Electrochemical Energy Reviews (2021) 4:101–135
https://doi.org/10.1007/s41918-020-00081-4

REVIEW ARTICLE

All-Solid-State Lithium Batteries with Sulfide Electrolytes and Oxide Cathodes

Jinghua Wu[1,2] · Lin Shen[1,2] · Zhihua Zhang[1] · Gaozhan Liu[1,2] · Zhiyan Wang[1,2] · Dong Zhou[1] · Hongli Wan[1,2] · Xiaoxiong Xu[3,4] · Xiayin Yao[1,2]

Received: 18 February 2020 / Revised: 19 June 2020 / Accepted: 22 August 2020 / Published online: 13 November 2020

Abstract
All-solid-state lithium batteries (ASSLBs) have attracted increasing attention due to their high safety and energy density. Among all corresponding solid electrolytes, sulfide electrolytes are considered to be the most promising ion conductors due to high ionic conductivities. Despite this, many challenges remain in the application of ASSLBs, including the stability of sulfide electrolytes, complex interfacial issues between sulfide electrolytes and oxide electrodes as well as unstable anodic interfaces. Although oxide cathodes remain the most viable electrode materials due to high stability and industrialization degrees, the matching of sulfide electrolytes with oxide cathodes is challenging for commercial use in ASSLBs. Based on this, this review will present an overview of emerging ASSLBs based on sulfide electrolytes and oxide cathodes and highlight critical properties such as compatible electrolyte/electrode interfaces. And by considering the current challenges and opportunities of sulfide electrolyte-based ASSLBs, possible research directions and perspectives are discussed.

Keywords All-solid-state lithium batteries · Sulfide electrolytes · Oxide cathodes · Interfaces

1 Introduction

Driven by the emergence of electric vehicles, great efforts have recently been devoted to the development of better rechargeable lithium ion batteries in terms of higher specific energy density, longer cycle lifes and better safety [1]. Although significant efforts have been devoted to lithium ion batteries based on organic liquid electrolytes in the past 30 years, the limited electrochemical and thermal stability, low ion selectivity and poor safety of organic liquid electrolyte-based lithium ion batteries hinder application. In particular, the combustible characteristic of organic electrolytes is a significant security risk for vehicle or grid applications that require large battery sizes. Here, the replacement of liquid electrolytes with solid electrolytes is regarded to be the ultimate solution to these problems in which the nonflammable nature of solid electrolytes can avoid fire and explosion even in a large scale [2–7]. Based on this, a variety of solid ionic conductors have been investigated as solid electrolytes to replace liquid ones [8]. However, their application is limited by low ionic conductivity. Sulfide-based electrolytes have been explored as alternatives to oxide-based electrolytes due to the more polarizable nature of sulfur anions, which can allow for more facile lithium ion conduction and higher ionic conductivity [9, 10]. And in recent years, the realization of sulfide electrolytes with unprecedented ionic conductivities equal to or greater than liquid electrolytes has been achieved in which $Li_{10}GeP_2S_{12}$ and $Li_{9.54}Si_{1.74}P_{1.44}S_{11.7}Cl_{0.3}$ have been demonstrated to possess ionic conductivities of 1.2×10^{-2} S cm^{-1} and 2.5×10^{-2} S cm^{-1}, respectively [11, 12]. Various systems from glass to glass–ceramics and crystalline conductors have also been studied, and an exciting new area in solid electrolytes has been presented. Due to these prominent performances, sulfide electrolytes can

✉ Xiaoxiong Xu
xuxiaoxiong@ganfenglithium.com

✉ Xiayin Yao
yaoxy@nimte.ac.cn

[1] Ningbo Institute of Materials Technology and Engineering, Chinese Academy of Sciences, Ningbo 315201, Zhejiang, China

[2] Center of Materials Science and Optoelectronics Engineering, University of Chinese Academy of Sciences, Beijing 100049, China

[3] Zhejiang Funlithium New Energy Technology Co., Ltd., Ningbo 315201, Zhejiang, China

[4] Ganfeng Lithium Co., Ltd., Xinyu 338015, Jiangxi, China

provide opportunities in the development of ASSLBs for electric vehicle applications.

Despite these promising findings, many challenges still exist in ASSLBs based on sulfide electrolytes. First, many sulfide electrolytes are unstable at low potentials, making their matching with lithium metal anodes difficult. Second, numerous studies have reported that the complex reactions between electrodes and electrolytes can result in low interfacial charge–transfer kinetics. Third, damage caused by Li dendrite formation in sulfide electrolytes is far worse than predicted and will shorten battery lifespans. Finally, the comprehensive understanding of sulfide electrolytes remains lacking. As for cathodes, lithium transition metal oxides have been extensively used in traditional lithium ion batteries because of their high electrochemical potential and moderate capacity [13, 14] and are commercially successful. However, poor rate and cyclic performances are generally observed in ASSLBs that combine sulfide electrolytes with oxide cathodes due to interfacial instability between the two, which is a major issue limiting the application of oxide cathodes in ASSLBs. In terms of anodes, although the use of lithium metal is necessary to obtain high-energy density, recent research has revealed that Li dendrites can easily form in the bulk or grain boundaries of inorganic sulfide electrolytes [15, 16]. In addition, sulfide electrolytes can show severe thermodynamic and dynamic instability against metallic lithium and the huge volume change of lithium anodes during lithium ion deposition/dissolution can lead to virtually infinite volume expansion to further deteriorate interfacial stability. Overall, the insufficient fundamental understanding of interfacial evolution processes during charge/discharge severally hinders the realization of ASSLBs based on sulfide electrolytes, oxide cathodes and lithium metal anodes.

Herein, we present an overview of the recent progress of ASSLBs using sulfide electrolytes and oxide cathodes. This review starts with a brief description of sulfide electrolytes. The corresponding electrolyte structures, preparation methods and ionic conductivity improvement strategies are summarized in detail. It is then followed by detailed discussions on the mechanisms of interfacial issues between sulfide electrolytes and electrodes with oxide cathodes and lithium metal anodes being the main focus. In addition, various design strategies including electrode coating, electrolyte component tuning and interfacial construction are proposed. At the end, a brief perspective concerning future development is presented.

2 Sulfide Electrolytes

The study of sulfide-type solid electrolytes began in 1981 with a Li_2S–P_2S_5 system [17] and although conductivities were improved through the doping of Li_xMO_y (M = Si, P and Ge), ionic conductivities remained lacking [18]. In 2001, a series of crystalline sulfide electrolytes based on the Li_2S–P_2S_5 system was reported by Kanno et al. [19] that possessed high lithium ion conductivities. As compared with Li_2S–SiS_2, Li_2S–P_2S_5 systems possess better physicochemical properties and have therefore been widely employed in all-solid-state batteries. In particular, Li_2S–P_2S_5 systems possess high room-temperature ionic conductivities of 0.1×10^{-3}–1×10^{-3} S cm^{-1} and wide electrochemical windows in which the materials in this family are referred to as "thio-LISICON" because their structures are similar to lithium superionic conductor (LISICON) materials [20]. Different from LISICON materials that possess poor room-temperature ionic conductivities, thio-LISICON materials possess much higher ionic conductivities due to the replacement of larger and more polarizable S^{2-} for O^{2-}, which can enlarge lithium ion migration tunnels and weaken interactions to result in higher ionic conductivities as compared with oxide analogs [21].

Based on the crystalline state, sulfide electrolytes can be divided into three categories, including glass (amorphous), crystal and glass–ceramic phases in which glassy electrolytes are attractive due to their isotropic ion conduction, zero grain boundary resistance and low costs with conductivities reaching ~ 10^{-4} S cm^{-1} at room temperature. Alternatively, glass–ceramic electrolytes obtained through the crystallization of glassy electrolytes can possess higher conductivities of 10^{-3} S cm^{-1} (even up to 10^{-2} S cm^{-1}). Tatsumisago et al. [22–25] systematically investigated the conductivity of $(100-x)Li_2S$–xP_2S_5 systems by controlling composition and heat treatment temperature and found that for all these electrolytes, glass–ceramic type electrolytes exhibited higher ionic conductivity as compared with glass or crystalline materials. Here, these researchers attributed this ionic conductivity enhancement mainly to the appearance of new metastable thio-LISICON analogs as confirmed by XRD analysis.

Sulfide electrolytes can also be divided into three categories based on structure, including binary systems of Li_2S–MS_x (M = P, Si and Ge), ternary systems of Li_2S–P_2S_5–MeS_x (Me = Si, Ge and Sn) and the argyrodite type. In this section, the crystal structure, conductivity and stability of these sulfide electrolyte systems will be discussed in detail.

2.1 Structure of Different Sulfide Electrolytes

2.1.1 Structure of Binary Sulfide Electrolytes

The chemical composition and conductivities of representative binary sulfide electrolytes include Li_2S–P_2S_5, Li_2S–SiS_2, Li_2S–GeS_2 and Li_2S–SnS_2 are summarized in Table 1. Among these, Li_2S–P_2S_5 has been the most studied system due to superior ionic conductivities. Taking into consideration good compatibility with metallic lithium and relatively high conductivity,

Table 1 Summary of the conductivity of representative binary sulfide electrolytes

Composition	Material type	Preparation method	Conductivity (S cm^{-1})	Reference
$Li_7Ni_{0.2}P_{3.1}S_{11}$	Crystal	High-energy ball-milling	2.22×10^{-3}	[44]
$Li_7P_{2.9}S_{10.85}Mo_{0.01}$	Crystal	High-energy ball-milling	4.8×10^{-3}	[67]
$90(0.7Li_2S–0.29P_2S_5–0.01WS_2)–10LiBr$	Glass–ceramic	High-energy ball-milling	1.82×10^{-3}	[175]
$75Li_2S–24P_2S_5–1P_2O_5$	Glass–ceramic	High-energy ball-milling	8×10^{-4}	[52]
$70Li_2S–27P_2S_5–3P_2O_5$	Glass–ceramic	High-energy ball-milling	3×10^{-3}	[176]
$Li_{3.06}P_{0.98}Zn_{0.02}S_{3.98}O_{0.02}$	Glass–ceramic	High-energy ball-milling	1.12×10^{-3}	[147]
$Li_3P_{0.98}Sb_{0.02}S_{3.95}O_{0.05}$	Glass–ceramic	High-energy ball-milling	1.08×10^{-3}	[146]
$70Li_2S–29P_2S_5–1Li_3PO_4$	Glass–ceramic	High-energy ball-milling	1.87×10^{-3}	[70]
$63Li_2S–27P_2S_5–10LiBr$	Glass–ceramic	High-energy ball-milling	6.5×10^{-3}	[72]
$Li_7P_3S_{11}$	Glass–ceramic	High-energy ball-milling	5.2×10^{-3}	[79]
$Li_7P_3S_{11}$	Glass–ceramic	Solid-state reaction	1.7×10^{-2}	[31]
$Li_7P_3S_{11}$	Crystal	Spark–plasma–sintering	1.16×10^{-2}	[32]
$0.59Li_2S–0.38SiS_2–0.03Li_3PO_4$	Glass	Solid-state reaction	6.9×10^{-4}	[177]
$2Li_2S–1GeS_2$	Glass	Solid-state reaction	2×10^{-7}	[178]
$2Li_2S–1SnS_2$	Crystal	Liquid-phase method	7.5×10^{-5}	[179]

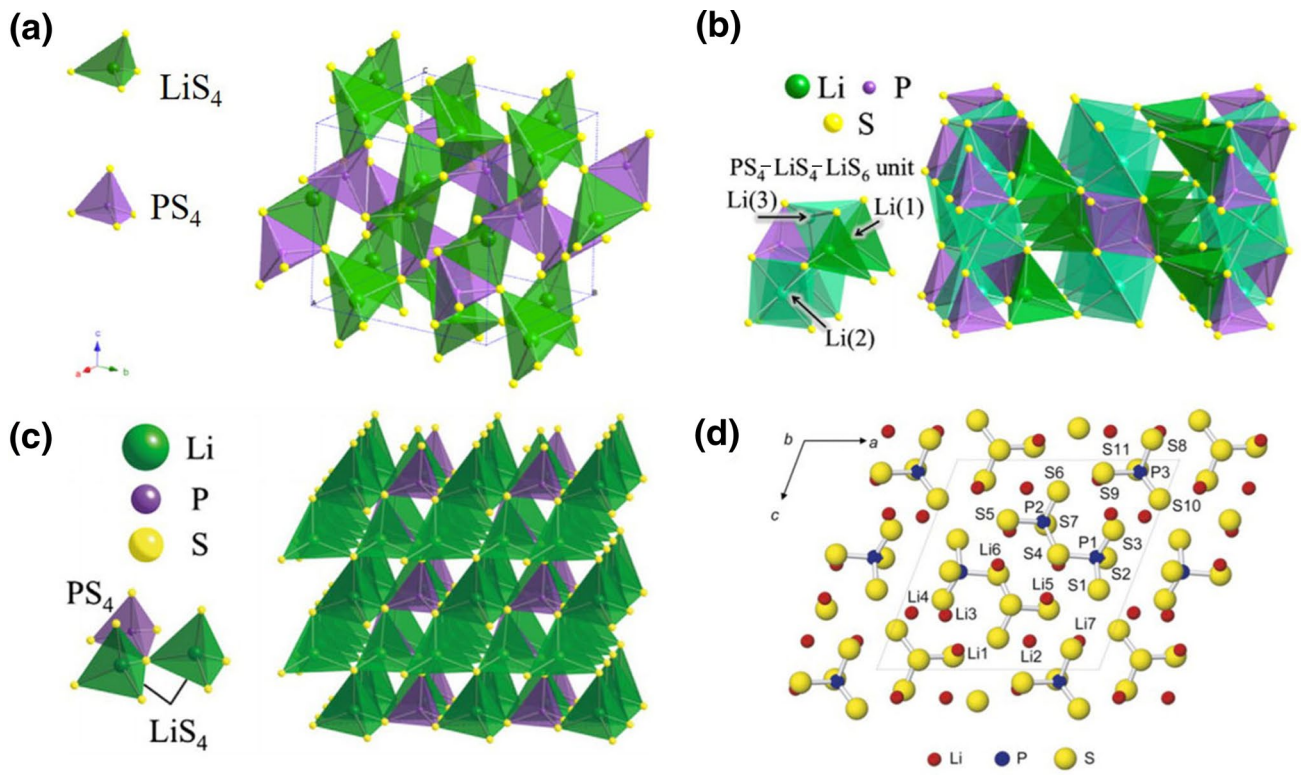

Fig. 1 Structure of **a** α-Li_3PS_4. Reprinted with permission from Ref. [27]. Copyright 2010, The Physical Society of Japan. **b** Structure of β-Li_3PS_4. **c** Structure of γ-Li_3PS_4. Reprinted with permission from Ref. [29]. Copyright 2007, Elsevier. **d** $Li_7P_3S_{11}$ viewed along the [010] direction. Reprinted with permission from Ref. [30]. Copyright 2007, Elsevier

Li_3PS_4 with a stoichiometry of $75\%Li_2S–25\%P_2S_5$ has also been extensively studied. In addition, Li_3PS_4 is usually regarded as the stablest composition in $Li_2S–P_2S_5$ systems and thus far, three types of Li_3PS_4 systems have been reported, including α-Li_3PS_4, β-Li_3PS_4 and γ-Li_3PS_4 (Fig. 1a–c) [26]. Among these crystal phases, the γ-Li_3PS_4 phase possesses the lowest ionic conductivity of 3×10^{-7} S cm^{-1}, whereas the β-Li_3PS_4 phase can deliver the highest ionic conductivity of ~ 10^{-4} S cm^{-1} in

which the different arrangements of PS_4 tetrahedra in Li_3PS_4 are the main reason for these differences in conductivity. In terms of structure, α-Li_3PS_4 is composed of LiS_4 tetrahedra and isolated PS_4 tetrahedra in which one LiS_4 tetrahedron is connected to four LiS_4 tetrahedra through corner sharing, one PS_4 tetrahedron through edge sharing and two PS_4 tetrahedra through corner sharing [27]. By contrast, γ-Li_3PS_4 is stable at low temperatures [27, 28] and possesses an ordered arrangement with the apex of the PS_4 tetrahedron orderly arranged in the same direction and the apex of the LiS_4 tetrahedron showing the same ordering as that of the PS_4 tetrahedron [27]. In terms of the structure of β-Li_3PS_4, this is particularly interesting due to its high lithium ion conductivity in which corresponding PS_4 tetrahedra are isolated from each other and connected with LiS_6 octahedra through edge sharing [29]. Here, lithium ions located in the tetrahedral (Wyckoff 4*c*) and octahedral (Wyckoff 4*b*) positions can form face-sharing octahedral–tetrahedral chains across the *b*-axis [26]. And unlike the ordered arrangement of PS_4 tetrahedra in γ-Li_3PS_4, β-Li_3PS_4 possesses a zig-zagged arrangement of PS_4^{3-} tetrahedra that can provide lithium ion positions in both octahedral and tetrahedral sites, allowing for more mobile lithium ions [27, 29].

As an example of a binary sulfide electrolyte, a newly emerged $Li_7P_3S_{11}$ phase developed by Yamane et al. [30] has attracted increasing attention due to its superior conductivity of up to 1.7×10^{-2} S cm^{-1} as reported by Seino et al. [31]. Here, the stoichiometry of $Li_7P_3S_{11}$ corresponds to a 70%Li_2S–30%P_2S_5 mixture with the crystalline structure of $Li_7P_3S_{11}$ (Fig. 1d) being composed of corner-sharing PS_4^{3-} and $P_2S_7^{4-}$ anions in a 1:1 ratio in which nearly all lithium sites are tetrahedrally coordinated (LiS_4) and interconnected by further empty tetrahedral sites ($\square S_4$) to provide three-dimensional diffusion tunnels [26]. And unlike other ionic conductors involving Li_2S–P_2S_5 systems, Chu et al. [32] proposed that the ionic conductivity of $Li_7P_3S_{11}$ does not proceed through the slow diffusion of isolated defects (i.e., lithium ion vacancies), but rather through the collective motion of multiple defects. Despite the favorable ionic conductivity of $Li_7P_3S_{11}$, it is metastable and can easily transform into other low-conductivity crystalline structures due to its narrow thermal stability window in which if heated to over 420 °C, it will decompose into Li_3PS_4 and $Li_4P_2S_7$, the latter of which tends to form $Li_4P_2S_6$ with extremely low conductivity (10^{-8} S cm^{-1}).

2.1.2 Structure of Ternary Sulfide Electrolytes

The electrochemical performance of Li_2S–P_2S_5 binary systems, especially ionic conductivity at room temperature remains unsatisfactory. To further optimize ionic conductivity and electrochemical performance, Li_2S–P_2S_5 ternary systems can be obtained through the introduction of tertiary components such as GeS_2, SiS_2, SnS_2 or Al_2S_3. The conductivities of representative ternary sulfide electrolytes are summarized in Table 2. Of these ternary systems, Li_2S–GeS_2–P_2S_5 is the most studied due to high ionic conductivities in which X-ray diffraction analysis has demonstrated that the introduction of GeS_2 can enlarge lattice structures, which is beneficial to lithium ion transport and

Table 2 Summary of the conductivity of representative ternary sulfide electrolytes

Composition	Material type	Preparation method	Conductivity (S cm^{-1})	Reference
$Li_{3.25}Ge_{0.25}P_{0.75}S_4$	Crystal	Solid-state reaction	2.2×10^{-3}	[19]
$Li_{3.05}Ge_{0.05}P_{0.95}S_4$	Glass–ceramic	High-energy ball-milling	1.2×10^{-3}	[180]
$Li_{10}GeP_2S_{12}$	Crystal	Solid-state reaction	1.2×10^{-2}	[11]
$Li_{10}GeP_2S_{12}$	Crystal	Solid-state reaction	1.0×10^{-2}	[181]
$Li_{10.35}Ge_{1.35}P_{1.65}S_{12}$	Crystal	Solid-state reaction	1.42×10^{-2}	[182]
$Li_{10}SnP_2S_{12}$	Crystal	Solid-state reaction	4.0×10^{-3}	[34]
$Li_{10}SnP_2S_{12}$	Crystal	Solid-state reaction	3.2×10^{-3}	[183]
$Li_{10}SiP_2S_{12}$	Crystal	Solid-state reaction	2.3×10^{-3}	[35]
$Li_{10}Si_{0.3}Sn_{0.7}P_2S_{12}$	Crystal	Solid-state reaction	8.0×10^{-3}	[184]
$Li_{10.3}Al_{0.3}Sn_{0.7}P_2S_{12}$	Crystal	Solid-state reaction	2.0×10^{-3}	[184]
$Li_{11}AlP_2S_{12}$	Crystal	Solid-state reaction	8.02×10^{-4}	[36]
$86.9Li_3PS_4{\cdot}13.1LiAlS_2$	Glass–ceramic	High-energy ball-milling	6.0×10^{-4}	[185]
$95Li_3PS_4{\cdot}5Li_4GeS_4$	Glass–ceramic	High-energy ball-milling	4.0×10^{-4}	[53]
$Li_{10}Ge_{0.95}Si_{0.05}P_2S_{12}$	Crystal	Solid-state reaction	8.6×10^{-3}	[186]
$Li_{10.35}(Sn_{0.27}Si_{1.08})P_2S_{12}$	Crystal	Solid-state reaction	1.1×10^{-2}	[151]
$Li_{10}Ge_{0.6}Sn_{0.4}P_2S_{11.2}Se_{0.8}$	Crystal	Solid-state reaction	2.75×10^{-3}	[77]
$Li_{10}SiP_2S_{11.3}O_{0.7}$	Crystal	Solid-state reaction	3.1×10^{-3}	[71]
$Li_{10}GeP_2S_{11.7}O_{0.3}$	Crystal	Solid-state reaction	1.03×10^{-2}	[78]
$Li_{9.54}Si_{1.74}P_{1.44}S_{11.7}Cl_{0.3}$	Crystal	Solid-state reaction	2.5×10^{-2}	[12]
$67(0.75Li_2S{\cdot}0.25P_2S_5){\cdot}33LiBH_4$	Glass	Mechanical milling	1.6×10^{-3}	[69]
$Li_{9.4}Ba_{0.3}GeP_2S_{12}$	Crystal	Solid-state reaction	7.04×10^{-4}	[149]

enhanced ionic conductivity. This structure was first discovered by Kanno et al. [19] based on a Li_4GeS_4–Li_3PS_4 solid solution system with a structural formula of $Li_{4-x}Ge_{1-x}P_xS_4$ in which corresponding $Li_{4-x}Ge_{1-x}P_xS_4$ crystals possess a similar structure to γ-Li_3PO_4 and can be divided into three compositional regions depending on monoclinic superstructures with different types of cation ordering, including region I ($0 < x \leqslant 0.6$), which possesses a monoclinic superlattice cell of $a \times 3b \times 2c$ that is related to orthorhombic Li_4GeS_4; regions II ($0.6 < x < 0.8$) and III ($0.8 \leqslant x < 1.0$) that possess different monoclinic cells of $a \times 3b \times 3c$ and $a \times 3b \times 2c$, respectively, and region II has been reported to possess the highest conductivity of 2.2×10^{-3} S cm^{-1} ($Li_{3.25}Ge_{0.25}P_{0.75}S_4$) at room temperature among the three regions. This $Li_{3.25}Ge_{0.25}P_{0.75}S_4$ electrolyte also possesses advantages including negligible electronic conductivity, high electrochemical stability and good physicochemical stability.

In 2011, Kanno et al. [11] discovered a new lithium superionic conductor $Li_{10}GeP_2S_{12}$ with an extremely high room-temperature ionic conductivity of 12 mS cm^{-1} that was even higher than that of organic liquid electrolytes used in commercial lithium ion systems. X-ray diffraction patterns indicated that the three-dimensional network structure of $Li_{10}GeP_2S_{12}$ differed from previously reported thio-LISICONs (Fig. 2a) in which the framework was composed of $(Ge_{0.5}P_{0.5})S_4$ tetrahedra, PS_4 tetrahedra, LiS_4 tetrahedra and LiS_6 octahedra. Among these $(Ge_{0.5}P_{0.5})S_4$ tetrahedra and LiS_6 octahedra shared the same edges and can form one-dimensional long chains along the *c*-axis to act as one-dimensional lithium conduction pathways. These one-dimensional chains were further connected to one another through PS_4 tetrahedra that were connected to LiS_6

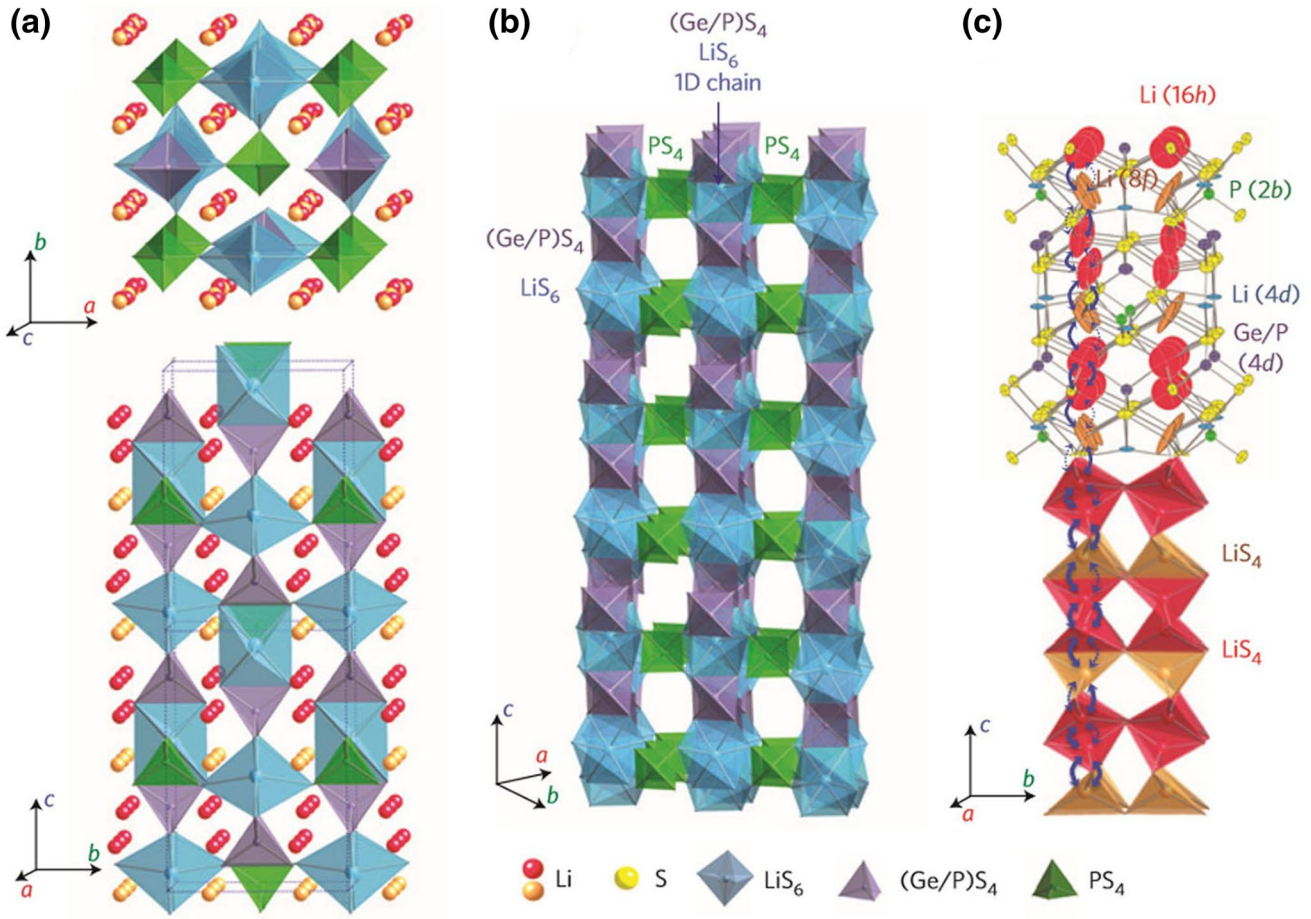

Fig. 2 Crystal structure of $Li_{10}GeP_2S_{12}$. **a** The framework structure and lithium ions that participate in ionic conduction. **b** Framework structure of $Li_{10}GeP_2S_{12}$. One-dimensional (1D) chains formed by LiS_6 octahedra and $(Ge_{0.5}P_{0.5})S_4$ tetrahedra, which are connected by a common edge. These chains are connected by a common corner with PS_4 tetrahedra. **c** Conduction pathways of lithium ions. Zigzag conduction pathways along the *c* axis are indicated. Lithium ions in the LiS4 tetrahedra (16*h* site) and LiS4 tetrahedra (8*f* site) participate in ionic conduction. Thermal ellipsoids are drawn with a 30% probability. The anisotropic character of the thermal vibration of lithium ions in three tetrahedral sites gives rise to 1D conduction pathways. Reprinted with permission from Ref. [11]. Copyright 2011, Nature Publishing Group

octahedra through a common corner (Fig. 2b). As a result, high ionic conductivities can be achieved through the zigzag conduction pathways formed by LiS_4 tetrahedra in 16*h* and 8*f* sites along the *c*-axis direction (Fig. 2c).

Despite the high ionic conductivity of $Li_{10}GeP_2S_{12}$, the high cost of elemental Ge and its instability with lithium metal limit large-scale application in ASSLBs. Because of this, many cheaper elements have been employed to replace Ge. For example, Ong et al. [33] investigated the ionic conductivity of a $Li_{10\pm1}MP_2X_{12}$ family of materials (M = Ge, Si, Sn, Al or P and X = O, S or Se) using first principle calculations and found that conductivity will not be affected by substituting Ge with relatively cheaper Sn or Si. Bron et al. [34] also reported the successful synthesis of $Li_{10}SnP_2S_{12}$ with a high grain conductivity of 7 mS cm^{-1} and a total conductivity of 4 mS cm^{-1} in which structural characterizations indicated that $Li_{10}SnP_2S_{12}$ was isostructural to the Ge analog with regard to the $P4_2/mc$ space group, thus ensuring high ionic conductivity. This high conductivity as well as the reduced cost of $Li_{10}SnP_2S_{12}$ makes it an attractive and affordable candidate for application in ASSLBs. White et al. [35] further prepared $Li_{10}SiP_2S_{12}$ as another $Li_{10}GeP_2S_{12}$ analog through the replacement of Ge by Si and obtained a conductivity of 2.3 mS cm^{-1}, which was greater than that of $Li_{10}GeP_2S_{12}$ prepared in the same conditions. Elemental Al has also been used to replace Ge. For example, Zhou et al. [36] prepared $Li_{11}AlP_2S_{12}$ with a $Li_{10}GeP_2S_{12}$ analogous structure through sintering and reported that although their ternary electrolyte provided an ionic conductivity (0.82 mS cm^{-1}) that was lower than that of $Li_{10}GeP_2S_{12}$, it provided a wider electrochemical window and excellent electrochemical performances.

2.1.3 Argyrodite-Type Solid Electrolytes

Argyrodite is another important class of solid electrolytes derived from the mineral Ag_8GeS_6 and possesses high Ag^+ conductivities [37]. In addition, the replacement of Ag^+ ions by other cations does not damage the cubic structure of argyrodite. And based on efforts to enhance lithium ion mobility, lithium argyrodites have been explored as solid electrolytes. A summary of the conductivity of representative argyrodite-type solid electrolytes is presented in Table 3. Li_7PS_6 as a lithium argyrodite was reported to have a cubic phase at high temperature or an orthorhombic phase at low temperature, and the cubic high-temperature phase possesses higher ionic conductivity and can be stabilized by the replacement of sulfur by halogen anions [38]. Deiseroth et al. [39] explored a series of lithium argyrodites with the general formula Li_6PS_5X (X=Cl, Br, I) as characterized by the partial replacement of S^{2-} by halogen anions. Theoretical calculations demonstrated that the incorporation of halogen ions can stabilize the corresponding cubic structure at room temperature and improve ionic conductivity [40]. For example, Li_6PS_5Cl and Li_6PS_5Br prepared through solid phase methods can reach ionic conductivities of 1.9×10^{-3} S cm^{-1} and 6.8×10^{-3} S cm^{-1}, respectively [41], whereas the ionic conductivity of Li_6PS_5I is low. Here, high-resolution neutron

Table 3 Summary of the conductivity of representative argyrodite-type solid electrolytes

Composition	Material type	Preparation method	Conductivity (S cm^{-1})	Reference
Li_6PS_5Cl (with excess Li_2S)	Crystal	Solid-state reaction	1.8×10^{-3}	[44]
Li_6PS_5Cl	Crystal	High-energy ball-milling	1.33×10^{-3}	[55]
Li_6PS_5Cl	Crystal	High-energy ball-milling	1.1×10^{-3}	[56]
Li_6PS_5Cl	Crystal	Liquid-phase method	1.1×10^{-3}	[65]
Li_6PS_5Cl	Crystal	Liquid-phase method	2.4×10^{-3}	[66]
$Li_6PS_5Cl_{0.75}Br_{0.25}$	Crystal	Liquid-phase method	3.2×10^{-3}	[66]
$Li_6PS_5Cl_{0.5}Br_{0.5}$	Crystal	Liquid-phase method	3.9×10^{-3}	[66]
$Li_6PS_5Cl_{0.25}Br_{0.75}$	Crystal	Liquid-phase method	3.4×10^{-3}	[66]
$Li_{5.75}PS_{4.75}Cl_{1.25}$	Crystal	Liquid-phase method	3.0×10^{-3}	[66]
$Li_{5.5}PS_{4.5}Cl_{1.5}$	Crystal	Liquid-phase method	3.9×10^{-3}	[66]
$Li_{6.6}Si_{0.6}Sb_{0.4}S_5I$	Crystal	Solid-state reaction	2.4×10^{-2}	[187]
$Li_{5.5}PS_{4.5}Cl_{1.5}$	Crystal	Solid-state reaction	9.4×10^{-3}	[74]
Li_6PS_5Br	Crystal	Solid-state reaction	2.58×10^{-3}	[45]
Li_6PS_5Br (with excess Li_2S)	Crystal	Solid-state reaction	1.3×10^{-3}	[44]
$Li_{6+x}P_{1-x}Si_xS_5Br$ ($x=0.35$)	Crystal	Solid-state reaction	2.4×10^{-3}	[188]
Li_6PS_5Br	Crystal	Liquid-phase method	1.9×10^{-4}	[189]
Li_6PS_5Br	Crystal	Liquid-phase method	1.9×10^{-3}	[66]
Li_6PS_5I (with excess Li_2S)	Crystal	Solid-state reaction	1.5×10^{-5}	[44]
$Li_{6+x}P_{1-x}Ge_xS_5I$ ($x=0.6$)	Crystal	Solid-state reaction	$(5.4\pm0.8)\times10^{-3}$ (cold-pressed) $(1.84\pm0.27)\times10^{-2}$ (sintered)	[43]

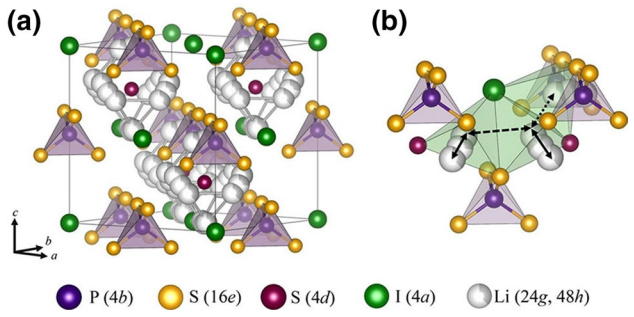

Fig. 3 **a** Crystal structure of Li_6PS_5X in the case of X = I, **b** rate-determining step of the inter-cage 48*h*–48*h* jump in lithium ion migration as shown by LiS_3I polyhedra. Reprinted with permission from Ref. [43]. Copyright 2018, American Chemical Society

and X-ray diffraction analyses showed that aside from lithium distribution disorder, disorder caused by Cl^- and Br^- can promote lithium ion mobility. However, I^- cannot exchange with S^{2-} due to its large size, resulting in more ordered structure and low conductivity, which cannot compete with those of Li_6PS_5Cl and Li_6PS_5Br [42]. In addition, Li_6PS_5X electrolytes can also possess wide electrochemical windows and cheaper precursors of this system allow for great potential as practical candidates for further application.

Li_6PS_5X can crystallize into a structure based on the tetrahedral close packing of anions (a cubic unit cell with the space group $F\bar{4}3m$ and a space group number 216, see Fig. 3). The halide anions X^- can form a face-centered cubic lattice (4*a*) with isolated PS_4 tetrahedra on octahedral sites (P on 4*b*) and free S in half of the tetrahedral sites (4*d*), while Li^+ ions are randomly distributed over the tetrahedral interstices (48*h* and 24*g* sites) [7, 43]. In the case of Li_6PS_5I, S and I atoms at 4*d* and 4*a* sites are fully ordered due to the small size mismatch between S and I, while it is fully disordered for Li_6PS_5Cl. Li_6PS_5Br consists of both ordered and disordered structures with 84% S and 16% Br at 4*d* sites and 60% Br and 40% S at 4*a* sites [7]. Here, the absence of disorder in Li_6PS_5I will lead to higher activation barriers for ion migration and lower ionic conductivities as compared with other argyrodite systems.

2.2 Synthesis Methods

In general, sulfide electrolyte preparation methods can be divided into three categories, including solid-state reaction, mechanical ball-milling and wet chemistry methods. Of these methods, the solid-state reaction method involves the heating of a precursor material mixture in stoichiometric ratios at the melting point followed by the cooling of the molten sample to room temperature. The preparation possess of the solid-state method is harsh and direct solid-state methods can produce impurities due to lithium and sulfur volatilization under high temperatures. Now, these issues can be alleviated through sealing techniques in which precursor powders can be pressed into pellets and filled into quartz ampoules that are sealed under vacuum conditions. By providing a sealed sintering environment, electrolyte purity can be ensured and high conductivities up to 10^{-3} S cm^{-1} can be achieved [43–45]. For example, Seino et al. [31] synthesized a Li_2S–P_2S_5 glass ceramic electrolyte that possessed a high conductivity of 1.7×10^{-2} S cm^{-1} through the solid-state reaction followed by hot pressing in which a mixture of Li_2S and P_2S_5 was sealed in a quartz tube and heated at 700 °C for 2 h followed by rapid quenching in ice water and hot-press sintering under 94 MPa at 280 °C or 300 °C to obtain the densified glass ceramic sample. These researchers also reported that grain boundary resistances can be reduced through optimized heat treatment conditions and allow for higher lithium ion mobility than that of organic liquid electrolytes. Ternary sulfide electrolytes with high conductivities can also be obtained through the solid-state method. For example, Kanno et al. obtained $Li_{10}GeP_2S_{12}$ by reacting stoichiometric quantities of Li_2S, GeS_2 and P_2S_5 at 550 °C in an evacuated quartz tube followed by a slow cooling process, whereas for $Li_{9.54}Si_{1.74}P_{1.44}S_{11.7}Cl_{0.3}$, the synthesis process was almost the same but with different initial precursor materials and reaction temperatures [11, 12]. The solid-state reaction method can further be used in the synthesis of argyrodite-type solid electrolytes. As examples, Deiseroth et al. [39] and Kraft et al. [46] both used the simple direct heating of precursor mixtures to prepare Li_6PS_5X despite long heating times, even up to 2 weeks. However, Wang et al. [47] also investigated the influence of sintering temperature and time on the structure and conductivity of Li_6PS_5Cl and found that 10 min of heating at 550 °C was sufficient to obtain Li_6PS_5Cl with a high conductivity of 3.15×10^{-3} S cm^{-1}. Similarly, Yu et al. [48] achieved a higher conductivity of 5×10^{-3} S cm^{-1} for Li_6PS_5Cl after long-term annealing with pellets pressed under high pressure.

Mechanical ball-milling, especially high-energy ball-milling, has been widely used to prepare sulfide electrolytes in which precursor particles can collide, diffuse and react if induced energy through high-speed impact is sufficient [49]. And unlike solid-state reactions that require intricate processes involving mixing, pulverization and high-temperature treatment, mechanical ball-milling processes are simple, with the entire process being able to be completed at room temperature. More importantly, the preparation of amorphous electrolytes can be easily achieved through mechanical ball-milling due to low reaction temperatures. Using this technology, a series of binary and ternary electrolytes has been synthesized, including $70Li_2S$–$30P_2S_5$ (8.6 mS cm^{-1}) [50], $77.5Li_2S$–$22.5P_2S_5$ (1 mS cm^{-1}) [51], $75Li_2S$–$25P_2S_5$ (0.5 mS cm^{-1}) [52] and ternary Li_2S–M_xS_y–P_2S_5 electrolytes [53]. High-energy ball-milling can also widen the region of

amorphous-sample formation as compared with the solid-state method. For example, Adams et al. [41] recently synthesized Li_6PS_5X (X = Cl, Br, I) argyrodite through mechanical ball-milling followed by annealing and reported that the use of their process allowed for faster synthesis than earlier reported methods with longer annealing times. Subsequently, a series of studies was conducted in their group to optimize the synthesis route, allowing for crystalline phases that can exhibit high ionic conductivities reaching 7×10^{-4} S cm^{-1} for X = Cl or Br [42, 54]. Boulineau et al. [55] were also able to obtain Li_6PS_5Cl with an ionic conductivity of 1.33×10^{-3} S cm^{-1} and a wide electrochemical window by optimizing ball-milling times to 10 h. The attractive electrochemical properties were attributed to the spontaneous formation of crystallized argyrodite during ball-milling. Similarly, Yu et al. [56] investigated the effects of mechanical milling times and subsequent heat treatment processes on electrolyte structure and were able to improve the ionic conductivity of Li_6PS_5Cl to 1.1×10^{-3} S cm^{-1}, revealing that further annealing can increase crystallinity and contact between grains to result in higher ionic conductivity. A major disadvantage of the ball-milling process is the long processing times. In addition, contamination as induced by the milling ball can compromise the purity of final electrolytes. In fact, it is difficult to completely distinguish ball-milling from solid-state processes because the latter requires ball-milling to mix materials in advance. Likewise, annealing after ball-milling is usually required to further improve the conductivity or crystallinity of electrolytes and the combination of ball-milling with solid-state methods can effectively reduce the reaction time of solid electrolyte synthesis.

In recent years, wet chemical methods by using liquid solvents as media have received increasing attention in the synthesis of sulfide electrolytes due to simple procedures, time-saving processes and the uniformity of resulting electrolytes. The use of the wet chemical method for the synthesis of Li_2S–P_2S_5 binary systems was first developed by Liu et al. [57] in 2013 in which the reaction between Li_2S and P_2S_5 was mediated by tetrahydrofuran to form β-Li_3PS_4. Subsequently, wet chemical methods have become more popular in the synthesis of sulfide electrolytes in which by using stable organic liquid solvents with low boiling points as reaction media, perfect homogeneity can be achieved and solvents can be removed through evaporation. Unfortunately, commonly adopted organic solvents such as anhydrous acetonitrile [58], tetrahydrofuran [57], ethyl acetate [59], N-methyl formamide [60] and 1,2-dimethoxyethane [61] are not environmentally friendly and the conductivity of electrolytes synthesized through the liquid-phase method is usually lower than those obtained through high-energy mechanical ball-milling methods. It was presumed that impurities from solvents and remaining amorphous phases precipitated at the interface between crystal particles were responsible for the low conductivity [61, 62]. Similar to the case of binary electrolytes, the purpose of the liquid-phase method in synthesizing argyrodite-type solid electrolytes is to improve homogeneity through dispersion in liquid media. Tatsumisago et al. [63] were the first to prepare argyrodite-type solid electrolytes through the liquid-phase method in which preparation conditions such as solvent, dissolution time and drying temperature were examined, resulting in a Li_6PS_5Br electrolyte with a relatively high ionic conductivity of 1.9×10^{-4} S cm^{-1}. And with the further development of their synthetic procedure, these researchers further improved the conductivity to 10^{-3} S cm^{-1} [64]. Choi et al. [65] also prepared argyrodite-type Li_6PS_5Cl solid electrolytes using a liquid-phase process with ethyl acetate as the solvent along with subsequent heat treatment at 550 °C to obtain a Li_6PS_5Cl solid electrolyte with a relatively high conductivity of 1.1×10^{-3} S cm^{-1} at room temperature. In addition, Zhou et al. [66] synthesized Li_6PS_5X (X = Cl, Br) through a liquid-phase method using tetrahydrofuran/ethanol mixtures as solvate complexes that enabled shorter reaction times as compared with the use of dimethoxyethane and acetonitrile to achieve a high conductivity of 3.9×10^{-3} S cm^{-1} for a resulting Li_6PS_5Cl electrolyte. Furthermore, Yubuchi et al. [64] employed a similar method using tetrahydrofuran as a solvent and were able to obtain a Li_6PS_5Br electrolyte with a conductivity of 3.1×10^{-3} S cm^{-1}. The preparation of ternary electrolytes by using wet chemical methods has seldomly been reported, possibly due to the unstable characteristic of high valent cations in organic solvents. Overall, the liquid-phase method is more applicable in scalable manufacturing processes as compared with solid-state and mechanical ball-milling methods and can be applied to synthesize various compounds through appropriate solvent selection. Another unique advantage of the liquid-phase method is that resulting morphology and particles sizes can be controllably adjusted by changing reaction conditions [65]. Despite all of this, the involvement of toxic organic solutions restricts application.

2.3 Strategies for Improving Electrochemical Properties

2.3.1 Cation Substitution

Lithium ion diffusion in solid materials mainly depends on migration tunnels in which a lithium ion can diffuse from one lattice site to adjacent vacant sites as individual lithium ion hops and is governed by corresponding crystalline structures, specifically the size of migration tunnels. Higher lithium ion concentrations can also enhance conductivity because more lithium ions can participate in diffusion. Various strategies have been proposed to enhance the room-temperature conductivity of sulfide electrolytes. In general,

aliovalent cation substitution has proven to be effective in which the incorporation of different valence cations can induce new vacancies and the migration of ion concentrations can increase in order to compensate for the valence imbalance of main skeletons. As examples, Ge et al. [44] reported that a 2 mol% Ni_2P-doped $Li_7P_3S_{11}$ electrolyte can exhibit an enhanced conductivity of 2.22×10^{-3} S cm^{-1} that is 1.6 times higher than that of the pristine electrolyte. Xu et al. [67] prepared $Li_7P_{2.9}S_{10.85}Mo_{0.01}$ through high-energy ball-milling using Li_2S, P_2S_5 and high-quality MoS_2 as starting materials with a stoichiometric ratio of 7:2.9:0.1. The resultant $Li_7P_{2.9}S_{10.85}Mo_{0.01}$ electrolyte possessed a high room-temperature conductivity of 4.8×10^{-3} S cm^{-1}. Wu et al. [68] prepared a series of $70Li_2S{\cdot}(30-x)P_2S_5{\cdot}xSeS_2$ ($x = 0$, 0.3, 0.5, 1, 3 and 5) glass–ceramic electrolytes through ball-milling to obtain an optimal conductivity of 5.28×10^{-3} S cm^{-1} at 20 °C in $70Li_2S{\cdot}29P_2S_5{\cdot}1SeS_2$ and ascribed this conductivity to the partial replacement of P_2S_5 by SeS_2. Yamauchi et al. [69] also reported that the addition of $LiBH_4$ to $(100-x)(0.75Li_2S{\cdot}0.25P_2S_5){\cdot}xLiBH_4$ glass electrolytes can not only improve conductivity but also enlarge electrochemical windows by up to 5 V versus Li/Li$^+$. Furthermore, Kraft et al. [43] systematically explored the influence of aliovalent substitution in $Li_{6+x}P_{1-x}Ge_xS_5I$ and found that with an increased Ge content, anion site disorder is induced and activation barriers for ionic migration are significantly reduced, leading to a high ionic conductivity of (18.4 ± 2.7) mS cm^{-1} upon sintering.

2.3.2 Anion Substitution

Doping with appropriate amounts of oxides can simultaneously enhance the ionic conductivity and stability of Li metal anodes. For example, Tao et al. [52] reported that a $75Li_2S–25P_2S_5$ electrolyte with 1 mol% P_2O_5 doping presented an enhanced conductivity of 8×10^{-4} S cm^{-1} that was 56% higher than that of the undoped electrolyte. In addition, $1P_2O_5–75Li_2S–24P_2S_5$ exhibited good electrochemical stability with lithium metal. Similar conclusions were also drawn by Huang et al. [70], who reported that a Li_3PO_4-doped $Li_7P_3S_{11}$ electrolyte exhibited higher conductivities than the pristine material (1.87×10^{-3} S cm^{-1} as compared with 1.07×10^{-3} S cm^{-1}). In terms of ternary sulfide electrolytes, Kim et al. [71] investigated new $Li_{10}SiP_2S_{12-x}O_x$ solid-state electrolytes through the substitution of O for S and reported a maximum ionic conductivity of 3.1×10^{-3} S cm^{-1} at $x = 0.7$.

The addition of halides can also significantly improve the ionic conductivity of $Li_2S–P_2S_5$ sulfide electrolytes. For example, Ujiie et al. [72] compared the doping effects of different halides and found that the introduction of LiBr can effectively increase the conductivity of a $Li_7P_3S_{11}$ glass–ceramic electrolyte to 6.5×10^{-3} S cm^{-1}. $(100-x)(0.7Li_2S{\cdot}0.3P_2S_5){\cdot}xLiI$ glass and glass–ceramic electrolytes were also prepared through mechanical milling in the composition range of $0 \leqslant x$ (mol%) $\leqslant 20$ by the same group in which the conductivity of the glass electrolytes increased with an increasing LiI content and resulted in an optimal conductivity of 5.6×10^{-4} S cm^{-1} at $x = 20$ [73]. More importantly, they also found that the $80(0.7Li_2S{\cdot}0.3P_2S_5){\cdot}20LiI$ glass electrolyte exhibited a wide electrochemical window up to 10 V (vs. Li/Li$^+$) according to cyclic voltammetry results. However, the conductivity will decrease sharply if the LiI content increases continually.

As for Li_6PS_5X argyrodite electrolytes, the selection of different halide anions is crucial to the determination of conductive properties in which structural changes can strongly affect activation barriers and further optimize electrolytes to obtain higher ionic conductivities. After systematic investigations, the optimized electrolyte system is determined as Li_6PS_5Cl [55, 66]. Adeli et al. found that in the halide-rich $Li_{6-x}PS_{5-x}Cl_{1+x}$ system the Cl^-/S^{2-} ratio has remarkable impacts on lithium ion diffusivity in the lattice in which $Li_{5.5}PS_{4.5}Cl_{1.5}$ can reach a high room-temperature conductivity of (12.0 ± 0.2) mS cm^{-1}, which was almost four-fold greater than Li_6PS_5Cl under identical processing conditions. Here, these researchers suggested that the weakened interactions between mobile lithium ions and surrounding framework anions as incurred by the substitution of Cl^- for S^- played a major role in the enhancement of lithium ion diffusivity [74].

2.3.3 Multi-element Substitution

Aside from single element doping, multi-element substitution, especially dual-cation doping, has been demonstrated to be an effective method to enhance the electrochemical performance of electrolytes due to the synergistic effect between different cations [75, 76]. For example, Yang et al. [77] studied the influence of multi-element doping on the ion channel width and the activation energy in which a Sn–Se co-doped $Li_{10}GeP_2S_{12}$ electrolyte was synthesized through a solid-state reaction method. Here, these researchers reported that in contrast to the limited benefits of single element doping, their Sn–Se dual-doped $5Li_2S{\cdot}P_2S_5{\cdot}0.6GeS_2{.}0.4SnSe_2$ ($Li_{10}Ge_{0.6}Sn_{0.4}P_2S_{11.2}Se_{0.8}$) electrolyte demonstrated a high ionic conductivity of 2.75×10^{-3} S cm^{-1} and extremely low activation energy of 16 kJ mol^{-1} at room temperature, which were some of the lowest reported values for lithium ion conductors, demonstrating the potential of the Sn–Se dual-doped $Li_{10}GeP_2S_{12}$ as a promising electrolyte for advanced all-solid-state batteries. Kanno et al. [78] also prepared a new $Li_{10+\delta}(Sn_ySi_{1-y})_{1+\delta}P_{2-\delta}S_{12}$ sulfide electrolyte through dual element substitution and found that changing Sn/Si ratios and (Sn^{4+} and Si^{4+})/P^{5+} ratios can adjust lithium conduction channel sizes and optimize conductivity, resulting in an optimized ionic conductivity of 1.1×10^{-2} S cm^{-1}.

Although this obtained conductivity was close to the value for the original $Li_{10}GeP_2S_{12}$ compound, the Ge-free electrolyte is more suitable for practical application.

2.3.4 Densification

The formation of micro-cracks and pores is inevitable in the processes of mass transport and grain growth in solid electrolytes. However, low-conductivity impurities tend to concentrate in these areas and block continuous lithium ion migration tunnels. In addition, electric charge accumulating in these defects can lead to the formation of lithium dendrites, which may further elevate lithium ion migration energy barriers. Because of this, the elimination of these cracks and pores through densification is a reasonable solution to improve ionic conductivity. For example, Chu et al. [32] reported that $Li_7P_3S_{11}$ prepared through spark–plasma sintering showed a high ionic conductivity of 1.16×10^{-2} S cm^{-1} at 27 °C that was higher than that prepared through general methods. Amorphous electrolyte materials can also be used for glass–ceramic electrolytes to fill cracks and pores and lower lithium ion migration energy barriers. Minami et al. [79] further reported that by optimizing heat treatment parameters, the conductivity of a $Li_7P_3S_{11}$ glass–ceramic electrolyte can reach 5.2×10^{-3} S cm^{-1} that was significantly higher than that of a $Li_7P_3S_{11}$ crystal electrolyte.

3 Sulfide Electrolyte/Oxide Cathode Interfaces

Oxide cathodes including lithium transition metal oxides and phosphates have been extensively used in commercial lithium ion batteries because of their high electrochemical potential and moderate capacity [80–82]. The combination of sulfide electrolytes with oxide cathodes can allow for the development of new ASSLBs with high safety and energy density. However, interfacial instability limits the application of oxide cathodes in ASSLBs. Because of this, extensive research has been conducted in this field and an overview of common interfacial behaviors between sulfide electrolytes and oxide cathodes is summarized in this section along with recent progress on strategies to improve interfacial stability.

3.1 Interface Behavior

In general, interfacial behaviors include the following aspects: (1) space charge layer effects, (2) interfacial reactions and (3) contact loss.

3.1.1 Space Charge Layer

Space charge layers are formed at the interface between two ionic conductors with significantly different lithium chemical potentials and can induce high interfacial resistances that severely affect the high-rate charge/discharge ability of ASSLBs. Because oxide cathodes are usually mixed conductors with high ion and electron conductivities, whereas sulfide electrolytes are single lithium ion conductors, contact between oxide cathodes with sulfide electrolytes will cause lithium ions to move from the sulfide electrolyte to the oxide cathode due to large chemical potential differences, resulting in the formation of space charge layers. Furthermore, because of the high electron conductivity of oxide cathodes, electrons can eliminate lithium ions on cathode sides to cause lithium ions to continue diffuse from the sulfide side to reach equilibrium. As a result, lithium-deficient space charge layers can form on the sulfide electrolyte side at equilibrium and grow after initial charging [83]. Takada et al. [84] investigated the effects of space charge layers and found that although the thickness of the space charge layer is only about 10 nm for a $Li_{1-x}Mn_2O_4/Li_{3.25}Ge_{0.25}P_{0.75}S_4$ interface, it can lead to huge electrode resistances as high as 1×10^4 Ω. In addition, Takada et al. [85] also found that space charge layers were detrimental for high-rate charge/discharge abilities in In-Li/$LiCoO_2$ cells in which only 4% of initial capacity was retained at 5 mA cm^{-2} in an ASSLB.

3.1.2 Interfacial Reactions

The interfaces between electrodes and electrolytes in ASSLBs are different from that in conventional organic liquid electrolyte-based lithium ion batteries in which electrochemical reactions are carried out through the solid–solid interface. Based on this, many studies have been conducted to understand the possible causes of these interfacial reactions. For example, Tateyama et al. [86] investigated cation mutual diffusion properties at sulfide electrolyte/cathode interfaces using DFT + U treatment. Their results for a representative $LiCoO_2$/β-Li_3PS_4 solid electrolyte interface revealed that Co and P exchange energy was negative, suggesting that elemental diffusion is energetically preferable and that interfaces kinetically is stabilized after diffusion. In addition, these researchers found that repetitions of these elemental diffusions can induce detrimental transformations at interfaces, such as phase transitions or resistive-layer formations. Calculated thermodynamic data also revealed that sulfide electrolytes possess higher reaction energy with high-voltage oxide cathodes because of high cathode potentials and strong reactions between PS_4 groups and oxide cathodes to form PO_4 groups [87–89]. Moreover, nearly all types of sulfide electrolytes have been found to be able to react with oxide cathodes, especially high-voltage cathodes [81,

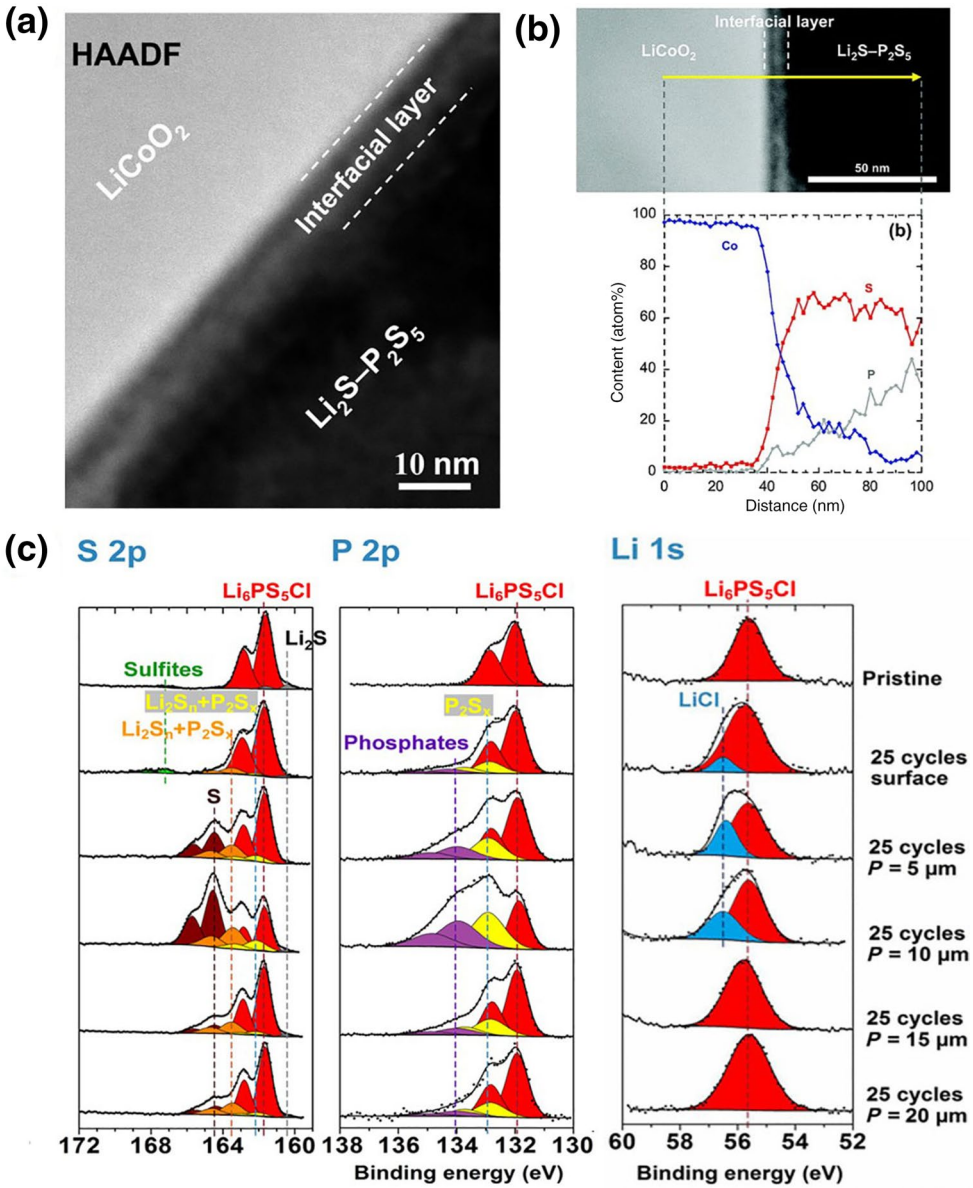

Fig. 4 **a** Cross-sectional high-angle annular dark-field transmission electron microscope image of the interface between a $LiCoO_2$ electrode and a $Li_2S–P_2S_5$ solid electrolyte. **b** Energy dispersive spectroscopy line profiles for Co, P and S elements near a $LiCoO_2$ electrode/$Li_2S–P_2S_5$ solid electrolyte interface after initial charging. Reprinted with permission from Ref. [90]. Copyright 2009, American Chemical Society. **c** S 2p, P 2p and Li 1s XPS spectra of a composite $LiCoO_2$ electrode in a $LiCoO_2$/Li_6PS_5Cl/Li-In half-battery: before cycling (pristine), after 25 cycles and after 25 cycles with increasing etching depths of the electrode from 5 to 20 μm. Reprinted with permission from Ref. [81]. Copyright 2017, American Chemical Society

90–92]. Kwak et al. [91] observed the interface between $LiCoO_2$ and $Li_2S–P_2S_5$ using transmission electron microscopy in which a 10-nm interfacial layer was found (Fig. 4a) and the coexistence of Co, S and P elements was observed (Fig. 4b), indicating that elements of $LiCoO_2$ and $Li_2S–P_2S_5$ can mutually diffuse. A similar interfacial layer was also found between a high Ni cathode and an O-doped binary sulfide electrolyte $75Li_2S–22P_2S_5–3Li_2SO_4$ in which large amounts of S and P penetrated into the oxide cathode and resulted in poor rate capability and capacity retention. Ternary sulfide electrolytes and argyrodite solid electrolytes have further been found to be unstable after contact with oxide cathodes. According to calculations by Mo et al. [92], $Li_{10}GeP_2S_{12}$ can decompose into Li_2S, Li_2SO_4, Li_3PO_4 and Li_4GeO_4 and argyrodite Li_6PS_5Cl can decompose into elemental S, lithium polysulfides, $P_2S_x(x \geqslant 5)$, phosphates and LiCl at the interface with different oxide cathodes as confirmed by XPS (Fig. 4c). Many components of interfacial layers are ionically insulating, which will further induce high interfacial resistances and even worse, some components are even electronically conductive (e.g., cobalt sulfides) and will lead to the continuous growth of ionically insulating interfacial layers [32]. As a result, interfacial reactions can explain experimentally observed high internal resistances that cause poor rate and cycle performances.

3.1.3 Contact Loss

Although sulfide electrolytes are soft and deformable enough to form better interfacial contact than oxide electrolytes, the

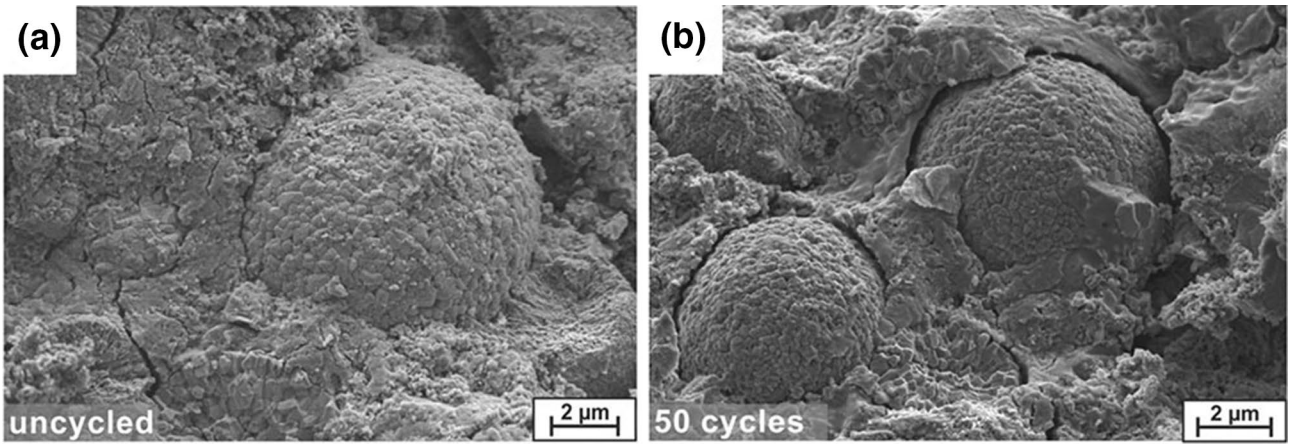

Fig. 5 **a** Scanning electron microscopy (SEM) image of a composite cathode of $LiNi_{0.8}Co_{0.1}Mn_{0.1}O_2$ (NCM811) in an ASSLB before electrochemical cycling. **b** SEM image of the composite cathode after 50 cycles. Reprinted with permission from Ref. [93]. Copyright 2017, American Chemical Society

repeated volume change of cathodes will inevitably cause contact loss between electrolytes and active material particles, resulting in increased interfacial resistance and capacity loss [93–96]. For example, Koerver et al. [93] investigated $LiNi_{0.8}Co_{0.1}Mn_{0.1}O_2$ composite morphology using scanning electron microscopy. The as-prepared sample showed close and intimate contact between the active material and the electrolyte before electrochemical cycling (Fig. 5a). But after 50 cycles, an obvious spherical gap appeared at the interface (Fig. 5b). Here, this mechanical deflation caused contact loss between the cathode and the electrolyte during cycling and had severe negative effects on battery performance because no additional solid electrolytes can fill the emerging voids. As a result, the corresponding ASSLB showed poor rate performances and capacity retention capabilities at low current rates with no reversible capacity at 1 C and a continuous capacity loss of 1%–2% per cycle at 0.1 C.

3.2 Interfacial Engineering

Due to poor interfacial behaviors, many approaches have been proposed to improve interfacial stability and promote the practical application of ASSLBs. These methods mainly include cathode coating, electrolyte compositional tuning and other methods.

3.2.1 Cathode Coating

The introduction of protective coatings on cathodes is the most efficient method to achieve the practical application of ASSLBs [97]. As shown in Fig. 6, an electrochemically stable interfacial coating layer can serve as a bridge to mitigate lithium chemical potential differences

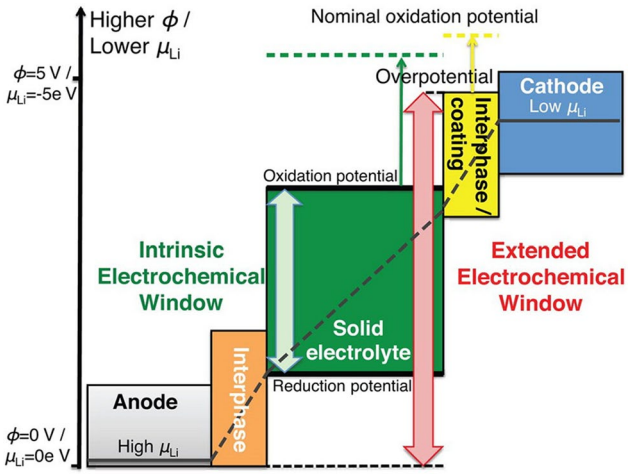

Fig. 6 Schematic diagram of an electrochemical window profile in an ASSLB. Reprinted with permission from Ref. [98]. Copyright 2015, American Chemical Society

between electrolytes and cathodes and significantly extend electrochemical windows and improve interfacial stability [98]. Based on the many types of materials used as effective coating layers (Table 4), ideal interfacial coating layers should possess several characteristics, including: (1) coating materials should be electronically insulating and possess similar lithium chemical potentials to oxide cathodes to efficiently shield sulfide electrolytes from high electrode potentials and reduce space charge layer effects; (2) ideal interfacial coating layers should possess wider electrochemical windows than sulfide electrolytes to prevent interfacial decomposition on cathodes [87]; (3) ideal interfacial coating layers need to possess excellent lithium ion conductivity because lithium ions have to migrate

Table 4 Summary of coating materials on oxide cathode surfaces in ASSLBs

Coating material	Cathode	Solid electrolyte	Reference
ZrO_2	$LiNi_{1/3}Mn_{1/3}Co_{1/3}O_2$	Li_3PS_4	[190]
Al_2O_3	$LiCoO_2$	$Li_{3.15}Ge_{0.15}P_{0.85}S_4$	[112]
SiO_2	$LiCoO_2$	$80Li_2S–20P_2S_5$	[105]
$LiNbO_3$	$LiNi_{0.8}Co_{0.15}Al_{0.05}O_2$	$Li_{10}GeP_2S_{12}$	[100]
$LiAlO_2$	$LiNi_{1/3}Mn_{1/3}Co_{1/3}O_2$	Li_3PS_4	[191]
$LiTaO_3$	$LiCoO_2$	$Li_{3.25}Ge_{0.25}P_{0.75}S_4$	[192]
$Li_4Ti_5O_{12}$	$LiNi_{0.8}Co_{0.15}Al_{0.05}O_2$	$70Li_2S–30P_2S_5$	[102]
Li_2SiO_3	$LiCoO_2$	$80Li_2S–20P_2S_5$	[105]
Li_3PO_4	$LiNi_{0.5}Mn_{1.5}O_4$	$80Li_2S–20P_2S_5$	[120]
Li_2CO_3	$LiCoO_2$	$78Li_2S–22P_2S_5$	[193]
$Li_2BO_3–Li_2CO_3$	$LiCoO_2$	Li_6PS_5Cl	[103]
$LiInO_2–LiI$	$LiNi_{0.8}Co_{0.15}Al_{0.05}O_2$	$75Li_2S–22P_2S_5–3Li_2SO_4$	[91]
$Li_2O–ZrO_2$	$LiNi_{0.8}Co_{0.15}Al_{0.05}O_2$	$80Li_2S–20P_2S_5$	[194]

through coating layers during battery cycling but also be selective toward other ions to suppress elemental diffusion; and finally, (4) because volume change (i.e., expansion and contraction) continuously occurs during battery cycling, coating materials should match with active material lattices and be mechanically plastic in response to active material deformation to maintain intimate contact between interfaces [99]. And according to these prerequisites for coating materials, various coating methods have been studied to improve battery performance in which ideal coating methods should be simple, nondestructive and cost-effective and corresponding ASSLB performances should be appreciably improved.

3.2.1.1 Liquid-Phase Method The liquid-phase method is the most common coating method due to associated low costs and simple procedures [91, 100, 101] in which two routes are most commonly adopted. In the first approach, a cathode is added into a precursor solution and a coating layer is obtained through co-precipitation or solution–evaporation. Although this approach is simple, economical and does not depend on expensive equipment, the thickness, homogeneity and morphology of resulting coating layers are difficult to control [90]. As for the second approach, precursor solution is sprayed onto a cathode material using a fluidized bed or through spray drying to obtain homogeneous coating layers with varying thicknesses [102]. This approach is more suitable for large-scale production processes. Based on these approaches, researchers have achieved a variety of coating layers, of which oxide-based $LiNbO_3$ is currently the most prevalent due to its excellent ionic conductivity (in the order of 10^{-5}–10^{-6} S cm^{-1}), low electronic conductivity (below 10^{-11} S cm^{-1}) [101, 103, 104], good lattice matching with oxide cathodes and wide electrochemical windows [87]. Zhang et al. [100] designed a novel double buffer layer strategy using the liquid-phase method (Fig. 7a) in which $LiNi_{0.8}Co_{0.15}Al_{0.05}O_2$ (NCA) was first designed as a core–shell structure through self-coating involving the coating of Ni-rich NCA with Al-rich NCA. Secondly, a thin $LiNbO_3$ layer was coated onto the core–shelled NCA (CS-NCA) through the solution–evaporation method by using metal lithium and $Nb(C_2H_5O)_5$ as precursors and ethanol as the solvent. Here, these researchers reported that the complete coating of the resulting CS-NCA with a thinner inactive $LiNbO_3$ layer was easier to achieve as compared with pristine NCA cathodes (Fig. 7b) and that after coating with the thin inactive $LiNbO_3$ buffer layer, space charge layers and interfacial reactions can be significantly suppressed in which CS-NCA@$LiNbO_3$ showed the lowest interfacial resistance (Fig. 7c). Spray coating can also be for $LiNbO_3$ coatings. For example, Takada et al. [84] investigated the effects of $LiNbO_3$ coating layers on the electrode properties of $LiMn_2O_4$ and $LiCoO_2$ cathodes through spray coating. Here, the thickness of the coating layers was controlled within 0–20 nm by altering the precursor solution amount as calculated from the specific gravity of $LiNbO_3$ and the BET surface area of the cathodes. As a result, these researchers found that $LiNbO_3$ coating layers can reduce electrode resistances by two orders of magnitude. In addition, these researchers found that the change trend in electrode resistance was similar for $LiMn_2O_4$ and $LiCoO_2$, suggesting that the space charge layer was the main cause for high interfacial resistance between high-voltage oxide cathodes and sulfide electrolytes because interfacial reactivity to sulfide electrolytes cannot be the same for $LiMn_2O_4$ and $LiCoO_2$ and that $LiNbO_3$ coating layers can effectively suppress space charge layers.

In addition to $LiNbO_3$, other coating materials have also been successfully applied through liquid-phase methods. For example, Kwak et al. [91] employed $LiInO_2–LiI$ as a novel coating layer in which LiI was added to improve the ionic conductivity of the coating layer and found the optimal coating amount to be 0.5 wt.% and that increases of

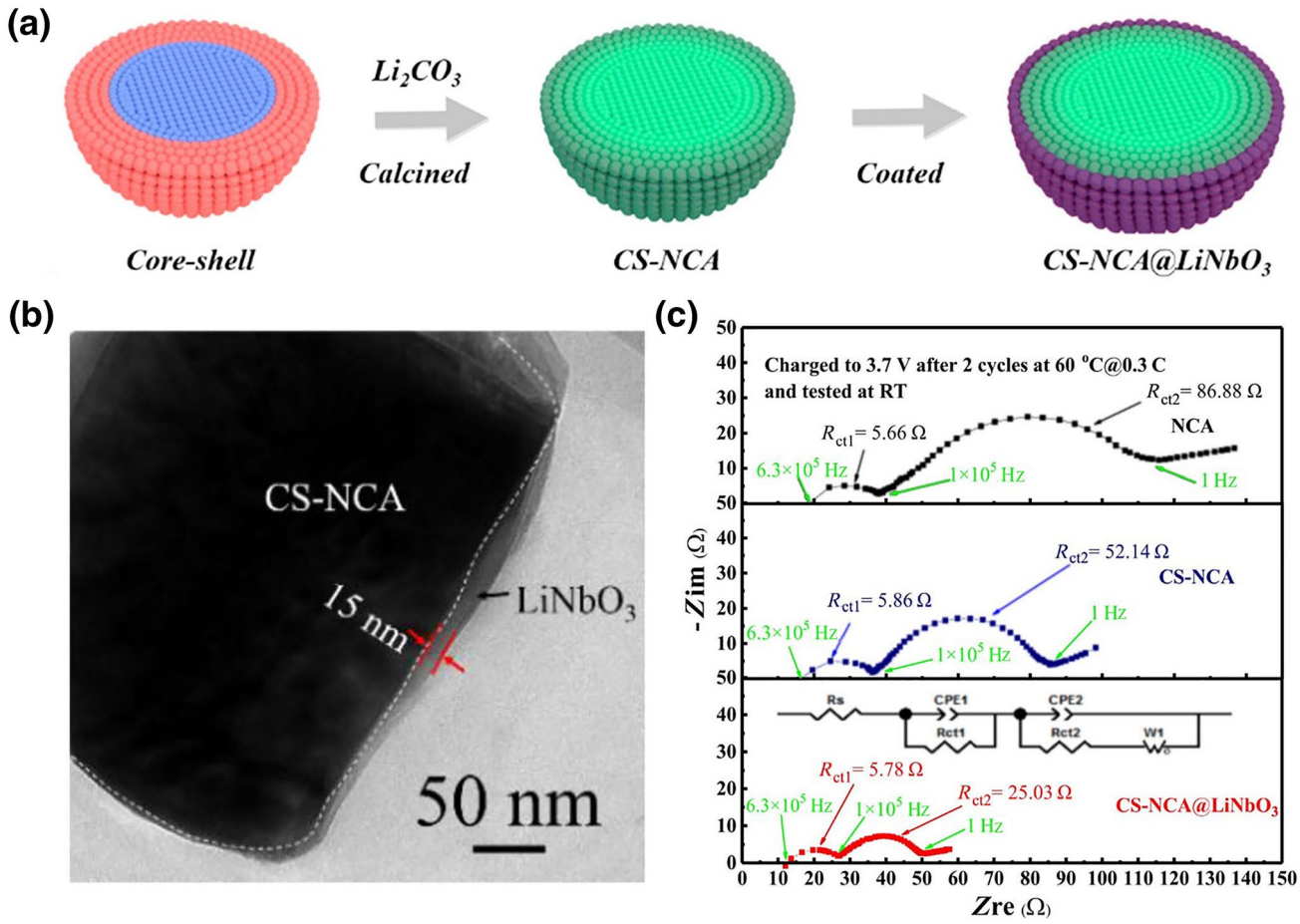

Fig. 7 **a** Schematic of the preparation process of CS-NCA@$LiNbO_3$. **b** HRTEM image of a CS-NCA@$LiNbO_3$ material. **c** Nyquist plots of charged ASSLBs by using NCA, CS-NCA and CS-NCA@$LiNbO_3$ cathodes after 2 cycles at 60 °C. EIS tests were conducted at room temperature. Reprinted with permission from Ref. [100]. Copyright 2018, Elsevier

coating amounts resulted in decreased capacity, implying that coating layers can introduce extra resistance if interlayers are too thick. Hayashi et al. [105] also investigated the electrochemical performance of $LiCoO_2$ coated with Li_2SiO_3 and SiO_2 and reported that batteries with Li_2SO_3-coated and SiO_2-coated $LiCoO_2$ showed higher discharge capacities as compared with batteries with uncoated $LiCoO_2$. Here, these researchers reported that the lithium ion conductive Li_2SiO_3 coating layer was more effective than inert SiO_2 in the improvement of battery performance and demonstrated that good ionic conduction was important in effective coating layers. These researchers further investigated interfacial behaviors using transmission electron microscopy and found that Co elemental diffusion from $LiCoO_2$ cathodes to Li_2S–P_2S_5 electrolytes can effectively be suppressed by means of Li_2SiO_3 coatings [90].

3.2.1.2 Atomic Layer Deposition (ALD) ALD is an attractive thin-film decomposition technique that can achieve atomic-scale coatings with excellent uniformity [106–109]. Different from traditional chemical vapor deposition, ALD is a self-limiting chemical reaction process that can achieve the thickness of about 0.1–0.2 nm for each ALD layer [110, 111] to allow for the precise control of coating layer thicknesses. To investigate the effects of ALD on ASSLB cycling stability, Lee et al. [112] conducted the ALD coating of ultrathin Al_2O_3 onto $LiCoO_2$ particle surfaces using trimethylaluminum and H_2O as precursors at a deposition temperature of 180 °C and reported that corresponding batteries using $LiCoO_2$ with 2–4 ALD Al_2O_3 layers exhibited improved capacity retention as compared with those using uncoated ones. Microstructural and elemental analyses also showed that the thickness of unfavorable interfacial layers can be reduced in coated $LiCoO_2$ as compared with uncoated $LiCoO_2$ (Fig. 8a, b), suggesting greatly suppressed interfacial reactions in coated $LiCoO_2$. As a result, the ALD Al_2O_3-coated $LiCoO_2$ in this study delivered superior cycling performances with 90% capacity retention within 25 cycles, whereas only 70% capacity retention was achieved for the uncoated $LiCoO_2$, indicating that the ALD Al_2O_3 film

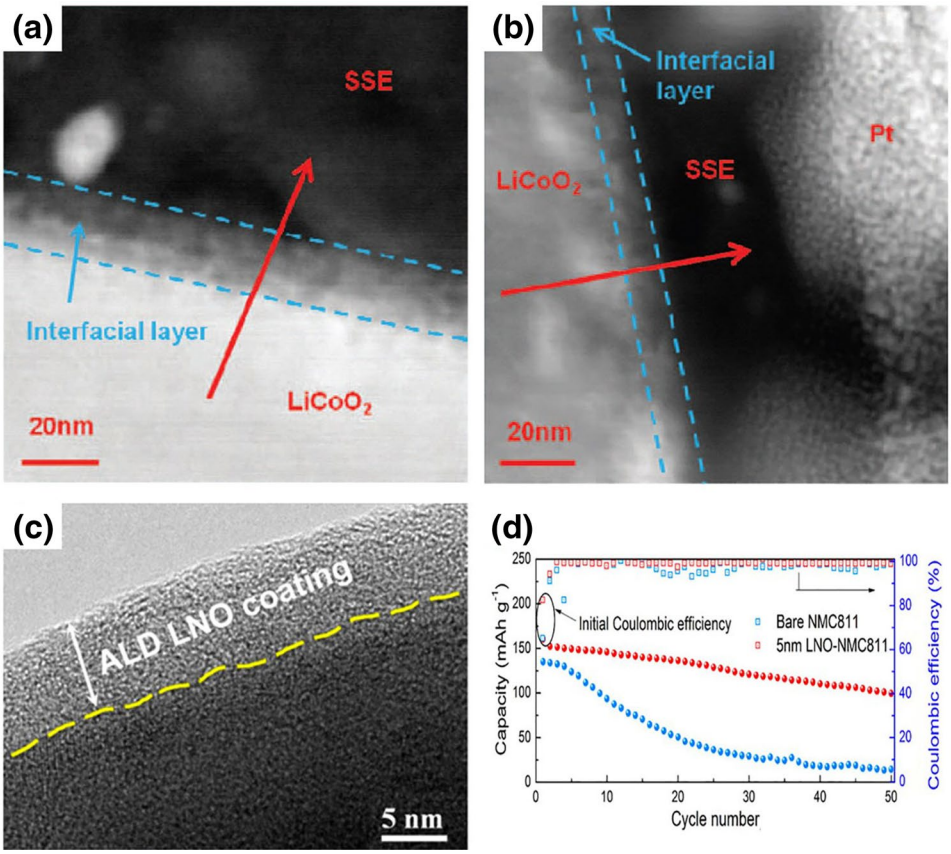

Fig. 8 **a** HAADF TEM image of an uncoated $LiCoO_2$/$Li_{3.15}Ge_{0.15}P_{0.85}S_4$ interface after the 33rd charge. **b** HAADF TEM image of an ALD Al_2O_3-coated $LiCoO_2$/$Li_{3.15}Ge_{0.15}P_{0.85}S_4$ interface after the 33rd charge. Reprinted with permission from Ref. [112]. Copyright 2012, The Electrochemical Society. **c** HRTEM image of an ALD $LiNbO_x$-coated $LiNi_{0.8}Co_{0.1}Mn_{0.1}O_2$. **d** Cycling performances of bare and $LiNbO_x$–$LiNi_{0.8}Co_{0.1}Mn_{0.1}O_2$ in an ASSLB. Reprinted with permission from Ref. [113]. Copyright 2019, American Chemical Society

was stable enough to inhibit Co dissolution and interfacial reactions. Despite these performances, the nonionic conductivity of metal oxides (e.g., Al_2O_3) can increase resistances and therefore, lithium-containing thin films should be more promising candidate materials due to their good ionic conductivity and excellent electrochemical stability. For example, Sun et al. [111] successfully achieved $LiNbO_x$ thin-film deposition with well-controlled thicknesses and composition through ALD at a deposition temperature of 235 °C using lithium tert-butoxide and niobium ethoxide as Li and Nb sources in which different thicknesses and composition were obtained by adjusting ALD cycle numbers and subcycle ratios of Li and Nb, respectively. A uniform and continuous $LiNbO_x$ thin film with an optimal lithium ion conductivity of 6×10^{-8} S cm^{-1} at room temperature can be obtained at a Li/Nb subcycle ratio of 1:4. In another example, Li et al. [113] developed an ALD $LiNbO_x$-coated $LiNi_{0.8}Mn_{0.1}Co_{0.1}O_2$ cathode to improve interfacial stability between $LiNi_{0.8}Mn_{0.1}Co_{0.1}O_2$ and $Li_{10}GeP_2S_{12}$ (Fig. 8c). These researchers also investigated the thickness effect of $LiNbO_x$ coating layers in which 2-, 5- and 10-nm-thick $LiNbO_x$ layers were deposited onto $LiNi_{0.8}Mn_{0.1}Co_{0.1}O_2$ surfaces. As a result, they found that 5-nm-thick $LiNbO_x$-coated $LiNi_{0.8}Mn_{0.1}Co_{0.1}O_2$ presented optimal electrochemical performances in terms of significantly improved cycling capacity and stability (Fig. 8d) because of a stabler interface and lower interfacial resistances. With the development of ALD techniques, many lithium-containing coating materials have also been successfully achieved, such as $Li_4Ti_5O_{12}$ [114], $LiSiO_x$ [115], $LiPO_x$ [116], $LiTaO_x$ [117], LiPON [118] and Li_3BO_3–Li_2CO_3 [119], all of which show promise as interfacial coating layers between cathodes and sulfide electrolytes because of their relatively high ionic conductivity and excellent electrochemical stability. Overall, the ALD technique can play an important role in addressing interfacial issues between oxide cathodes and sulfide electrolytes through well-controlled coatings.

3.2.1.3 Physical Vapor Deposition (PVD) and Chemical Vapor Deposition (CVD) Common PVD processes involve sputtering and evaporation in which pulsed laser deposition and magnetron sputtering are typical PVD techniques. Here, Tatsumisago et al. [120] extensively used the pulsed laser deposition method to mitigate interfacial impedance between cathodes and electrolytes. For example, they successfully deposited a 100-nm Li_3PO_4 thin film onto a 5 V class $LiNi_{0.5}Mn_{1.5}O_4$ cathode using pulsed laser deposition at room temperature (Fig. 9a) and reported that with an $80Li_2S$–$20P_2S_5$ solid electrolyte, the coating of Li_3PO_4 onto the $LiNi_{0.5}Mn_{1.5}O_4$ cathode allowed for operation in an

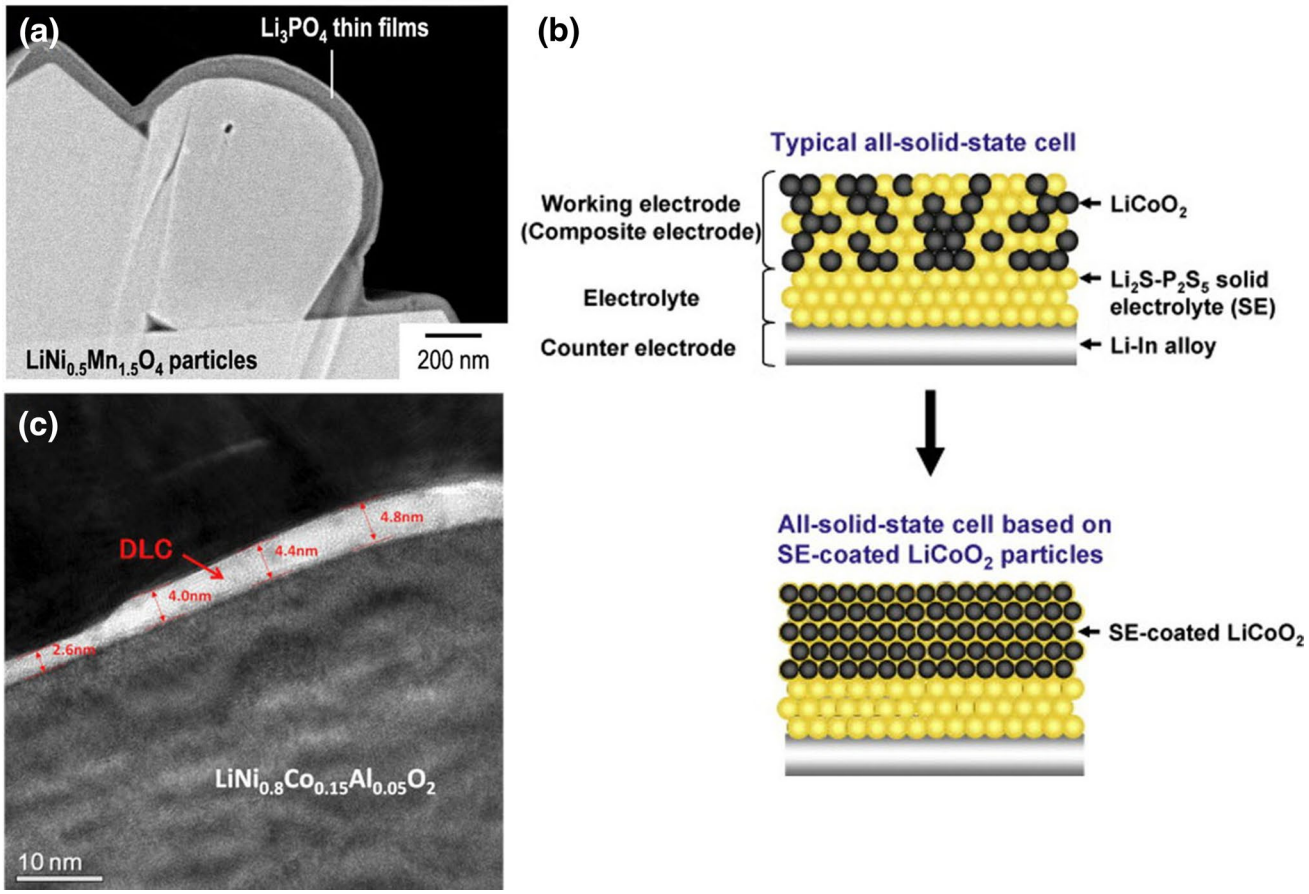

Fig. 9 **a** SEM image of pulsed laser deposition Li_3PO_4-coated $LiNi_{0.5}Mn_{1.5}O_4$ particles. Reprinted with permission from Ref. [120]. Copyright 2015, Elsevier. **b** Schematic of a typical ASSLB and an ASSLB based on sulfide electrolyte-coated $LiCoO_2$ particles. Reprinted with permission from Ref. [122]. Copyright 2010, Elsevier. **c** TEM image of CVD diamond-like carbon-coated $LiNi_{0.8}Co_{0.15}Al_{0.05}O_2$. Reprinted with permission from Ref. [126]. Copyright 2016, Elsevier

assembled ASSLB, whereas uncoated $LiNi_{0.5}Mn_{1.5}O_4$ could not achieve reversible cycling, indicating that the coating of Li_3PO_4 can significantly reduce interfacial impedance between cathodes and sulfide electrolytes. In addition, these researchers deposited the sulfide electrolyte onto an oxide cathode through the pulsed laser deposition method [121, 122] and achieved closer interfacial contact (Fig. 9b). The results indicated that a corresponding ASSLB using the sulfide electrolyte-coated $LiCoO_2$ delivered lower interfacial resistances and higher discharge capacities as compared with that using bare $LiCoO_2$.

Aside from pulsed laser deposition, magnetron sputtering is also an attractive physical coating method that can achieve uniform thin-film depositions on cathode surfaces through the sputtering of elemental (metallic) targets in inert gas (e.g., Ar) or inert/reactive mixture gas (e.g., Ar/O_2). This coating method has been applied successfully in organic liquid electrolyte-based lithium ion battery systems. For example, Zhou et al. [123] successfully coated $Li_4Ti_5O_{12}$ onto $LiCoO_2$ surfaces and reported significantly improved interfacial kinetics, cycling stability and rate performances for $Li_4Ti_5O_{12}$-coated $LiCoO_2$ as compared with bare $LiCoO_2$. Many other oxides can also be used as targets to coat cathodes to suppress interfacial reactions and improve cycling performances [124, 125]. Although the magnetron sputtering technique has yet to be widely used in ASSLB applications, it possesses significant application potential in the coating of proper interfacial materials onto oxide cathodes to improve interfacial compatibility between oxide cathodes and sulfide electrolytes.

CVD is another effective coating method that uses thermally induced chemical reactions on heated substrate surfaces. The difference between CVD and PVD is that PVD uses physical forces, whereas CVD uses chemical processes. Recently, CVD has also been applied in the coating of cathode materials to improve interfacial stability. Aihara et al. [126] used acetylene gas as a precursor and obtained a diamond-like carbon-coated (DLC) $LiNi_{0.8}Co_{0.15}Al_{0.05}O_2$ through CVD at a deposition temperature of 250 °C. Here, these researchers reported that the resulting diamond-like

carbon layer possessed a thickness of around 4 nm (Fig. 9c) as well as low electronic conductivity (unlike traditional graphitic carbon) and moderate ionic conductivity, which effectively hindered side reactions and provided an alternative method to improve the performance of ASSLBs by using nonmetal oxide materials.

3.2.2 Electrolyte Composition Tuning

Although cathode coatings can effectively improve interfacial stability, intrinsic tuning through electrolyte composition tuning to improve the inherent stability of solid electrolytes is also attractive. In general, electrolytes should possess high ionic conductivity, low electronic conductivity as well as close electrochemical potentials and low lattice mismatches with cathodes; however, perfect electrolytes remain unavailable. Here, the most commonly adopted strategy to improve electrolyte performance involves oxygen anion substitution due to inherently lower lattice mismatches with cathodes and the higher electrochemical stability of oxides. In addition, substitution of oxygen atoms for sulfur atoms in sulfide electrolytes can inhibit the diffusion of oxygen from oxide cathodes to sulfide electrolytes. For example, Kawamoto et al. [127] prepared a $7Li_2O–68Li_2S–25P_2S_5$ electrolyte through ball-milling and found that the resulting $7Li_2O–68Li_2S–25P_2S_5$ electrolyte can effectively inhibit elemental diffusion and side reactions to reduce interfacial resistance growth and capacity fading as compared with ASSLBs using a $75Li_2S–25P_2S_5$ electrolyte.

In addition to binary and ternary sulfide electrolytes, argyrodite Li_6PS_5X electrolytes have also been widely studied to improve interfacial stability with oxide cathodes. For example, Shao et al. [128] investigated the electrochemical stability of hali-chalcogenide Li_6PA_5Cl argyrodites involving a system of materials including pristine Li_6PS_5Cl, partial oxygen-substituted Li_6PO_4SCl and full oxygen-substituted Li_6PO_5Cl as formulated through extensive theoretical simulations. Here, results based on these theoretical calculations indicated that the Li_6PO_4SCl electrolyte possessed a wide electrochemical window from 0 to 2.62 V and the Li_6PO_5Cl electrolyte possessed a wider electrochemical window from 0 to 3.49 V, and that the electrochemical window of the Li_6PS_5Cl electrolyte was narrow, only being 0.49 V (1.7–2.19 V), indicating that the replacement of S by O can significantly improve the electrochemical stability window of argyrodite sulfides and suppress interfacial reactions under high cathode potentials. Zhang et al. [129] also studied an oxygen-substituted Li_6PS_5Br solid electrolyte $Li_6PS_{4.7}O_{0.3}Br$ and reported that an ASSLB using the $Li_6PS_{4.7}O_{0.3}Br$ as an electrolyte and NCM811 as a cathode achieved discharge capacities of 108.7 mAh g^{-1} at 0.1 C and 47.4 mAh g^{-1} at 0.8 C, which presented higher electrochemical performances as compared with an ASSLB using Li_6PS_5Br as the electrolyte. Here, the enhanced cycle and rate performances of the $Li_6PS_{4.7}O_{0.3}Br$-based ASSLB were attributed to the inhibition of space charge layer effects and interfacial reactions.

Clearly, compositional tuning is essential in the improvement of the intrinsic interfacial stability of sulfide electrolytes. Oxygen substitution, as the most prevalent modification method, can significantly improve the compatibility of oxide cathodes/sulfide-based solid electrolytes. However, mechanisms concerning how these substitutions can improve interfacial stability remain unclear and significant research is required to elucidate impact mechanisms and promote the development of novel electrolytes.

3.2.3 Others

Overall, cathode coating and electrolyte compositional tuning are two of the most promising approaches to improve interfacial stability. In addition to these two major methods, other methods have also been extensively employed to improve interfacial performance. As one method, the nano-crystallization of cathodes or electrolytes can increase contact areas between cathodes and electrolyte particles to reduce interfacial impedance. For example, Peng et al. [130] systematically investigated the fundamental lithium storage behaviors of $LiNi_{0.8}Co_{0.15}Al_{0.05}O_2$ in ASSLBs. They found that particle sizes can be decreased and surface impurities (e.g., Li_2CO_3) can be removed through ball-milling and that surface defects as caused by ball-milling such as cracks and pores can be eliminated through post-annealing. The decrease in particle size caused by ball-milling can increase the contact area between cathodes and sulfide electrolytes, and the interfacial impedances can be further reduced through post-annealing. Here, these researchers reported that their resulting $LiNi_{0.8}Co_{0.15}Al_{0.05}O_2$ in a $LiNi_{0.8}Co_{0.15}Al_{0.05}O_2/Li_{10}GeP_2S_{12}$/Li-In all-solid-state battery delivered an enhanced discharge capacity of 146 mAh g^{-1} at room temperature. To obtain uniform and continuous electrode–electrolyte interfaces, composite electrodes can also generally be prepared through the mixing of electrode active materials, sulfide electrolytes and conduction additives. For example, Navarro et al. [131] studied the electrochemical performance of a $LiNi_{1/3}Co_{1/3}Mn_{1/3}O_2$ composite cathode using a $Li_7P_3S_{11}$ solid electrolyte prepared through the liquid-phase method and ball-milling in which particle sizes of about 500 nm can be obtained through the liquid-phase process, whereas particle sizes larger than 10 μm can be obtained through ball-milling. As a result, the composite cathode composed of $LiNi_{1/3}Co_{1/3}Mn_{1/3}O_2$ and small-sized $Li_7P_3S_{11}$ prepared through the liquid-phase method exhibited excellent electrochemical performances (Fig. 10a). It is difficult to achieve uniform and continuous

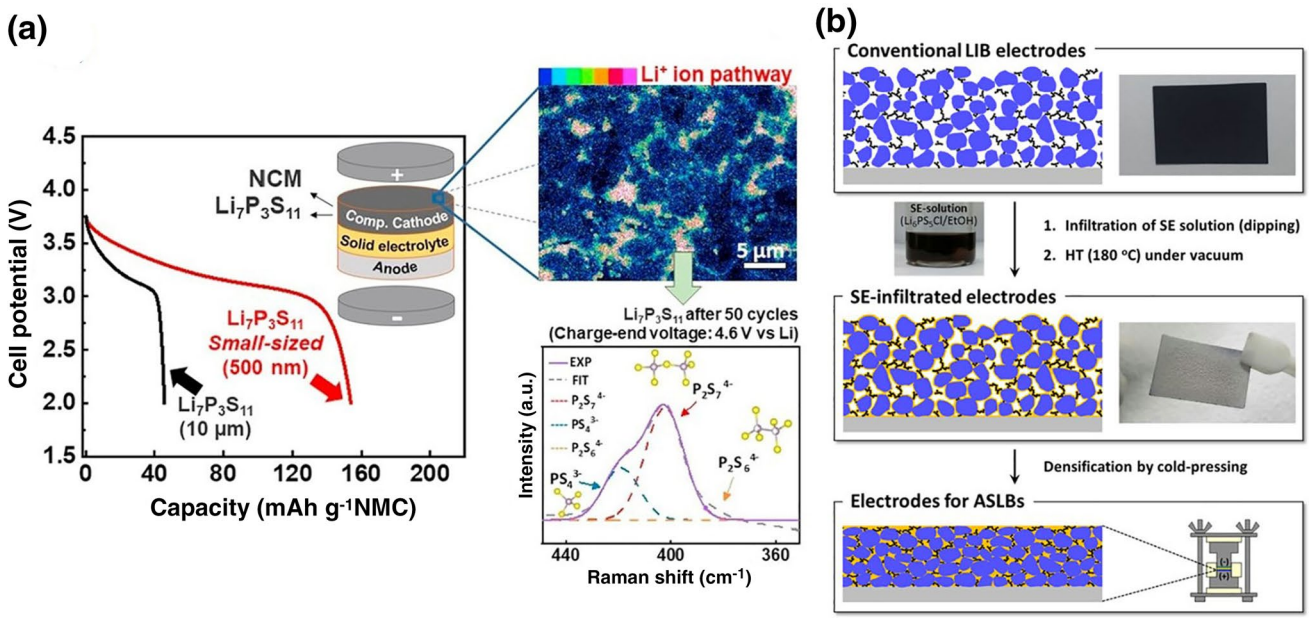

Fig. 10 **a** Initial discharge curves of an ASSLB using $LiNi_{1/3}Co_{1/3}Mn_{1/3}O_2$ as the active material and different particle sizes of $Li_7P_3S_{11}$ as ionic conductors in the composite cathode. Reprinted with permission from Ref. [131]. Copyright 2018, Elsevier. **b** Schematic illustrating the filtration of cathodes with solution-processable Li_6PS_5Cl. Reprinted with permission from Ref. [132]. Copyright 2017, American Chemical Society

interfaces in traditional composite cathodes prepared through mechanical dry-mixing with solid electrolyte particles. To address this issue (Fig. 10b), Jung et al. [132] infiltrated a Li_6PS_5Cl solution in ethanol into a cathode using a dip-coating method followed by the subsequent removal of the solvent and heat treatment at 180 °C under vacuum to obtain a densified composite cathode with very low porosity through cold pressing. Similarly, Tatsumisago et al. [133] and Navarro et al. [134] prepared composite cathodes through infiltration with sulfide electrolyte solutions to construct favorable electrode–electrolyte interfaces.

4 Sulfide Electrolyte/Anode Interfaces

4.1 Lithium Metal Anodes

Lithium metal is considered to be the most promising candidate for anodes in lithium batteries to meet the increasing energy demands of the modern world because of its extremely high theoretical specific capacity (3860 mAh g^{-1}) and low redox potential (−3.040 V vs. SHE). However, undesirable lithium dendrite growth and low Coulombic efficiency during repeated lithium plating and stripping hamper widespread application [135, 136].

Conventionally, solid electrolytes with high lithium ion transference numbers, mechanical strength and high chemical–electrochemical stability are expected to suppress Li dendrite growth and side reactions at Li/electrolyte interfaces. However, recent research has revealed that lithium dendrites can easily form in the grain boundaries of inorganic electrolytes [137]. In addition, ternary sulfide electrolytes such as $Li_{10}GeP_2S_{12}$ can show severe thermodynamic and dynamic instability against metallic lithium. Moreover, the huge volume change of lithium anodes during lithium ion deposition/dissolution can lead to virtually infinite volume expansion, which further deteriorates interfacial stability. As a consequence, the large-scale commercialization of high-energy density and safe ASSLBs by using sulfide electrolytes remains challenging.

4.1.1 Interfacial Reactions

Theoretical simulations have revealed that only a few solid electrolytes are thermodynamically stable in contact with lithium due to its strong reducing ability [92]. In terms of solid electrolyte/electrode interfaces, a simplified view of the molecular orbital theory structure is schematically shown in Fig. 11a, b. In the case of the stable interface (Fig. 11a), the lowest unoccupied molar orbital (LUMO) energy of a solid electrolyte should be higher than that of the highest occupied molar orbital (HOMO) of Li (or the Fermi level of Li) to prevent the transfer of electrons from the Fermi level of Li to the conduction band of the solid electrolyte. In the case of the instable interface (Fig. 11b), the Fermi level (HOMO) of Li is higher than that of the conduction band (LUMO) of

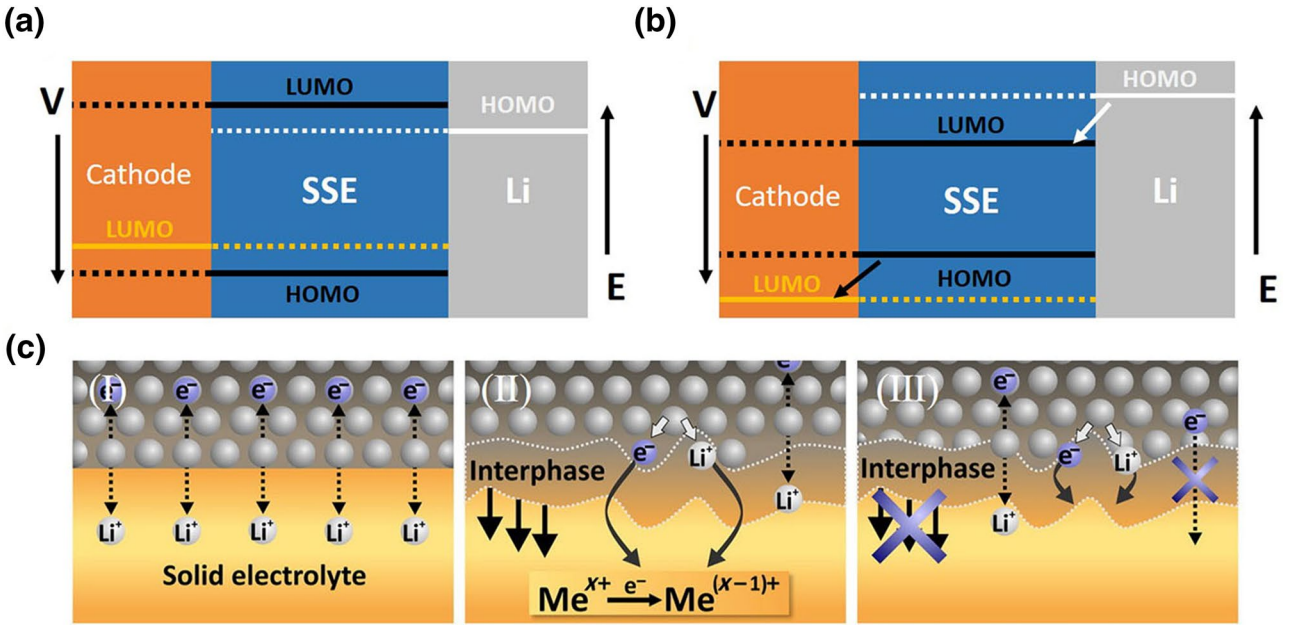

Fig. 11 Band structures for **a** stable and **b** unstable sulfide solid electrolyte/electrode interfaces. **c** Types of interphases between Li metal and the solid electrolyte. Reprinted with permission from Ref. [138]. Copyright 2015, Elsevier

a solid electrolyte, and electrons can transfer from lithium metal to the solid electrolyte to result in inevitable interfacial reactions. Likewise, the LUMO energy of cathodes should be higher than that HOMO of sulfide electrolytes so that electron transfer from the valence band of solid electrolytes to the Fermi level of cathodes can be prevented, allowing sulfide electrolytes to be thermodynamically stable with cathodes in which cathodes reacting with solid-state electrolytes can lead to altered conduction properties and the consumption of active materials (i.e., capacity loss).

Considering this interfacial behavior and interphase formation on solid electrolytes, Wenzel et al. [138] defined three types of interfaces based on thermodynamics (Fig. 11c), including: (1) interfaces that are thermodynamically stable against lithium in which no reactions occur at the interface; (2) interfaces that are thermodynamically unstable against lithium at which mixed conducting interphases with reasonably high ionic and electronic conductivities can form, resulting in high electronic conductivity interphases that cannot bridge the high chemical potential of lithium and leading to the continued reduction of inner fresh solid electrolytes [92]; and (3) interfaces that are thermodynamically unstable against lithium but with interphases that are kinetically stable against Li.

As for binary sulfide electrolytes with glass or glass–ceramic structures, P_2S_5, B_2S_3 or SiS_2 anions can form matrixes and Li_2S can provide lithium ion conduction. Here, increasing the Li_2S content can increase ionic conductivity due to increased mobile-ion concentrations; however, crystal structure stability also decreases. And due to the smaller electronic conductivity of interphases, binary sulfide electrolytes generally show thermodynamic instability but dynamic stability against lithium metal anodes. For example, the reaction between $Li_7P_3S_{11}$ and Li^0 is $Li_7P_3S_{11} + 24\ Li \rightarrow Li_2S + 3Li_3P$ [139], which is similar to other reactants such as Li_3PS_4 [140].

For ternary systems, Wenzel et al. [139, 141] found that strong increases in the overall impedance of a Li/$Li_{10}GeP_2S_{12}$/Li cell as well as the solid electrolyte interphase layer can be observed as compared with a Li_2S–P_2S_5 system in which operando XPS data showed that the content of Li_3P, Li_2S and Ge^0 interphases increased with lithium deposition time. For binary sulfide electrolytes such as $Li_7P_3S_{11}$ however, increases in Li_3P and Li_2S interphases resulted in an obvious decelerating trend, meaning that the interfacial decomposition of $Li_{10}GeP_2S_{12}$ can result in the deterioration of charge–transfer kinetics and the rapid increase of cell resistances in which the possible decomposition reaction can be expressed as: $Li_{10}GeP_2S_{12} + 20Li \rightarrow 12Li_2S + 2Li_3P + Ge$. Camacho-Forero et al. [142] also summarized the anion decomposition process of sulfide electrolytes through density functional theory optimizations and ab initio molecular dynamics (AIMD) simulations. As shown in Fig. 12, the PS_4^{3-} of $Li_{10}GeP_2S_{12}$, Li_3PS_4 and $Li_7P_3S_{11}$ decomposes sequentially through the breaking of each P–S bond. In most cases, final decomposition species involve S, P and some PS_x species remaining stable for long periods of

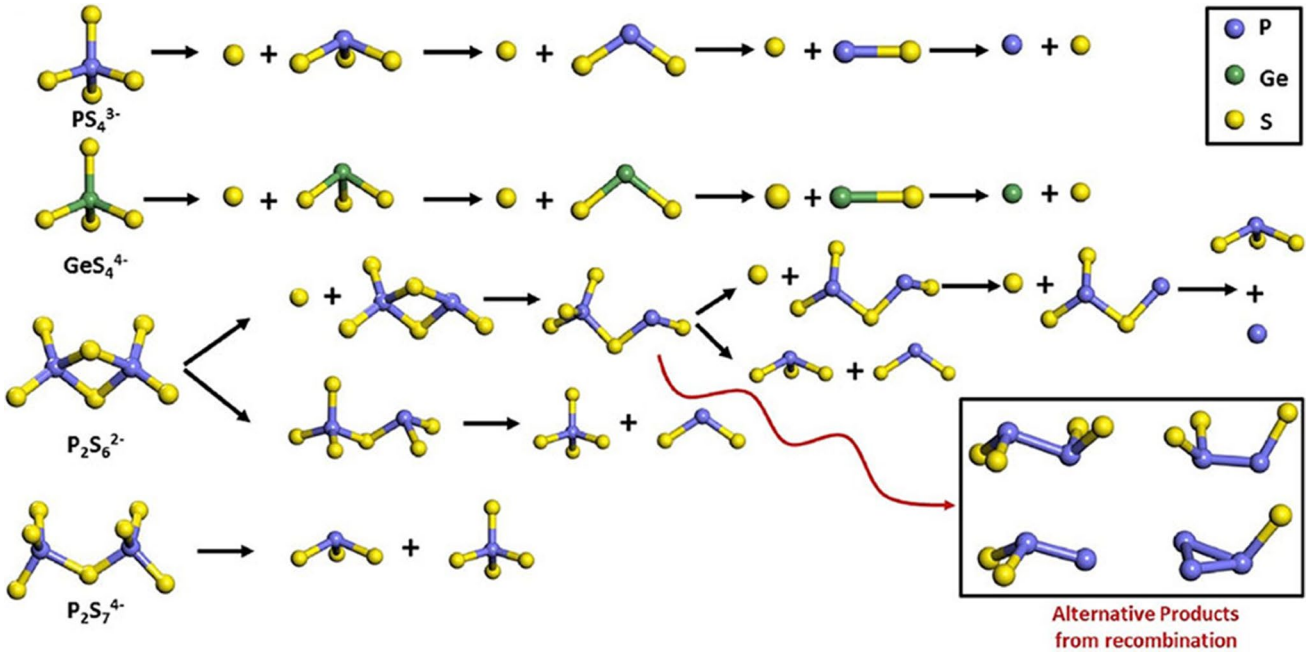

Fig. 12 Anion decomposition mechanism based on density functional theory optimization and AIMD simulation. Reprinted with permission from Ref. [142]. Copyright 2018, Elsevier

time. These researchers also reported that the GeS_4 group from $Li_{10}GeP_2S_{12}$ decomposed similarly to PS_4 anions and that P_2S_7 anions (from $Li_7P_3S_{11}$) reduced to PS_3 and PS_4, which can further break down to S and P. Overall, this study provided new insights into the time evolution and transient phenomena of interfacial structures, allowing for the identification of major interfacial products through theoretical calculation. Ong et al. [33] further reported that the replacement of Ge with cheaper Si or Sn still possessed limited influences on phase stability and electrochemical stability in $Li_{10\pm1}MP_2X_{12}$ (M = Ge, Si, Sn, Al or P, and X = O, S or Se). Bron et al. [143] tested the time-dependent parallel resistance R_{par} of $Li_{10}GeP_2S_{12}$, $Li_{10}SiP_2S_{12}$, $Li_{10}SnP_2S_{12}$ and $95(0.8Li_2S{\cdot}0.2P_2S_5){\cdot}5LiI$ as well as the corresponding time-dependent ionic resistance R_{ion} to find that the parallel resistance and ionic resistance of $Li_{10}GeP_2S_{12}$, $Li_{10}SiP_2S_{12}$ and $Li_{10}SnP_2S_{12}$ samples increased with contact time, reflecting continuous chemical reactions between lithium metal and sulfide electrolytes, whereas a stable solid electrolyte interphase formed at the interface between $95(0.8Li_2S{\cdot}0.2P_2S_5){\cdot}5LiI$ and lithium metal. As for argyrodite-type solid electrolytes, Wenzel et al. [144] reported that all three compounds including Li_6PS_5Cl, Li_6PS_5Br and Li_6PS_5I decomposed in contact with lithium and that growing interphases can lead to increased interfacial resistances, but that Li_6PS_5Cl was the stablest solid electrolyte against lithium because of its slower increasing resistance trend. In situ XPS data further showed that the main interphases of Li_6PS_5Cl/Li were Li_3P, Li_2S and Li, but that LiCl can inevitably be generated based on stoichiometry in which a possible decomposition reaction is: $Li_6PS_5X + 8Li \rightarrow 5Li_2S + Li_3P + LiX$.

4.1.2 Strategies to Inhibit Interfacial Reactions

Various approaches have been proposed to alleviate interfacial reaction issues and mainly include the design of electrolyte components and the construction of artificial protective layers.

4.1.2.1 Electrolyte Component Optimizations Although Li_3PS_4 can exhibit better stability against lithium reduction than other sulfide electrolytes with higher valence ions, interfacial reactions still exist, which can lead to large interfacial impedances in corresponding ASSLBs during charge–discharge processes. Here, theoretical calculations and experimental results have shown that oxygen doping can improve interfacial stability in which the stabilization of crystal phases and the improvement of ionic conductivities have been widely demonstrated. In addition, simulations of sulfide electrolyte/lithium interfaces indicated that oxygen doping can prevent interfacial reactions and avoid the formation of Li_2S-like buffer layers [145]. Furthermore, the replacement of P^{5+} with large radius ions can improve chemical stability in addition to enhancing ionic conductivity. For example, Xie et al.

[146] recently prepared a $Li_3P_{0.98}Sb_{0.02}S_{3.95}O_{0.05}$ electrolyte through the simultaneous introduction of Sb^{5+} and O^{2+} into a Li_3PS_4 structure in which structural characterizations showed that Sb and O can partially occupy P and S sites with no new phases observed, resulting in a higher ionic conductivity of 1.08 mS cm^{-1} at room temperature and excellent stability against lithium through this dual doping method. Similarly, Liu et al. [147] successfully synthesized $Li_{3.06}P_{0.98}Zn_{0.02}S_{3.98}O_{0.02}$ through the aliovalent substitution of 2 mol% ZnO in which P^{5+} and S^{2-} were partially substituted by Zn^{2+} and O^{2-} separately and reported a wider electrochemical window and better stability against lithium metal.

Theoretical calculations also indicate that the $Li_{10}GeP_2S_{12}$ ternary electrolyte is in a metastable phase that is not stable against lithium reduction at low voltages or lithium extraction with self-decomposition at high voltages [148]. Here, Sun et al. [149] suggested that oxygen doping can effectively suppress lithium anode reduction in ternary systems and Hu et al. [150] reported that both Coulombic interactions and Van der Waals forces can contribute to the structural stability of $Li_{10}GeP_2S_{12}$ in which if lithium ions were partially substituted by other divalent or trivalent cations, interactions between S^{2-} and di/trivalent cations can be enhanced, allowing for the reduction of $Li_{10}GeP_2S_{12}$ total energy and enhanced structural stability. Sun et al. [151] also partially substituted Li^+ by divalent Ba^{2+} cations to improve the structural stability of $Li_{10}GeP_2S_{12}$ and reported that due to stable interactions between Ba^{2+} and S^{2-}, an optimized composition of $Li_{9.4}Ba_{0.3}GeP_2S_{12}$ exhibited lower polarization and better stability against lithium reduction.

Oxygen doping is also applicable for argyrodite electrolytes. Different from other sulfide electrolytes, oxygen atoms in argyrodite electrolytes prefer to substitute S atoms at free S^{2-} sites rather than those at PS_4 tetrahedral sites. For example, Zhang et al. [129] systematically investigated the electrochemical properties of $Li_6PS_{5-x}O_xBr$ ($0 \leqslant x \leqslant 1$) solid electrolytes to study the effects of oxygen doping and found that without deteriorating ionic conductivities, an O-doped electrolyte can exhibit much better stability against lithium as compared with its undoped counterparts, the corresponding ASSLB using this electrolyte exhibited higher capacity and better cycling performance than that with oxygen free electrolyte. What′s more, using lithium metal as the anode, a $LiNi_{0.8}Co_{0.1}Mn_{0.1}O_2$ cathode achieved stable cycling for 92 cycles, whereas that with undoped electrolyte failed after only two cycles.

4.1.2.2 Construction of Artificial Protective Layers The addition of artificial protective layers has been extensively studied, and due to the severe instability of ternary sulfide electrolytes/Li interfaces, recent studies have mainly focused on the modification of $Li_{10\pm1}MP_2S_{12}$ (M = Ge, Si, Sn). For example, Zhang et al. [152] prepared a manipulated LiH_2PO_4 protective layer on the surface of lithium foil to circumvent the intrinsic chemical instability issues of $Li_{10}GeP_2S_{12}$ to lithium metal through the reaction of H_3PO_4 with lithium metal (Fig. 13a). As a result, their Li/Li symmetric cell showed that the LiH_2PO_4 protective layer can play a positive role in the stabilization of the $Li_{10}GeP_2S_{12}$/Li interface and enhance the stability of $Li_{10}GeP_2S_{12}$ to lithium metal. Lithium deficiency at sulfide electrolytes/Li interfaces as caused by interfacial reactions has also been proposed as a major cause of interfacial resistance; however, it is difficult to non-invasively observe lithium distribution in solid electrolytes by using traditional probing methods. To address this, Chien et al. [153] employed ^7Li magnetic resonance imaging to observe lithium distribution during electrochemical cycling and found that significant lithium loss occurred at the electrode/electrolyte interface upon electrochemical cycling. To address this issue, these researchers used a PEO-LiTFSI polymer electrolyte film to improve $Li_{10}GeP_2S_{12}$/Li interfacial stability in which results showed significant improvements in lithium distribution homogeneity as well as enhanced cycling stability in a corresponding ASSLB (Fig. 13b). Inspired by high ionic conductivity and good thermal stability in lithium ion batteries, succinonitrile-based plastic crystal electrolytes have also been adopted as buffer layers to address the instability of sulfide electrolytes to lithium metal. For example, Wang et al. [154] used a solid-state plastic crystal electrolyte to address interfacial issues between sulfide electrolytes and lithium metal and achieved significant progress toward high-energy density ASSLBs (Fig. 13c). Here, these researchers reported that if lithium metal was in direct contact with sulfide electrolytes, the sulfide electrolyte can easily reduce to form a high-resistance interphase that hindered lithium ion migration at the interface, whereas the coating of a layer of the plastic crystal electrolyte as an intermediate layer at the interface between lithium metal and the sulfide electrolyte can greatly suppress interfacial reactions between the sulfide electrolyte and lithium metal. As a result, a corresponding ASSLB with a $LiFePO_4$ cathode delivered an enhanced initial capacity of 148 mAh g^{-1} at 0.1 C and 131 mAh g^{-1} at 0.5 C. These researchers also reported that the chemical compatibility between the sulfide electrolyte and the plastic crystal electrolyte ensured the long-term cycling stability of the ASSLB. Gao et al. [155] further dripped a highly concentrated liquid electrolyte into a $Li_{10}GeP_2S_{12}$/Li interface and found that nanocomposites derived from commercial organic or inorganic lithium salts can act as interphases and that these composite interphases not only possessed high ionic conductivity but also cleanly separated lithium and $Li_{10}GeP_2S_{12}$ to result in stable interfaces. Overall, these promising results indicate that the rational design of buffer layer composition and structure to enhance interfacial compatibility between lithium and sulfide electrolytes is important.

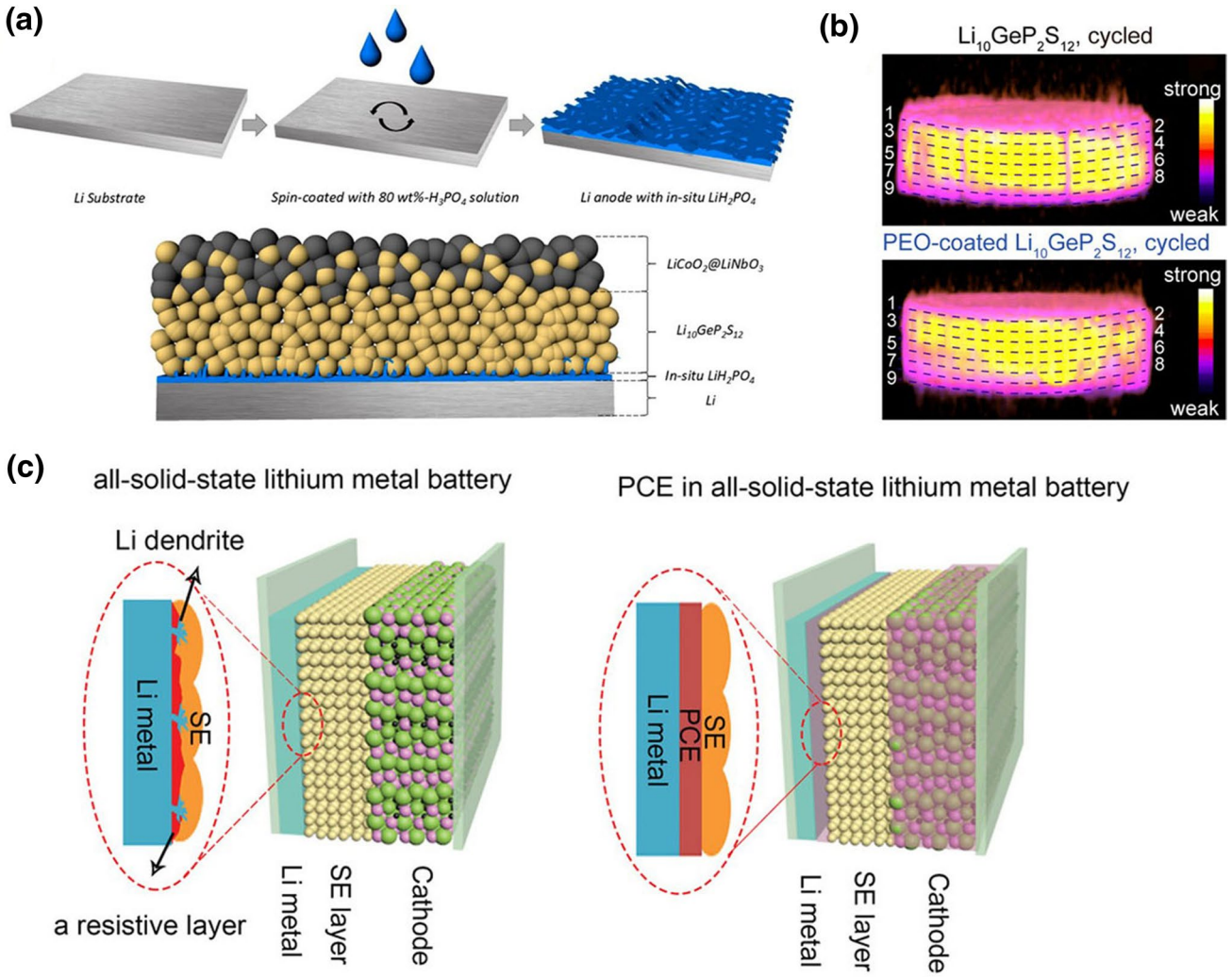

Fig. 13 **a** Schematic of the preparation of an in situ LiH_2PO_4 protective layer and a $LiCoO_2/Li_{10}GeP_2S_{12}/LiH_2PO_4$-Li ASSLB with an optimized structure. Reprinted with permission from Ref. [152]. Copyright 2018, American Chemical Society. **b** Lithium density profiles at different depths of electrochemically cycled $Li_{10}GeP_2S_{12}$ pellets. Reprinted with permission from Ref. [153]. Copyright 2018, American Chemical Society. **c** Schematic of ASSLBs with plastic crystal electrolyte interlayers. Reprinted with permission from Ref. [154]. Copyright 2019, Wiley–VCH

To take advantage of individual components, inorganic–organic composite electrolytes have also been frequently adopted to improve rigid interfacial issues and compatibility with lithium metal. For example, Ju et al. [156] fabricated a poly(vinyl carbonate) and $Li_{10}SnP_2S_{12}$ composite electrolyte (PVCA–LSnPS) through in situ polymerization and reported that the resulting PVCA–LSnPS composite possessed an indispensable combination of high ionic conductivity, wide electrochemical windows and large lithium ion transference numbers. More importantly, this composite electrolyte possessed good compatibility with lithium metal as engineered through in situ polymerization, leading to significant interfacial impedance reductions in corresponding solid-state Li–Li symmetric cells.

4.1.3 Lithium Dendrites

According to Li dendrite growth mechanisms in organic liquid electrolyte/polymer electrolyte batteries, researchers have generally proposed that the growth of dendrites can be physically limited by high shear modulus solid electrolytes ($G_{\text{solid electrolyte}} > 1.8G_{\text{Li}}$) [157]. However, recent research has shown that lithium dendrites are also found in ASSLBs using sulfide electrolytes, presenting a challenge in the application of lithium anodes in which lithium dendrites in ASSLBs are believed to be associated with the inherent physical defects of sulfide electrolytes or corresponding deterioration during cell cycling.

In general, lithium dendrite formation tends to occur under several situations, including: (1) along the grain

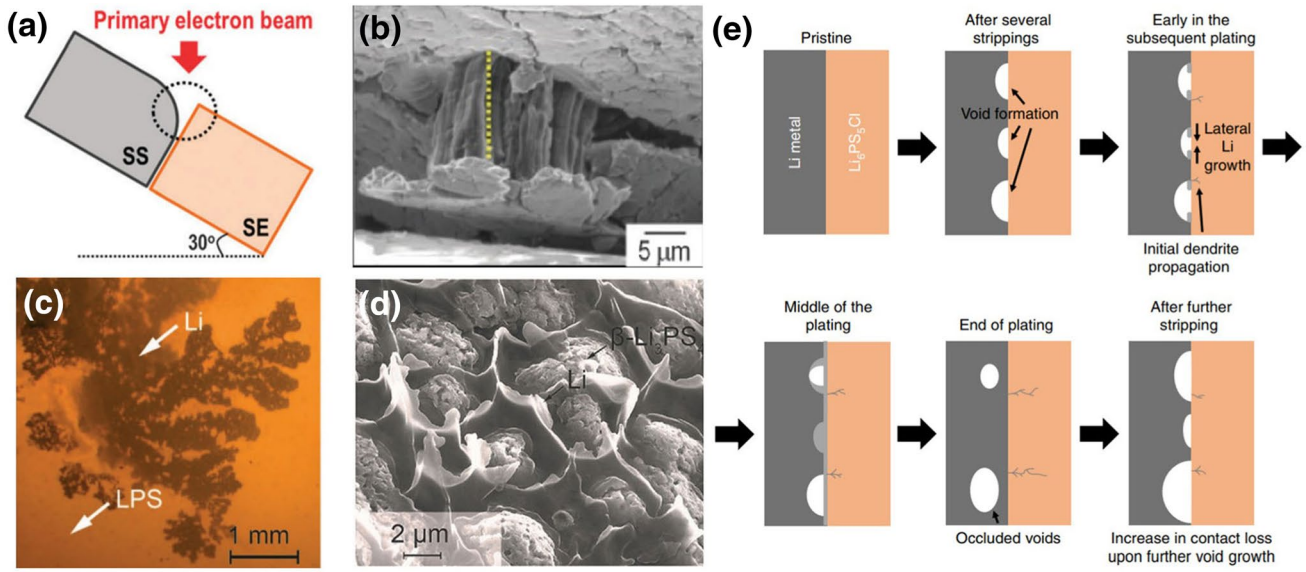

Fig. 14 **a** Cell schematic for in situ SEM observation and **b** lithium deposition at 5 mA cm^{-2} for 10 min after short circuiting. Reprinted with permission from Ref. [158]. Copyright 2013, The Royal Society of Chemistry. **c** Transmission optical microscopy and **d** fracture surface SEM images of a lithium metal network in a solid-state electrolyte. Reprinted with permission from Ref. [161]. Copyright 2017, Wiley–VCH. **e** Schematic of a Li/Li_6PS_5Cl interface cycled at an overall current density above critical current density. Reprinted with permission from Ref. [163]. Copyright 2019, Nature Publishing Group

boundary and voids of solid electrolytes in which low lithium ion diffusivity at grain boundaries was reported to be the intrinsic reason for dendrite formation along grain boundaries [158]; (2) pre-existing defects in the surface of or inside solid electrolytes, such as cracks, in which generated stress can further extend cracks and further promote lithium dendrite propagation [159]; (3) inhomogeneous lithium plating due to insufficient interfacial contact between lithium and sulfide electrolytes [160]; and (4) high electronic conductivity solid electrolytes that will accelerate dendrite formation and growth.

In one example, Nagao et al. [158] investigated lithium deposition/dissolution in an ASSLB with an $80Li_2S{\cdot}20P_2S_5$ electrolyte through in situ SEM using a stainless steel current collector with chamfered corners in which to observe the interface between the electrolyte and the electrode, SEM observations were carried out with a stage tilt at an angle of 30° (Fig. 14a). As a result, these researchers found that current density played a crucial role in deposition behavior in which at currents above 1 mA cm^{-2}, lithium deposited locally and triggered large cracks in the solid electrolyte that led to the short circuiting of the cell. In addition, these researchers reported that deposited lithium can push the solid electrolyte out to form pillared deposits 6.6 μm in length at the interface between the electrolyte and the electrode after short circuiting (Fig. 14b), whereas at current densities lower than 0.05 mA cm^{-2}, lithium metal deposited uniformly on the solid electrolyte surface and no cracks or pillared deposits formed, suggesting that the homogeneous deposition of lithium and the suppression of lithium growth along grain boundaries were important to achieve highly reversible lithium deposition and dissolution. These researchers also reported that the softening of amorphous electrolytes followed by pressurization can allow for solid electrolytes with fewer grain boundaries and pores, which is beneficial to the inhibition of dendrite growth.

Chiang et al. [161] further developed a new method to monitor lithium penetration in different types of solid electrolytes during lithium electrodeposition and found that the onset of lithium dendrite formation depended on the roughness of the solid electrolyte surface, particularly the size and density of defects. More importantly, these researchers found based on typical transmission optical microscopy and fracture surface SEM imaging that above a critical current density, lithium plating in surface cracks can produce crack-tip stress that can further drive crack propagation and extend to complex networks (Fig. 14c, d), meaning that the failure mechanism for brittle electrolytes is Griffith-like and that the suppression of lithium dendrite formation in solid-state electrolytes requires scrupulous attention to the minimization of interfacial defects.

Recently, Han et al. [162] also investigated the origins of dendrite formation in solid electrolytes by monitoring the dynamic evolution of lithium concentration profiles in different solid electrolytes during lithium electrodeposition. They found that lithium metal can directly deposit inside $Li_7La_3Zr_2O_{12}$ and Li_3PS_4 solid-state electrolytes, whereas no dendrites were found in LiPON, suggesting that high

electronic conductivity was most likely responsible for dendrite formation in solid electrolytes. Because of this, electronic conductivity is considered to be another critical criterion in the evaluation of solid-state electrolytes. In another study, Kasemchainan et al. [163] investigated the process of lithium plating/stripping at a Li/Li_6PS_5Cl interface and suggested that critical current density for stripping was the crucial factor affecting dendrite growth in which if stripping current removed lithium faster than what can be supplied, voids would form at the interface, leading to preferential lithium deposition in subsequent lithium plating and the formation of lithium dendrites near these voids (Fig. 14e). These researchers also found that pressure-dependent creep rather than lithium diffusion-dominated lithium transport at the interface and that considerable pressure was crucial for homogeneous lithium deposition and can effectively increase critical current density to achieve high power density or large rate capability.

4.1.4 Modifications to Alleviate Lithium Dendrite Formation

Due to high reactivity, the suppression of lithium dendrite growth in sulfide electrolytes is challenging because the mechanisms for "unexpected" dendrite formation are unclear and currently, methods to restrain lithium dendrite growth are mainly focused on the optimization of electrolyte composition and the application of artificial protective layers. In terms of the optimization of electrolyte composition, LiI has been demonstrated to be an effective additive to suppress lithium dendrite growth. For example, Suyama et al. [164] investigated the lithium dissolution/deposition behaviors of an all-solid-state lithium symmetric cell using a Li_3PS_4–LiI electrolyte system and their electrochemical tests showed that the introduction of LiI enhanced lithium dissolution/deposition performances in which the optimized electrolyte (46 mol% LiI) delivered ultralong cycling for 3400 h at 1.25 mA cm^{-2} without short circuiting and with a high areal capacity of 7.5 mAh cm^{-2}. Here, structural analysis revealed that electrolyte reduction by lithium metal can be inhibited with the addition of LiI in which good interfacial contact was maintained even after prolonged cycling, clearly demonstrating that the introduction of LiI improved the tolerance of sulfide electrolytes to lithium metal reduction. Similarly, Han et al. [160] demonstrated that lithium dendrites in a Li_2S–P_2S_5 glass electrolyte can be effectively suppressed by incorporating LiI into the electrolyte in which the ionically conductive but electronically insulating characteristic of LiI can improve lithium ion migration at the interface to suppress dendrite growth. As a result, these researchers reported significantly improved critical current densities, reaching 3.90 mA cm^{-2} at 100 °C as well as stable cycling for 200 h at 1.50 mA cm^{-2} in the corresponding lithium symmetric battery.

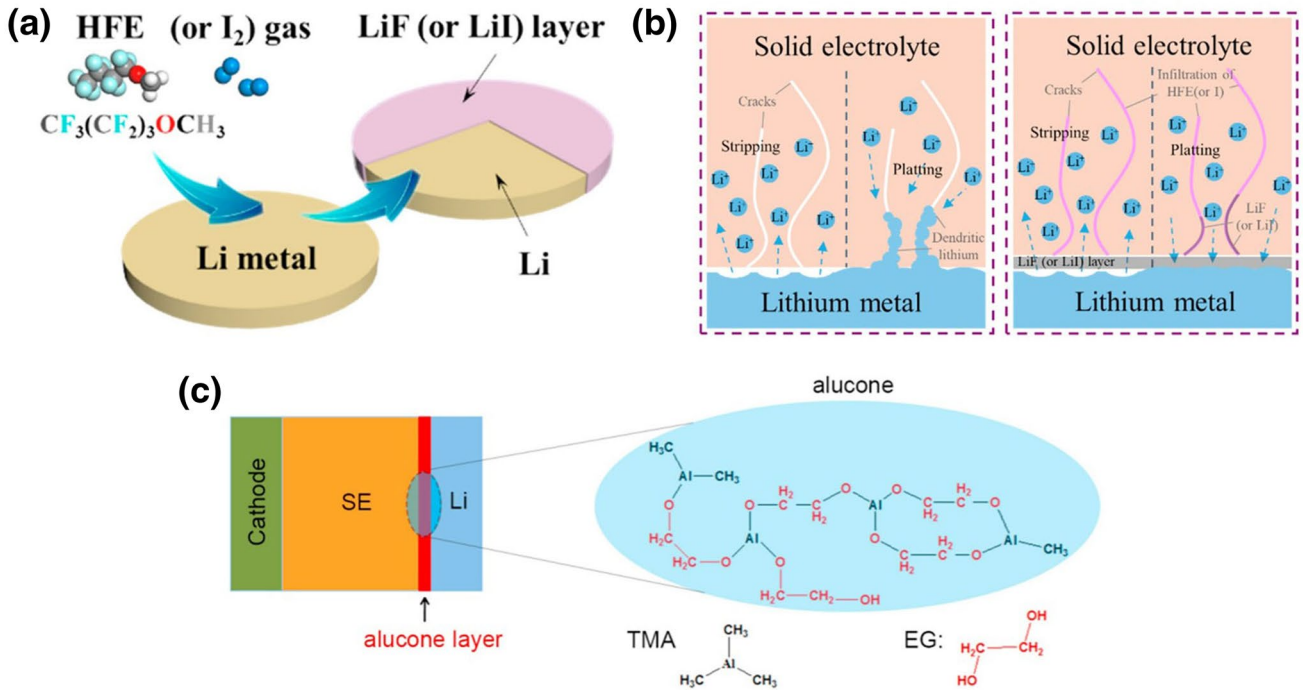

Fig. 15 **a** Schematic of LiF and LiI coating processes on lithium metal surfaces. **b** Schematic of lithium stripping/plating behaviors in bare lithium and LiF or LiI coated lithium with HFE or iodine infiltrated electrolytes. Reprinted with permission from Ref. [165]. Copyright 2018, Wiley–VCH. **c** Structure of a solid-state battery and chemical structure of the alucone layer. Reprinted with permission from Ref. [166]. Copyright 2018, Wiley–VCH

Aside from electrolyte composition optimization, the construction of buffer layers between lithium metal and electrolytes has also been demonstrated to be an effective method to suppress lithium dendrite formation. For example, Xu et al. [165] demonstrated that the coating of a uniform LiF (or LiI) interfacial layer at a Li/$Li_7P_3S_{11}$ interface can effectively inhibit lithium dendrite growth in which LiF or LiI can form on lithium surfaces after exposing lithium to methoxyperfluorobutane and I_2 gas at 150 °C (Fig. 15a). These researchers also reported that LiF interlayers exhibited much higher capabilities than LiI in the suppression of lithium dendrite formation due to the higher interfacial energy of LiF. More importantly, these researchers reported that even if the interfacial layer was broken by lithium dendrites, fresh lithium dendrites will be consumed by penetrative methoxyperfluorobutane (HFE) to form new solid electrolyte interphases (Fig. 15b). And as a result of this modification, a corresponding lithium symmetric battery showed enhanced cycling performances for over 200 cycles at 0.5 mA cm^{-2} and 0.1 mAh cm^{-2} and an assembled $LiNbO_3$@$LiCoO_2$/$Li_7P_3S_{11}$/LiF@Li ASSLB exhibited a reversible discharge capacity of 118.9 mAh g^{-1} at 0.1 mA cm^{-2} and retained 96.8 mAh g^{-1} after 100 cycles, demonstrating greatly enhanced performances as compared with ASSLBs using pure lithium metal anodes. Wang et al. [166] further developed an organic–inorganic hybrid interlayer (alucone) between $Li_{10}SnP_2S_{12}$ and lithium metal through molecular layer deposition (Fig. 15c) and found that the artificial interfacial layer can serve as an SEI to intrinsically block electron transfer at the Li/$Li_{10}SnP_2S_{12}$ interface to completely suppress interfacial reactions and lithium dendrite growth. As a result, an ASSLB employing the modified lithium metal anode exhibited smaller polarization, higher capacity and longer cycle lifes than that using bare lithium metal. More importantly, these researchers reported that their organic–inorganic hybrid molecular layer deposition method resulted in better flexibility than inorganic coatings and can better accommodate stress/strain as caused by volume change.

4.2 Other Anodes

Challenges such as uncontrollable lithium dendrite growth, interfacial reactions as well as volume effects facing ASSLBs are difficult to resolve in the short term. However, many anode materials used in traditional lithium ion batteries have been explored for application in ASSLBs, such as graphite, silicon and $Li_5Ti_7O_{12}$. In addition, the high environmental stability of these materials can lower the manufacturing costs of ASSLBs.

4.2.1 Graphite and Silicon

In general, the main issue between graphite or silicon anode powder materials and sulfide electrolytes is inferior contact. For example, Takeuchi et al. [167] prepared a graphite–sulfide electrolyte composite anode through spark–plasma–sintering (SPS) in which electrochemical tests showed that a corresponding ASSLB with a Li_2S cathode delivered a discharge capacity of 750 mAh g^{-1} (normalized by Li_2S mass). And although this capacity was lower than that of a battery employing an In/Li_2S anode (ca. 920 mAh g^{-1}), the estimate energy density was higher due to the low redox potential of graphite (0.1 V vs. Li/Li^+). More importantly, the graphite–sulfide composite anode exhibited enhanced rate capabilities as compared with the simply blended graphite–sulfide anode due to the intimate contact as a result of the SPS method. The selection of suitable electrolytes can also maintain electrochemical stability. For example, Takada et al. [168] designed a unique bilayer electrolyte structure in which a LiI–Li_2S–P_2S_5 glass electrolyte was used at the anode to suppress electrochemical reduction and Li_3PO_4–Li_2S–SiS_2 or Li_2S–GeS_2–P_2S_5 glass electrolytes were used at the cathode to suppress electrochemical oxidation. As a result, electrochemical testing showed no significant reactions between the LiI–Li_2S–P_2S_5 glass electrolyte and the graphite anode during lithium intercalation/deintercalation. This construction also allowed for the use of graphite as an anode and $LiCoO_2$ as a cathode in an ASSLB to achieve comparable performances to commercial lithium ion batteries. Similarly, Yamamoto et al. [169] found that $Li_7P_2S_8I$, a type of LiI–Li_2S–P_2S_5 electrolytes, exhibited wide electrochemical windows and was suitable to be paired with graphite anodes in which a half-cell with a graphite anode delivered an initial discharge of 372 mAh g^{-1} and highly reversible capacities.

Despite the high theoretical capacity of silicon (4200 mAh g^{-1} for $Li_{4.4}Si$), large volume change (~400%) during lithiation and de-lithiation as well as poor electronic conductivity must be overcome to allow for application. Based on this, great efforts have been devoted to the use of Si as anodes in traditional lithium ion batteries with strategies including the nano-crystallization of silicon particles, the construction of stress–relief buffer matrixes and the use of physical compartments to accommodate volume expansion [170]. Overall, the underlying mechanism of these strategies is to enhance adhesion between active materials and conducting matrixes to maintain better electrical contact during repeated volume change. In recent years, researchers have also applied Si in solid-state batteries. However, most studies have been based on dry-mixing with extremely low mass loadings and resulted in poor electrical contact

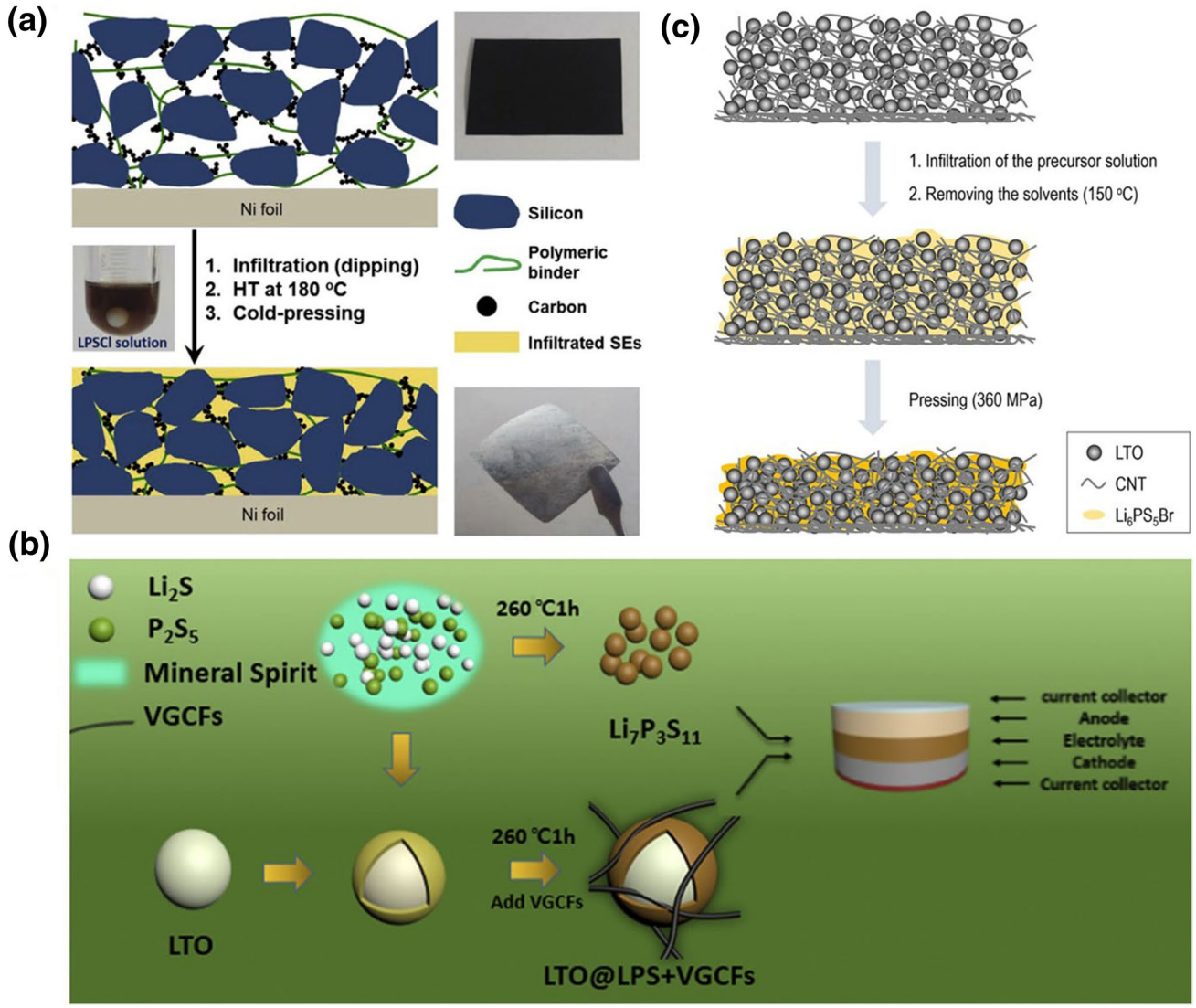

Fig. 16 **a** Schematic and photographs illustrating the infiltration process of conventional Si composite electrodes with solution-processable solid electrolytes. Reprinted with permission from Ref. [171]. Copyright 2019, Elsevier. **b** Schematic of the synthesis of a $Li_4Ti_5O_{12}$@LPS + VGCFs composite electrode and the assembly of a solid-state battery. Reprinted with permission from Ref. [173]. Copyright 2018, Elsevier. **c** Schematic of the infiltration of Li_6PS_5Br into a $Li_5Ti_7O_{12}$@CNT electrode by using the liquid-phase technique. Reprinted with permission from Ref. [133]. Copyright 2019, Elsevier

and low energy density. Kim et al. [171] prepared a sheet-like composite anode by infiltrating a traditional Si anode with a solution-processable Li_6PS_5Cl electrolyte (Fig. 16a) and reported that after the evaporation of the solvent, the electrolyte can solidify on the surface of the silicon particles to allow for compact ionic contact and favorable ionic transport. EDX mapping of the anode further showed that the penetration of the Li_6PS_5Cl solution into the Si electrode allowed for intimate contact between Si and Li_6PS_5Cl and electrochemical testing showed that a corresponding half-cell delivered a high capacity of 3246 mAh g^{-1} at 0.25 mA cm^{-2} that was much better than that of a traditional dry-mixed Si anode. In addition, a corresponding all-solid-state full cell using a $LiCO_2$ cathode was able to provide a high-energy density of 338 Wh kg^{-1}. Many results have also shown that encapsulating Si particles in robust matrixes can further suppress the volumetric expansion and pulverization of Si. Based on commercial considerations, Lee et al. [172] prepared a silicon–carbon composite derived from the industrial waste product coal–tar–pitch as an anode in an ASSLB in which the pyrolysis of coal–tar–pitch produced a mixed conducting amorphous carbon to encapsulate Si particles. Here, structural characterizations showed that the pitch-derived carbon was robust enough to suppress the volume change of silicon and resulted in impressive electrochemical properties in which an optimized sample displayed

stable specific capacities of 653.5 mAh g^{-1} (a mass electrode) and 1089.2 mAh g^{-1} (a mass Si–C) with Coulombic efficiency > 99%.

4.2.2 $Li_4Ti_5O_{12}$

Considering the good reversibility and negligible volume change of $Li_4Ti_5O_{12}$ in charge–discharge processes, the combination of $Li_4Ti_5O_{12}$ anodes with sulfide electrolytes should enable ASSLBs with high rate and cycle performances. And to enhance electrochemical performances, many strategies have been conducted to increase the contact area and enhance the compactness of contact interfaces. Similar to graphite and silicon anodes, these strategies mainly focus on liquid-phase or infiltration methods. For example, Cao et al. [173] developed a liquid-phase approach to in situ coat $70Li_2S–30P_2S_5$ onto $Li_4Ti_5O_{12}$ surfaces using mineral spirit as a solvent (Fig. 16b) and reported that a cell employing the $Li_4Ti_5O_{12}$@$70Li_2S–30P_2S_5$ and vapor-grown carbon fibers as the working electrode exhibited excellent rate capacities and cycling stability. In addition, these researchers successfully prepared a Li_6PS_5Cl-coated $Li_4Ti_5O_{12}$ using a kind of paint as the solvent [174] in which SEM and energy dispersive spectroscopy mapping showed the homogenous coating of nano-sized Li_6PS_5Cl onto the $Li_4Ti_5O_{12}$ surface, allowing for a stable interface between the active material and the solid electrolyte and resulting in low interfacial resistances and excellent electrochemical activities. Similar to that of silicon anodes, the infiltration method can also be used to enhance compactness and facilitate electric/ionic conduction. For example, Yubuchi et al. [133] prepared a homogenous $Li_4Ti_5O_{12}$-carbon nanotube-Li_6PS_5Br composite electrode using infiltration followed by cold pressing (Fig. 16c) to achieve an electrochemically active interface with a large contact area and favorable electric/ionic conduction pathways, resulting in a corresponding ASSLB demonstrating an improved capacity of 100 mAh g^{-1} at 4 °C and 100 °C.

5 Summary and Outlook

ASSLBs based on sulfide electrolytes are attracting significant interest due to their potential to address safety concerns and improve energy density. The metal oxide cathodes have been extensively used in commercial lithium ion batteries. Based on this, this review has comprehensively presented the progress in ASSLBs using sulfide electrolytes and oxide cathodes. In addition, related interfacial issues at sulfide electrolyte/oxide cathode interfaces as well as unstable anodic interfaces have been systematically discussed. Moreover, major challenges as well as corresponding improvement strategies for ASSLBs using lithium anodes have been proposed. Different sulfide electrolytes have also been summarized and ionic conductivities have been compared based on the type and the preparation method. In terms of practical commercialization, the stability of sulfide electrolytes was also considered. As for oxide-based cathodes, various types of interfacial behaviors including space charge layer effects, interfacial reactions and contact losses were classified and discussed in detail.

Overall, to improve interfacial stability and promote practical application, various strategies have been adopted, mainly including cathode coating and electrolyte compositional tuning. New strategies such as the reduction of particle size and the mixing of electrolytes with electrodes through ball-milling have also been proposed to enhance the performance of ASSLBs. As for anodes, main methods including artificial solid electrolyte interphase construction and electrolyte component optimization have routinely been used to minimize interfacial resistance. And despite Li_3PS_4 and derivatives exhibiting relative stability with lithium metal, the capacity utilization and working current density of lithium metal anodes are far from meeting practical requirements. Therefore, the resolution of interfacial contact and dendrite formation issues for lithium metal anodes used with sulfide electrolytes remains challenging.

Despite these challenges, ASSLBs with oxide-based cathodes and sulfide electrolytes are still considered to be promising candidates for next-generation energy storage systems in which enhancements in electrolyte conductivity and interfacial stability are still needed. Here, the adoption of straightforward strategies alone is insufficient for the practical application of ASSLBs and combined solutions such as suitable electrolyte components and artificial interfaces between electrolytes and electrodes need to be considered to achieve joint modifications for high-performance ASSLBs. Several design principles and solutions regarding ASSLBs with oxide-based cathodes and sulfide electrolytes are listed as follow:

(1) New sulfide electrolytes. Although sulfide electrolytes possess unparalleled ionic conductivities, poor electrochemical and chemical stability greatly limits practical application. Therefore, the exploration for new electrolytes is needed to further improve the performance of corresponding ASSLBs. Here, both ionic and electronic conductivities need to be taken into consideration and recently, theoretical calculations have been reported to be an important tool in the design of new electrolytes by allowing for the prediction or selection of suitable components and physicochemical properties in advance. Overall, a combination of experimental results with theoretical calculations is necessary to explore new electrolytes.

(2) Optimized electrolyte/cathode interfaces. The different chemical potentials of lithium ions between sulfide electrolytes and oxide cathodes can induce high interfacial resistance that can severely affect the high-rate capability of ASSLBs. Therefore, optimized interfaces are necessary to act as bridges to mitigate lithium chemical potential differences between electrolytes and cathodes. These interfaces should possess high ionic conductivity to ensure smooth lithium ion migration as well as good compatibility with electrodes and stability to shield sulfide electrolytes from high electrode potentials.

(3) Dendrite control in lithium anodes. Low relative density, grain boundaries, defects and high electronic conductivity in sulfide electrolytes are believed to be the reasons for lithium dendrite formation. Here, the mechanisms of lithium dendrite formation in solid electrolytes are being actively studied and a single method to suppress all aspects of lithium dendrite formation remains lacking. Therefore, combined modifications are better choices to achieve dendrite-free anodes in ASSLBs, such as the construction of artificial interfaces, the design of 3D lithium matrixes and the adoption of lithium alloys. In addition, the development of new sulfide electrolytes with high ionic conductivity and low electronic conductivity can also inhibit dendrite formation.

(4) Optimized battery assembly. Well-designed battery assembly technologies are also important. For example, suitable pressures are crucial to achieve homogeneous lithium deposition and can effectively increase critical current densities to achieve high power density ASSLBs.

Acknowledgements This work was supported by the National Key R&D Program of China (Grant No. 2018YFB0905400), the National Natural Science Foundation of China (Grant Nos. 51872303, U1964205, 51902321), the Zhejiang Provincial Natural Science Foundation of China (Grant No. LD18E020004, LY18E020018), the Ningbo S&T Innovation 2025 Major Special Programme (Grant Nos. 2018B10061, 2018B10087, 2019B10044), the Natural Science Foundation of Ningbo (Grant Nos. 2018A610010, 2019A610007), the Jiangxi Provincial Key R&D Program of China (Grant No. 20182ABC28007) and the Youth Innovation Promotion Association CAS (2017342).

References

1. Zhao, Y., Li, X.F., Yan, B., et al.: Recent developments and understanding of novel mixed transition–metal oxides as anodes in lithium ion batteries. Adv. Energy Mater. **6**, 1502175 (2016). https://doi.org/10.1002/aenm.201502175
2. Lian, P.J., Zhao, B.S., Zhang, L.Q., et al.: Inorganic sulfide solid electrolytes for all-solid-state lithium secondary batteries. J. Mater. Chem. A **7**, 20540–20557 (2019). https://doi.org/10.1039/c9ta04555d
3. Cheng, X.B., Zhang, R., Zhao, C.Z., et al.: A review of solid electrolyte interphases on lithium metal anode. Adv. Sci. **3**, 1500213 (2016). https://doi.org/10.1002/advs.201500213
4. Sun, C., Liu, J., Gong, Y., et al.: Recent advances in all-solid-state rechargeable lithium batteries. Nano Energy **33**, 363–386 (2017). https://doi.org/10.1016/j.nanoen.2017.01.028
5. Manthiram, A., Yu, X.W., Wang, S.F.: Lithium battery chemistries enabled by solid-state electrolytes. Nat. Rev. Mater. **2**, 16103 (2017). https://doi.org/10.1038/natrevmats.2016.103
6. Takada, K.: Progress and prospective of solid-state lithium batteries. Acta Mater. **61**, 759–770 (2013)
7. Bachman, J.C., Muy, S., Grimaud, A., et al.: Inorganic solid-state electrolytes for lithium batteries: mechanisms and properties governing ion conduction. Chem. Rev. **116**, 140–162 (2016). https://doi.org/10.1021/acs.chemrev.5b00563
8. Gao, Z.H., Sun, H.B., Fu, L., et al.: All-solid-state batteries: Promises, challenges, and recent progress of inorganic solid-state electrolytes for all-solid-state lithium batteries. Adv. Mater. **30**, 1870122 (2018). https://doi.org/10.1002/adma.201870122
9. Lau, J., DeBlock, R.H., Butts, D.M., et al.: Sulfide solid electrolytes for lithium battery applications. Adv. Energy Mater. **8**, 1800933 (2018). https://doi.org/10.1002/aenm.201800933
10. Zhang, Q., Cao, D.X., Ma, Y., et al.: Sulfide-based solid-state electrolytes: synthesis, stability, and potential for all-solid-state batteries. Adv. Mater. **31**, 1901131 (2019). https://doi.org/10.1002/adma.201901131
11. Kamaya, N., Homma, K., Yamakawa, Y., et al.: A lithium superionic conductor. Nat. Mater. **10**, 682–686 (2011). https://doi.org/10.1038/nmat3066
12. Kato, Y., Hori, S., Saito, T., et al.: High-power all-solid-state batteries using sulfide superionic conductors. Nat. Energy **1**, 16030 (2016). https://doi.org/10.1038/nenergy.2016.30
13. Jung, S.K., Gwon, H., Hong, J., et al.: Understanding the degradation mechanisms of $LiNi_{0.5}Co_{0.2}Mn_{0.3}O_2$ cathode material in lithium ion batteries. Adv. Energy Mater. **4**, 1300787 (2014). https://doi.org/10.1002/aenm.201300787
14. Poizot, P., Laruelle, S., Grugeon, S., et al.: Nano-sized transition–metal oxides as negative-electrode materials for lithium-ion batteries. Nature **407**, 496–499 (2000). https://doi.org/10.1038/35035045
15. Xin, S., You, Y., Wang, S.F., et al.: Solid-state lithium metal batteries promoted by nanotechnology: progress and prospects. ACS Energy Lett. **2**, 1385–1394 (2017). https://doi.org/10.1021/acsenergylett.7b00175
16. Chen, L., Fan, L.Z.: Dendrite-free Li metal deposition in all-solid-state lithium sulfur batteries with polymer-in-salt polysiloxane electrolyte. Energy Storage Mater. **15**, 37–45 (2018). https://doi.org/10.1016/j.ensm.2018.03.015
17. Mercier, R., Malugani, J.P., Fahys, B., et al.: Superionic conduction in Li_2S–P_2S_5–LiI-glasses. Solid State Ionics **5**, 663–666 (1981). https://doi.org/10.1016/0167-2738(81)90341-6
18. Hayashi, A., Yamashita, H., Tatsumisago, M., et al.: Characterization of Li_2S–SiS_2–Li_xMO_y (M = Si, P, Ge) amorphous solid electrolytes prepared by melt-quenching and mechanical milling. Solid State Ionics **148**, 381–389 (2002). https://doi.org/10.1016/S0167-2738(02)00077-2
19. Kanno, R., Murayama, M.: Lithium ionic conductor thio-LISICON: the Li_2S–GeS_2–P_2S_5 system. J. Electrochem. Soc. **148**, A742–A746 (2001)
20. Hong, H.Y.: Crystal structure and ionic conductivity of $Li_{14}Zn(GeO_4)_4$ and other new Li^+ superionic conductors. Mater. Res. Bull. **13**, 117–124 (1978). https://doi.org/10.1016/0025-5408(78)90075-2

21. Zhang, Z.Z., Shao, Y.J., Lotsch, B., et al.: New horizons for inorganic solid state ion conductors. Energy Environ. Sci. **11**, 1945–1976 (2018). https://doi.org/10.1039/c8ee01053f
22. Hayashi, A., Hama, S., Minami, T., et al.: Formation of superionic crystals from mechanically milled Li_2S–P_2S_5 glasses. Electrochem. Commun. **5**, 111–114 (2003). https://doi.org/10.1016/s1388-2481(02)00555-6
23. Mizuno, F., Hayashi, A., Tadanaga, K., et al.: High lithium ion conducting glass–ceramics in the system Li_2S–P_2S_5. Solid State Ionics **177**, 2721–2725 (2006). https://doi.org/10.1016/j.ssi.2006.04.017
24. Hayashi, A., Hama, S., Morimoto, H., et al.: Preparation of Li_2S–P_2S_5 amorphous solid electrolytes by mechanical milling. J. Am. Ceram. Soc. **84**, 477–479 (2004). https://doi.org/10.1111/j.1151-2916.2001.tb00685.x
25. Mizuno, F., Hayashi, A., Tadanaga, K., et al.: New, highly ion-conductive crystals precipitated from Li_2S–P_2S_5 glasses. Adv. Mater. **17**, 918–921 (2005). https://doi.org/10.1002/adma.200401286
26. Kudu, Ö.U., Famprikis, T., Fleutot, B., et al.: A review of structural properties and synthesis methods of solid electrolyte materials in the Li_2S–P_2S_5 binary system. J. Power Sources **407**, 31–43 (2018). https://doi.org/10.1016/j.jpowsour.2018.10.037
27. Homma, K., Yonemura, M., Nagao, M., et al.: Crystal structure of high-temperature phase of lithium ionic conductor, Li_3PS_4. J. Phys. Soc. Jpn. **79**, 90–93 (2010). https://doi.org/10.1143/jpsjs.79sa.90
28. Iikubo, S., Shimoyama, K., Kawano, S., et al.: Novel stable structure of Li_3PS_4 predicted by evolutionary algorithm under high-pressure. AIP Adv. **8**, 015008 (2018). https://doi.org/10.1063/1.5011401
29. Homma, K., Yonemura, M., Kobayashi, T., et al.: Crystal structure and phase transitions of the lithium ionic conductor Li_3PS_4. Solid State Ionics **182**, 53–58 (2011). https://doi.org/10.1016/j.ssi.2010.10.001
30. Yamane, H., Shibata, M., Shimane, Y., et al.: Crystal structure of a superionic conductor, $Li_7P_3S_{11}$. Solid State Ionics **178**, 1163–1167 (2007). https://doi.org/10.1016/j.ssi.2007.05.020
31. Seino, Y., Ota, T., Takada, K., et al.: A sulphide lithium super ion conductor is superior to liquid ion conductors for use in rechargeable batteries. Energy Environ. Sci. **7**, 627–631 (2014). https://doi.org/10.1039/c3ee41655k
32. Chu, I.H., Nguyen, H., Hy, S., et al.: Insights into the performance limits of the $Li_7P_3S_{11}$ superionic conductor: a combined first-principles and experimental study. ACS Appl. Mater. Interfaces **8**, 7843–7853 (2016). https://doi.org/10.1021/acsami.6b00833
33. Ong, S.P., Mo, Y.F., Richards, W.D., et al.: Phase stability, electrochemical stability and ionic conductivity of the $Li_{10\pm1}MP_2X_{12}$ (M = Ge, Si, Sn, Al or P, and X = O, S or Se) family of superionic conductors. Energy Environ. Sci. **6**, 148–156 (2013). https://doi.org/10.1039/c2ee23355j
34. Bron, P., Johansson, S., Zick, K., et al.: $Li_{10}SnP_2S_{12}$: an affordable lithium superionic conductor. J. Am. Chem. Soc. **135**, 15694–15697 (2013). https://doi.org/10.1021/ja407393y
35. Whiteley, J.M., Woo, J.H., Hu, E.Y., et al.: Empowering the lithium metal battery through a silicon-based superionic conductor. J. Electrochem. Soc. **161**, A1812–A1817 (2014). https://doi.org/10.1149/2.0501412jes
36. Zhou, P.F., Wang, J.B., Cheng, F.Y., et al.: A solid lithium superionic conductor $Li_{11}AlP_2S_{12}$ with a thio-LISICON analogous structure. Chem. Commun. **52**, 6091–6094 (2016). https://doi.org/10.1039/c6cc02131j
37. Hayashi, A., Nishio, Y., Kitaura, H., et al.: Novel technique to form electrode–electrolyte nanointerface in all-solid-state rechargeable lithium batteries. Electrochem. Commun. **10**, 1860–1863 (2008). https://doi.org/10.1016/j.elecom.2008.09.026
38. Ziolkowska, D.A., Arnold, W., Druffel, T., et al.: Rapid and economic synthesis of a Li_7PS_6 solid electrolyte from a liquid approach. ACS Appl. Mater. Interfaces **11**, 6015–6021 (2019). https://doi.org/10.1021/acsami.8b19181
39. Deiseroth, H.J., Kong, S.T., Eckert, H., et al.: Li_6PS_5X: a class of crystalline Li-rich solids with an unusually high Li^+ mobility. Angew. Chem. Int. Ed. **47**, 755–758 (2008). https://doi.org/10.1002/anie.200703900
40. de Klerk, N.J.J., Roslon, I., Wagemaker, M.: Diffusion mechanism of Li argyrodite solid electrolytes for Li-ion batteries and prediction of optimized halogen doping: the effect of Li vacancies, halogens, and halogen disorder. Chem. Mater. **28**, 7955–7963 (2016). https://doi.org/10.1021/acs.chemmater.6b03630
41. Rao, R., Adams, S.: Studies of lithium argyrodite solid electrolytes for all-solid-state batteries. Phys. Status Solidi A **208**, 1804–1807 (2011). https://doi.org/10.1002/pssa.201001117
42. Rayavarapu, P.R., Sharma, N., Peterson, V.K., et al.: Variation in structure and Li^+-ion migration in argyrodite-type Li_6PS_5X (X = Cl, Br, I) solid electrolytes. J. Solid State Electrochem. **16**, 1807–1813 (2012). https://doi.org/10.1007/s10008-011-1572-8
43. Kraft, M.A., Ohno, S., Zinkevich, T., et al.: Inducing high ionic conductivity in the lithium superionic argyrodites $Li_{6+x}P_{1-x}Ge_xS_5I$ for all-solid-state batteries. J. Am. Chem. Soc. **140**, 16330–16339 (2018). https://doi.org/10.1021/jacs.8b10282
44. Ge, Q., Zhou, L., Lian, Y.M., et al.: Metal-phosphide-doped $Li_7P_3S_{11}$ glass-ceramic electrolyte with high ionic conductivity for all-solid-state lithium-sulfur batteries. Electrochem. Commun. **97**, 100–104 (2018). https://doi.org/10.1016/j.elecom.2018.10.024
45. Yu, C., Hageman, J., Ganapathy, S., et al.: Tailoring Li_6PS_5Br ionic conductivity and understanding of its role in cathode mixtures for high performance all-solid-state Li–S batteries. J. Mater. Chem. A **7**, 10412–10421 (2019). https://doi.org/10.1039/c9ta02126d
46. Kraft, M.A., Culver, S.P., Calderon, M., et al.: Influence of lattice polarizability on the ionic conductivity in the lithium superionic argyrodites Li_6PS_5X (X = Cl, Br, I). J. Am. Chem. Soc. **139**, 10909–10918 (2017). https://doi.org/10.1021/jacs.7b06327
47. Wang, S., Zhang, Y.B., Zhang, X., et al.: High-conductivity argyrodite Li_6PS_5Cl solid electrolytes prepared via optimized sintering processes for all-solid-state lithium–sulfur batteries. ACS Appl. Mater. Interfaces **10**, 42279–42285 (2018). https://doi.org/10.1021/acsami.8b15121
48. Yu, C., Ganapathy, S., Hageman, J., et al.: Facile synthesis toward the optimal structure-conductivity characteristics of the argyrodite Li_6PS_5Cl solid-state electrolyte. ACS Appl. Mater. Interfaces **10**, 33296–33306 (2018). https://doi.org/10.1021/acsami.8b07476
49. Zhang, D.: Processing of advanced materials using high-energy mechanical milling. Prog. Mater Sci. **49**, 537–560 (2004). https://doi.org/10.1016/S0079-6425(03)00034-3
50. Busche, M.R., Weber, D.A., Schneider, Y., et al.: In situ monitoring of fast Li-ion conductor $Li_7P_3S_{11}$ crystallization inside a hot-press setup. Chem. Mater. **28**, 6152–6165 (2016). https://doi.org/10.1021/acs.chemmater.6b02163
51. Trevey, J., Jang, J.S., Jung, Y.S., et al.: Glass–ceramic Li_2S–P_2S_5 electrolytes prepared by a single step ball billing process and their application for all-solid-state lithium–ion batteries. Electrochem. Commun. **11**, 1830–1833 (2009). https://doi.org/10.1016/j.elecom.2009.07.028
52. Tao, Y.C., Chen, S.J., Liu, D., et al.: Lithium superionic conducting oxysulfide solid electrolyte with excellent stability against lithium metal for all-solid-state cells. J. Electrochem. Soc. **163**, A96–A101 (2016). https://doi.org/10.1149/2.0311602jes

53. Yamamoto, H., Machida, N., Shigematsu, T.: A mixed-former effect on lithium-ion conductivities of the Li_2S–GeS_2–P_2S_5 amorphous materials prepared by a high-energy ball-milling process. Solid State Ionics **175**, 707–711 (2004). https://doi.org/10.1016/j.ssi.2004.08.028
54. Chen, M.H., Adams, S.: High performance all-solid-state lithium/sulfur batteries using lithium argyrodite electrolyte. J. Solid State Electrochem. **19**, 697–702 (2015). https://doi.org/10.1007/s10008-014-2654-1
55. Boulineau, S., Courty, M., Tarascon, J.M., et al.: Mechanochemical synthesis of Li-argyrodite Li_6PS_5X (X = Cl, Br, I) as sulfur-based solid electrolytes for all solid state batteries application. Solid State Ionics **221**, 1–5 (2012). https://doi.org/10.1016/j.ssi.2012.06.008
56. Yu, C., van Eijck, L., Ganapathy, S., et al.: Synthesis, structure and electrochemical performance of the argyrodite Li_6PS_5Cl solid electrolyte for Li-ion solid state batteries. Electrochim. Acta **215**, 93–99 (2016). https://doi.org/10.1016/j.electacta.2016.08.081
57. Liu, Z.C., Fu, W.J., Payzant, E.A., et al.: Anomalous high ionic conductivity of nanoporous β-Li_3PS_4. J. Am. Chem. Soc. **135**, 975–978 (2013). https://doi.org/10.1021/ja3110895
58. Yao, X.Y., Liu, D., Wang, C.S., et al.: High-energy all-solid-state lithium batteries with ultralong cycle life. Nano Lett. **16**, 7148–7154 (2016). https://doi.org/10.1021/acs.nanolett.6b03448
59. Phuc, N.H.H., Totani, M., Morikawa, K., et al.: Preparation of Li_3PS_4 solid electrolyte using ethyl acetate as synthetic medium. Solid State Ionics **288**, 240–243 (2016). https://doi.org/10.1016/j.ssi.2015.11.032
60. Teragawa, S., Aso, K., Tadanaga, K., et al.: Liquid-phase synthesis of a Li_3PS_4 solid electrolyte using *N*-methylformamide for all-solid-state lithium batteries. J. Mater. Chem. A **2**, 5095 (2014). https://doi.org/10.1039/c3ta15090a
61. Ito, S., Nakakita, M., Aihara, Y., et al.: A synthesis of crystalline $Li_7P_3S_{11}$ solid electrolyte from 1,2-dimethoxyethane solvent. J. Power Sources **271**, 342–345 (2014). https://doi.org/10.1016/j.jpowsour.2014.08.024
62. Wan, H., Mwizerwa, J.P., Han, F., et al.: Grain-boundary-resistance-less $Na_3SbS_{4-x}Se_x$ solid electrolytes for all-solid-state sodium batteries. Nano Energy **66**, 104109 (2019). https://doi.org/10.1016/j.nanoen.2019.104109
63. Yubuchi, S., Teragawa, S., Aso, K., et al.: Preparation of high lithium-ion conducting Li_6PS_5Cl solid electrolyte from ethanol solution for all-solid-state lithium batteries. J. Power Sources **293**, 941–945 (2015). https://doi.org/10.1016/j.jpowsour.2015.05.093
64. Yubuchi, S., Uematsu, M., Hotehama, C., et al.: An argyrodite sulfide-based superionic conductor synthesized by a liquid-phase technique with tetrahydrofuran and ethanol. J. Mater. Chem. A **7**, 558–566 (2019). https://doi.org/10.1039/c8ta09477b
65. Choi, S., Ann, J., Do, J., et al.: Application of rod-like Li_6PS_5Cl directly synthesized by a liquid phase process to sheet-type electrodes for all-solid-state lithium batteries. J. Electrochem. Soc. **166**, A5193–A5200 (2019). https://doi.org/10.1149/2.0301903jes
66. Zhou, L.D., Park, K.H., Sun, X.Q., et al.: Solvent-engineered design of argyrodite Li_6PS_5X (X = Cl, Br, I) solid electrolytes with high ionic conductivity. ACS Energy Lett. **4**, 265–270 (2019). https://doi.org/10.1021/acsenergylett.8b01997
67. Xu, R.C., Xia, X.H., Wang, X.L., et al.: Tailored Li_2S–P_2S_5 glass–ceramic electrolyte by MoS_2 doping, possessing high ionic conductivity for all-solid-state lithium–sulfur batteries. J. Mater. Chem. A **5**, 2829–2834 (2017). https://doi.org/10.1039/c6ta10142a
68. Wu, Z.J., Xie, Z.K., Yoshida, A., et al.: Novel SeS_2 doped Li_2S–P_2S_5 solid electrolyte with high ionic conductivity for all-solid-state lithium sulfur batteries. Chem. Eng. J. **380**, 122419 (2020). https://doi.org/10.1016/j.cej.2019.122419
69. Yamauchi, A., Sakuda, A., Hayashi, A., et al.: Preparation and ionic conductivities of $(100-x)(0.75Li_2S{\cdot}0.25P_2S_5){\cdot}xLiBH_4$ glass electrolytes. J. Power Sources **244**, 707–710 (2013). https://doi.org/10.1016/j.jpowsour.2012.12.001
70. Huang, B.X., Yao, X.Y., Huang, Z., et al.: Li_3PO_4-doped $Li_7P_3S_{11}$ glass–ceramic electrolytes with enhanced lithium ion conductivities and application in all-solid-state batteries. J. Power Sources **284**, 206–211 (2015). https://doi.org/10.1016/j.jpowsour.2015.02.160
71. Kim, K., Martin, S.W.: Structures and properties of oxygen-substituted $Li_{10}SiP_2S_{12-x}O_x$ solid-state electrolytes. Chem. Mater. **31**, 3984–3991 (2019). https://doi.org/10.1021/acs.chemmater.9b00505
72. Ujiie, S., Inagaki, T., Hayashi, A., et al.: Conductivity of $70Li_2S{\cdot}30P_2S_5$ glasses and glass–ceramics added with lithium halides. Solid State Ionics **263**, 57–61 (2014). https://doi.org/10.1016/j.ssi.2014.05.002
73. Ujiie, S., Hayashi, A., Tatsumisago, M.: Structure, ionic conductivity and electrochemical stability of Li_2S–P_2S_5–LiI glass and glass–ceramic electrolytes. Solid State Ionics **211**, 42–45 (2012). https://doi.org/10.1016/j.ssi.2012.01.017
74. Adeli, P., Bazak, J.D., Park, K.H., et al.: Boosting solid-state diffusivity and conductivity in lithium superionic argyrodites by halide substitution. Angew. Chem. Int. Ed. **58**, 8681–8686 (2019). https://doi.org/10.1002/anie.201814222
75. Xiong, L.L., Xu, Y.L., Tao, T., et al.: Synthesis and electrochemical characterization of multi-cations doped spinel $LiMn_2O_4$ used for lithium ion batteries. J. Power Sources **199**, 214–219 (2012). https://doi.org/10.1016/j.jpowsour.2011.09.062
76. Guo, H.L., Gao, Q.M.: Boron and nitrogen co-doped porous carbon and its enhanced properties as supercapacitor. J. Power Sources **186**, 551–556 (2009). https://doi.org/10.1016/j.jpowsour.2008.10.024
77. Yang, K., Dong, J.Y., Zhang, L., et al.: Dual doping: an effective method to enhance the electrochemical properties of $Li_{10}GeP_2S_{12}$-based solid electrolytes. J. Am. Ceram. Soc. **98**, 3831–3835 (2015). https://doi.org/10.1111/jace.13800
78. Sun, Y.L., Suzuki, K., Hori, S., et al.: Superionic conductors: $Li_{10+\delta}[Sn_ySi_{1-y}]_{1+\delta}P_{2-\delta}S_{12}$ with a $Li_{10}GeP_2S_{12}$-type structure In the Li_3PS_4–Li_4SnS_4–Li_4SiS_4 quasi-ternary system. Chem. Mater. **29**, 5858–5864 (2017). https://doi.org/10.1021/acs.chemmater.7b00886
79. Minami, K., Hayashi, A., Tatsumisago, M.: Crystallization process for superionic $Li_7P_3S_{11}$ glass–ceramic electrolytes. J. Am. Ceram. Soc. **94**, 1779–1783 (2011). https://doi.org/10.1111/j.1551-2916.2010.04335.x
80. Chen, S.J., Xie, D.J., Liu, G.Z., et al.: Sulfide solid electrolytes for all-solid-state lithium batteries: structure, conductivity, stability and application. Energy Storage Mater. **14**, 58–74 (2018). https://doi.org/10.1016/j.ensm.2018.02.020
81. Auvergniot, J., Cassel, A., Ledeuil, J.B., et al.: Interface stability of argyrodite Li_6PS_5Cl toward $LiCoO_2$, $LiNi_{1/3}Co_{1/3}Mn_{1/3}O_2$, and $LiMn_2O_4$ in bulk all-solid-state batteries. Chem. Mater. **29**, 3883–3890 (2017). https://doi.org/10.1021/acs.chemmater.6b04990
82. Sumita, M., Tanaka, Y., Ohno, T.: Possible polymerization of PS_4 at a Li_3PS_4/$FePO_4$ interface with reduction of the $FePO_4$ phase. J. Phys. Chem. C **121**, 9698–9704 (2017). https://doi.org/10.1021/acs.jpcc.7b01009
83. Haruyama, J., Sodeyama, K., Han, L.Y., et al.: Space–charge layer effect at interface between oxide cathode and sulfide electrolyte in all-solid-state lithium-ion battery. Chem. Mater. **26**, 4248–4255 (2014). https://doi.org/10.1021/cm5016959

84. Takada, K., Ohta, N., Zhang, L.Q., et al.: Interfacial phenomena in solid-state lithium battery with sulfide solid electrolyte. Solid State Ionics **225**, 594–597 (2012). https://doi.org/10.1016/j.ssi.2012.01.009
85. Ohta, N., Takada, K., Zhang, L., et al.: Enhancement of the high-rate capability of solid-state lithium batteries by nanoscale interfacial modification. Adv. Mater. **18**, 2226–2229 (2006). https://doi.org/10.1002/adma.200502604
86. Haruyama, J., Sodeyama, K., Tateyama, Y.: Cation mixing properties toward Co diffusion at the $LiCoO_2$ cathode/sulfide electrolyte interface in a solid-state battery. ACS Appl. Mater Interfaces **9**, 286–292 (2017). https://doi.org/10.1021/acsami.6b08435
87. Richards, W.D., Miara, L.J., Wang, Y., et al.: Interface stability in solid-state batteries. Chem. Mater. **28**, 266–273 (2016). https://doi.org/10.1021/acs.chemmater.5b04082
88. Sumita, M., Tanaka, Y., Ikeda, M., et al.: Charged and discharged states of cathode/sulfide electrolyte interfaces in all-solid-state lithium ion batteries. J. Phys. Chem. C **120**, 13332–13339 (2016). https://doi.org/10.1021/acs.jpcc.6b01207
89. Oh, G., Hirayama, M., Kwon, O., et al.: Bulk-type all solid-state batteries with 5 V class $LiNi_{0.5}Mn_{1.5}O_4$ cathode and $Li_{10}GeP_2S_{12}$ solid electrolyte. Chem. Mater. **28**, 2634–2640 (2016). https://doi.org/10.1021/acs.chemmater.5b04940
90. Sakuda, A., Hayashi, A., Tatsumisago, M.: Interfacial observation between $LiCoO_2$ electrode and Li_2S–P_2S_5 solid electrolytes of all-solid-state lithium secondary batteries using transmission electron microscopy. Chem. Mater. **22**, 949–956 (2010). https://doi.org/10.1021/cm901819c
91. Kwak, H.W., Park, Y.J.: Cathode coating using $LiInO_2$−LiI composite for stable sulfide-based all-solid-state batteries. Sci. Rep. **9**, 8099 (2019). https://doi.org/10.1038/s41598-019-44629-x
92. Zhu, Y.Z., He, X.F., Mo, Y.F.: First principles study on electrochemical and chemical stability of solid electrolyte–electrode interfaces in all-solid-state Li-ion batteries. J. Mater. Chem. **4**, 3253–3266 (2016). https://doi.org/10.1039/C5TA08574H
93. Koerver, R., Aygün, I., Leichtweiß, T., et al.: Capacity fade in solid-state batteries: interphase formation and chemomechanical processes in nickel-rich layered oxide cathodes and lithium thiophosphate solid electrolytes. Chem. Mater. **29**, 5574–5582 (2017)
94. Takada, K.: Interfacial nanoarchitectonics for solid-state lithium batteries. Langmuir **29**, 7538–7541 (2013). https://doi.org/10.1021/la3045253
95. Xu, L., Tang, S., Cheng, Y., et al.: Interfaces in solid-state lithium batteries. Joule **2**, 1991–2015 (2018). https://doi.org/10.1016/j.joule.2018.07.009
96. Nam, Y.J., Cho, S.J., Oh, D.Y., et al.: Bendable and thin sulfide solid electrolyte film: a new electrolyte opportunity for free-standing and stackable high-energy all-solid-state lithium-ion batteries. Nano Lett. **15**, 3317–3323 (2015). https://doi.org/10.1021/acs.nanolett.5b00538
97. Yao, L., Liang, F.Q., Jin, J., et al.: Improved electrochemical property of Ni-rich $LiNi_{0.6}Co_{0.2}Mn_{0.2}O_2$ cathode via in situ ZrO_2 coating for high energy density lithium ion batteries. Chem. Eng. J. **389**, 124403 (2020). https://doi.org/10.1016/j.cej.2020.124403
98. Zhu, Y., He, X., Mo, Y.: Origin of outstanding stability in the lithium solid electrolyte materials: Insights from thermodynamic analyses based on first-principles calculations. ACS Appl. Mater. Interfaces **7**, 23685–23693 (2015). https://doi.org/10.1021/acsami.5b07517
99. McGrogan, F.P., Swamy, T., Bishop, S.R., et al.: Compliant yet brittle mechanical behavior of Li_2S–P_2S_5 lithium-ion-conducting solid electrolyte. Adv. Energy Mater. **7**, 1602011 (2017). https://doi.org/10.1002/aenm.201602011
100. Li, X.L., Liang, M., Sheng, J., et al.: Constructing double buffer layers to boost electrochemical performances of NCA cathode for ASSLB. Energy Storage Mater. **18**, 100–106 (2019). https://doi.org/10.1016/j.ensm.2018.10.003
101. Ohta, N., Takada, K., Sakaguchi, I., et al.: $LiNbO_3$-coated $LiCoO_2$ as cathode material for all solid-state lithium secondary batteries. Electrochem. Commun. **9**, 1486–1490 (2007). https://doi.org/10.1016/j.elecom.2007.02.008
102. Seino, Y., Ota, T., Takada, K.: High rate capabilities of all-solid-state lithium secondary batteries using $Li_4Ti_5O_{12}$-coated $LiNi_{0.8}Co_{0.15}Al_{0.05}O_2$ and a sulfide-based solid electrolyte. J. Power Sources **196**, 6488–6492 (2011). https://doi.org/10.1016/j.jpowsour.2011.03.090
103. Jung, S.H., Oh, K., Nam, Y.J., et al.: Li_3BO_3–Li_2CO_3: rationally designed buffering phase for sulfide all-solid-state Li-ion batteries. Chem. Mater. **30**, 8190–8200 (2018). https://doi.org/10.1021/acs.chemmater.8b03321
104. Glass, A.M., Nassau, K., Negran, T.J.: Ionic conductivity of quenched alkali niobate and tantalate glasses. J. Appl. Phys. **49**, 4808–4811 (1978). https://doi.org/10.1063/1.325509
105. Sakuda, A., Kitaura, H., Hayashi, A., et al.: All-solid-state lithium secondary batteries with oxide-coated $LiCoO_2$ electrode and Li_2S–P_2S_5 electrolyte. J. Power Sources **189**, 527–530 (2009). https://doi.org/10.1016/j.jpowsour.2008.10.129
106. Zhao, Y., Zheng, K., Sun, X.: Addressing interfacial issues in liquid-based and solid-state batteries by atomic and molecular layer deposition. Joule **2**, 2583–2604 (2018). https://doi.org/10.1016/j.joule.2018.11.012
107. Ahmed, B., Xia, C., Alshareef, H.N.: Electrode surface engineering by atomic layer deposition: a promising pathway toward better energy storage. Nano Today **11**, 250–271 (2016). https://doi.org/10.1016/j.nantod.2016.04.004
108. Wang, B.Q., Liu, J., Sun, Q., et al.: Titanium dioxide/lithium phosphate nanocomposite derived from atomic layer deposition as a high-performance anode for lithium ion batteries. Adv. Mater. Interfaces **3**, 1600369 (2016). https://doi.org/10.1002/admi.201600369
109. Li, X.F., Liu, J., Banis, M.N., et al.: Atomic layer deposition of solid-state electrolyte coated cathode materials with superior high-voltage cycling behavior for lithium ion battery application. Energy Environ. Sci. **7**, 768–778 (2014). https://doi.org/10.1039/c3ee42704h
110. Groner, M.D., Fabreguette, F.H., Elam, J.W., et al.: Low-temperature Al_2O_3 atomic layer deposition. Chem. Mater. **16**, 639–645 (2004). https://doi.org/10.1021/cm0304546
111. Wang, B.Q., Zhao, Y., Banis, M.N., et al.: Atomic layer deposition of lithium niobium oxides as potential solid-state electrolytes for lithium-ion batteries. ACS Appl. Mater. Interfaces. **10**, 1654–1661 (2018). https://doi.org/10.1021/acsami.7b13467
112. Woo, J.H., Trevey, J.E., Cavanagh, A.S., et al.: Nanoscale interface modification of $LiCoO_2$ by Al_2O_3 atomic layer deposition for solid-state Li batteries. J. Electrochem. Soc. **159**, A1120–A1124 (2012). https://doi.org/10.1149/2.085207jes
113. Li, X., Ren, Z.H., Norouzi Banis, M., et al.: Unravelling the chemistry and microstructure evolution of a cathodic interface in sulfide-based all-solid-state Li-ion batteries. ACS Energy Lett. **4**, 2480–2488 (2019). https://doi.org/10.1021/acsenergylett.9b01676
114. Meng, X.B., Liu, J., Li, X.F., et al.: Atomic layer deposited $Li_4Ti_5O_{12}$ on nitrogen-doped carbon nanotubes. RSC Advances **3**, 7285–7288 (2013)
115. Wang, B.Q., Liu, J., Banis, M.N., et al.: Atomic layer deposited lithium silicates as solid-state electrolytes for all-solid-state batteries. ACS Appl. Mater. Interfaces **9**, 31786–31793 (2017). https://doi.org/10.1021/acsami.7b07113

116. Wang, B., Liu, J., Sun, Q., et al.: Atomic layer deposition of lithium phosphates as solid-state electrolytes for all-solid-state microbatteries. Nanotechnology **25**, 504007 (2014). https://doi.org/10.1088/0957-4484/25/50/504007
117. Liu, J., Banis, M.N., Li, X.F., et al.: Atomic layer deposition of lithium tantalate solid-state electrolytes. J. Phys. Chem. C **117**, 20260–20267 (2013). https://doi.org/10.1021/jp4063302
118. Kozen, A.C., Pearse, A.J., Lin, C.F., et al.: Atomic layer deposition of the solid electrolyte LiPON. Chem. Mater. **27**, 5324–5331 (2015). https://doi.org/10.1021/acs.chemmater.5b01654
119. Kazyak, E., Chen, K.H., Davis, A.L., et al.: Atomic layer deposition and first principles modeling of glassy Li_3BO_3–Li_2CO_3 electrolytes for solid-state Li metal batteries. J. Mater. Chem. A **6**, 19425–19437 (2018). https://doi.org/10.1039/c8ta08761j
120. Yubuchi, S., Ito, Y., Matsuyama, T., et al.: 5 V class $LiNi_{0.5}Mn_{1.5}O_4$ positive electrode coated with Li_3PO_4 thin film for all-solid-state batteries using sulfide solid electrolyte. Solid State Ionics **285**, 79–82 (2016). https://doi.org/10.1016/j.ssi.2015.08.001
121. Sakuda, A., Hayashi, A., Ohtomo, T., et al.: $LiCoO_2$ electrode particles coated with Li_2S–P_2S_5 solid electrolyte for all-solid-state batteries. Electrochem. Solid-State Lett. **13**, A73 (2010). https://doi.org/10.1149/1.3376620
122. Sakuda, A., Hayashi, A., Ohtomo, T., et al.: All-solid-state lithium secondary batteries using $LiCoO_2$ particles with pulsed laser deposition coatings of Li_2S–P_2S_5 solid electrolytes. J. Power Sources **196**, 6735–6741 (2011). https://doi.org/10.1016/j.jpowsour.2010.10.103
123. Zhou, A., Dai, X., Lu, Y., et al.: Enhanced interfacial kinetics and high-voltage/high-rate performance of $LiCoO_2$ cathode by controlled sputter-coating with a nanoscale $Li_4Ti_5O_{12}$ ionic conductor. ACS Appl. Mater. Interfaces **8**, 34123–34131 (2016). https://doi.org/10.1021/acsami.6b11630%5bPubMed]
124. Dai, X.Y., Wang, L.P., Xu, J., et al.: Improved electrochemical performance of $LiCoO_2$ electrodes with ZnO coating by radio frequency magnetron sputtering. ACS Appl. Mater. Interfaces **6**, 15853–15859 (2014). https://doi.org/10.1021/am503260s
125. Qiu, B., Wang, J., Xia, Y.G., et al.: Enhanced electrochemical performance with surface coating by reactive magnetron sputtering on lithium-rich layered oxide electrodes. ACS Appl. Mater. Interfaces **6**, 9185–9193 (2014). https://doi.org/10.1021/am501293y
126. Visbal, H., Aihara, Y., Ito, S., et al.: The effect of diamond-like carbon coating on $LiNi_{0.8}Co_{0.15}Al_{0.05}O_2$ particles for all solid-state lithium-ion batteries based on Li_2S–P_2S_5 glass–ceramics. J. Power Sources **314**, 85–92 (2016). https://doi.org/10.1016/j.jpowsour.2016.02.088
127. Ohtomo, T., Hayashi, A., Tatsumisago, M., et al.: All-solid-state batteries with Li_2O–Li_2S–P_2S_5 glass electrolytes synthesized by two-step mechanical milling. J. Solid State Electrochem. **17**, 2551–2557 (2013). https://doi.org/10.1007/s10008-013-2149-5
128. Xu, H.J., Yu, Y.R., Wang, Z., et al.: A theoretical approach to address interfacial problems in all-solid-state lithium ion batteries: tuning materials chemistry for electrolyte and buffer coatings based on Li6PA5Cl hali-chalcogenides. J. Mater. Chem. A **7**, 5239–5247 (2019). https://doi.org/10.1039/c8ta11151k
129. Zhang, Z.X., Zhang, L., Yan, X.L., et al.: All-in-one improvement toward $Li_6PS_5Br^-$ based solid electrolytes triggered by compositional tune. J. Power Sources **410**(411), 162–170 (2019). https://doi.org/10.1016/j.jpowsour.2018.11.016
130. Peng, G., Yao, X.Y., Wan, H.L., et al.: Insights on the fundamental lithium storage behavior of all-solid-state lithium batteries containing the $LiNi_{0.8}Co_{0.15}Al_{0.05}O_2$ cathode and sulfide electrolyte. J. Power Sources **307**, 724–730 (2016). https://doi.org/10.1016/j.jpowsour.2016.01.039
131. Calpa, M., Rosero-Navarro, N.C., Miura, A., et al.: Electrochemical performance of bulk-type all-solid-state batteries using small-sized $Li_7P_3S_{11}$ solid electrolyte prepared by liquid phase as the ionic conductor in the composite cathode. Electrochim. Acta **296**, 473–480 (2019). https://doi.org/10.1016/j.electacta.2018.11.035
132. Kim, D.H., Oh, D.Y., Park, K.H., et al.: Infiltration of solution-processable solid electrolytes into conventional Li-ion-battery electrodes for all-solid-state Li-ion batteries. Nano Lett. **17**, 3013–3020 (2017). https://doi.org/10.1021/acs.nanolett.7b00330
133. Yubuchi, S., Nakamura, W., Bibienne, T., et al.: All-solid-state cells with $Li_4Ti_5O_{12}$/carbon nanotube composite electrodes prepared by infiltration with argyrodite sulfide-based solid electrolytes via liquid-phase processing. J. Power Sources **417**, 125–131 (2019). https://doi.org/10.1016/j.jpowsour.2019.01.070
134. Rosero-Navarro, N.C., Miura, A., Tadanaga, K.: Composite cathode prepared by argyrodite precursor solution assisted by dispersant agents for bulk-type all-solid-state batteries. J. Power Sources **396**, 33–40 (2018). https://doi.org/10.1016/j.jpowsour.2018.06.011
135. Wang, D., Zhang, W., Zheng, W.T., et al.: Towards high-safe lithium metal anodes: suppressing lithium dendrites via tuning surface energy. Adv. Sci. **4**, 1600168 (2017). https://doi.org/10.1002/advs.201600168
136. Cheng, X.B., Hou, T.Z., Zhang, R., et al.: Dendrite-free lithium deposition induced by uniformly distributed lithium ions for efficient lithium metal batteries. Adv. Mater. **28**, 2888–2895 (2016). https://doi.org/10.1002/adma.201506124
137. Sun, C.Z., Ruan, Y.D., Zha, W.P., et al.: Recent advances in anodic interface engineering for solid-state lithium-metal batteries. Mater. Horiz. **7**, 1667–1696 (2020). https://doi.org/10.1039/d0mh00050g
138. Wenzel, S., Leichtweiss, T., Krüger, D., et al.: Interphase formation on lithium solid electrolytes: an in situ approach to study interfacial reactions by photoelectron spectroscopy. Solid State Ionics **278**, 98–105 (2015). https://doi.org/10.1016/j.ssi.2015.06.001
139. Wenzel, S., Randau, S., Leichtweiß, T., et al.: Direct observation of the interfacial instability of the fast ionic conductor $Li_{10}GeP_2S_{12}$ at the lithium metal anode. Chem. Mater. **28**, 2400–2407 (2016). https://doi.org/10.1021/acs.chemmater.6b00610
140. Hakari, T., Deguchi, M., Mitsuhara, K., et al.: Structural and electronic-state changes of a sulfide solid electrolyte during the Li deinsertion–insertion processes. Chem. Mater. **29**, 4768–4774 (2017). https://doi.org/10.1021/acs.chemmater.7b00551
141. Wenzel, S., Weber, D.A., Leichtweiss, T., et al.: Interphase formation and degradation of charge transfer kinetics between a lithium metal anode and highly crystalline $Li_7P_3S_{11}$ solid electrolyte. Solid State Ionics **286**, 24–33 (2016). https://doi.org/10.1016/j.ssi.2015.11.034
142. Camacho-Forero, L.E., Balbuena, P.B.: Exploring interfacial stability of solid-state electrolytes at the lithium-metal anode surface. J. Power Sources **396**, 782–790 (2018). https://doi.org/10.1016/j.jpowsour.2018.06.092
143. Bron, P., Roling, B., Dehnen, S.: Impedance characterization reveals mixed conducting interphases between sulfidic superionic conductors and lithium metal electrodes. J. Power Sources **352**, 127–134 (2017). https://doi.org/10.1016/j.jpowsour.2017.03.103
144. Wenzel, S., Sedlmaier, S.J., Dietrich, C., et al.: Interfacial reactivity and interphase growth of argyrodite solid electrolytes at lithium metal electrodes. Solid State Ionics **318**, 102–112 (2018). https://doi.org/10.1016/j.ssi.2017.07.005
145. Wang, X.L., Xiao, R.J., Li, H., et al.: Oxygen-driven transition from two-dimensional to three-dimensional transport behaviour in β-Li_3PS_4 electrolyte. Phys. Chem. Chem. Phys. **18**, 21269–21277 (2016). https://doi.org/10.1039/c6cp03179j

146. Xie, D.J., Chen, S.J., Zhang, Z.H., et al.: High ion conductive Sb_2O_5-doped β-Li_3PS_4 with excellent stability against Li for all-solid-state lithium batteries. J. Power Sources **389**, 140–147 (2018). https://doi.org/10.1016/j.jpowsour.2018.04.021
147. Liu, G.Z., Xie, D.J., Wang, X.L., et al.: High air-stability and superior lithium ion conduction of $Li_{3+3x}P_{1-x}Zn_xS_{4-x}O_x$ by aliovalent substitution of ZnO for all-solid-state lithium batteries. Energy Storage Mater. **17**, 266–274 (2019). https://doi.org/10.1016/j.ensm.2018.07.008
148. Mo, Y., Ong, S.P., Ceder, G.: First principles study of the $Li_{10}GeP_2S_{12}$ lithium super ionic conductor material. Chem. Mater. **24**, 15–17 (2012). https://doi.org/10.1021/cm203303y
149. Sun, Y.L., Suzuki, K., Hara, K., et al.: Oxygen substitution effects in $Li_{10}GeP_2S_{12}$ solid electrolyte. J. Power Sources **324**, 798–803 (2016). https://doi.org/10.1016/j.jpowsour.2016.05.100
150. Hu, C.H., Wang, Z.Q., Sun, Z.Y., et al.: Insights into structural stability and Li superionic conductivity of $Li_{10}GeP_2S_{12}$ from first-principles calculations. Chem. Phys. Lett. **591**, 16–20 (2014). https://doi.org/10.1016/j.cplett.2013.11.003
151. Sun, Y., Yan, W.N., An, L., et al.: A facile strategy to improve the electrochemical stability of a lithium ion conducting $Li_{10}GeP_2S_{12}$ solid electrolyte. Solid State Ionics **301**, 59–63 (2017). https://doi.org/10.1016/j.ssi.2017.01.014
152. Zhang, Z., Chen, S., Yang, J., et al.: Interface Re-engineering of $Li_{10}GeP_2S_{12}$ electrolyte and lithium anode for all-solid-state lithium batteries with ultralong cycle life. ACS Appl. Mater. Interfaces **10**, 2556–2565 (2018). https://doi.org/10.1021/acsami.7b16176
153. Chien, P.H., Feng, X., Tang, M., et al.: Li Distribution heterogeneity in solid electrolyte $Li_{10}GeP_2S_{12}$ upon electrochemical cycling probed by ^{7}Li MRI. J. Phys. Chem. Lett. **9**, 1990–1998 (2018)
154. Wang, C.H., Adair, K.R., Liang, J.W., et al.: Solid-state plastic crystal electrolytes: effective protection interlayers for sulfide-based all-solid-state lithium metal batteries. Adv. Funct. Mater. **29**, 1900392 (2019). https://doi.org/10.1002/adfm.201900392
155. Gao, Y., Wang, D.W., Li, Y.C., et al.: Salt-based organic-inorganic nanocomposites: towards A stable lithium metal/$Li_{10}GeP_2S_{12}$ solid electrolyte interface. Angew. Chem. Int. Ed. **57**, 13608–13612 (2018). https://doi.org/10.1002/anie.201807304
156. Ju, J.W., Wang, Y.T., Chen, B.B., et al.: Integrated interface strategy toward room temperature solid-state lithium batteries. ACS Appl. Mater. Interfaces **10**, 13588–13597 (2018). https://doi.org/10.1021/acsami.8b02240
157. Monroe, C., Newman, J.: The impact of elastic deformation on deposition kinetics at lithium/polymer interfaces. J. Electrochem. Soc. **152**, A396 (2005). https://doi.org/10.1149/1.1850854
158. Nagao, M., Hayashi, A., Tatsumisago, M., et al.: In situ SEM study of a lithium deposition and dissolution mechanism in a bulk-type solid-state cell with a Li_2S–P_2S_5 solid electrolyte. Phys. Chem. Chem. Phys. **15**, 18600 (2013). https://doi.org/10.1039/c3cp51059j
159. Kerman, K., Luntz, A., Viswanathan, V., et al.: Review: practical challenges hindering the development of solid state Li ion batteries. J. Electrochem. Soc. **164**, A1731–A1744 (2017). https://doi.org/10.1149/2.1571707jes
160. Han, F.D., Yue, J., Zhu, X.Y., et al.: Suppressing Li dendrite formation in Li_2S–P_2S_5 solid electrolyte by LiI incorporation. Adv. Energy Mater. **8**, 1703644 (2018). https://doi.org/10.1002/aenm.201703644
161. Porz, L., Swamy, T., Sheldon, B.W., et al.: Mechanism of lithium metal penetration through inorganic solid electrolytes. Adv. Energy Mater. **7**, 1701003 (2017). https://doi.org/10.1002/aenm.201701003
162. Han, F.D., Westover, A.S., Yue, J., et al.: High electronic conductivity as the origin of lithium dendrite formation within solid electrolytes. Nat. Energy **4**, 187–196 (2019). https://doi.org/10.1038/s41560-018-0312-z
163. Kasemchainan, J., Zekoll, S., Spencer Jolly, D., et al.: Critical stripping current leads to dendrite formation on plating in lithium anode solid electrolyte cells. Nat. Mater. **18**, 1105–1111 (2019). https://doi.org/10.1038/s41563-019-0438-9
164. Suyama, M., Kato, A., Sakuda, A., et al.: Lithium dissolution/deposition behavior with Li_3PS_4–LiI electrolyte for all-solid-state batteries operating at high temperatures. Electrochim. Acta **286**, 158–162 (2018). https://doi.org/10.1016/j.electacta.2018.07.227
165. Xu, R.C., Han, F.D., Ji, X., et al.: Interface engineering of sulfide electrolytes for all-solid-state lithium batteries. Nano Energy **53**, 958–966 (2018). https://doi.org/10.1016/j.nanoen.2018.09.061
166. Wang, C., Zhao, Y., Sun, Q., et al.: Stabilizing interface between $Li_{10}SnP_2S_{12}$ and Li metal by molecular layer deposition. Nano Energy **53**, 168–174 (2018). https://doi.org/10.1016/j.nanoen.2018.08.030
167. Takeuchi, T., Kageyama, H., Nakanishi, K., et al.: Application of graphite–solid electrolyte composite anode in all-solid-state lithium secondary battery with Li_2S positive electrode. Solid State Ionics **262**, 138–142 (2014). https://doi.org/10.1016/j.ssi.2013.09.046
168. Takada, K.: Solid-state lithium battery with graphite anode. Solid State Ionics **158**, 269–274 (2003). https://doi.org/10.1016/s0167-2738(02)00823-8
169. Yamamoto, T., Phuc, N.H.H., Muto, H., et al.: Preparation of $Li_7P_2S_8I$ solid electrolyte and its application in all-solid-state lithium-ion batteries with graphite anode. Electron. Mater. Lett. **15**, 409–414 (2019). https://doi.org/10.1007/s13391-019-00133-y
170. Zuo, X., Zhu, J., Mullerbuschbaum, P., et al.: Silicon based lithium-ion battery anodes: a chronicle perspective review. Nano Energy **31**, 113–143 (2017). https://doi.org/10.1016/j.nanoen.2016.11.013
171. Kim, D.H., Lee, H.A., Song, Y.B., et al.: Sheet-type Li_6PS_5Cl-infiltrated Si anodes fabricated by solution process for all-solid-state lithium-ion batteries. J. Power Sources **426**, 143–150 (2019). https://doi.org/10.1016/j.jpowsour.2019.04.028
172. Dunlap, N.A., Kim, S., Jeong, J.J., et al.: Simple and inexpensive coal-tar-pitch derived Si–C anode composite for all-solid-state Li-ion batteries. Solid State Ionics **324**, 207–217 (2018). https://doi.org/10.1016/j.ssi.2018.07.013
173. Cao, Y., Li, Q., Lou, S.F., et al.: Enhanced electrochemical performance of $Li_4Ti_5O_{12}$ through in situ coating $70Li_2S$–$30P_2S_5$ solid electrolyte for all-solid-state lithium batteries. J. Alloys Compd. **752**, 8–13 (2018). https://doi.org/10.1016/j.jallcom.2018.04.149
174. Hwang, A., Ma, Y., Cao, Y., et al.: Fabrication and electrochemical properties of $Li_4Ti_5O_{12}$@Li_6PS_5Cl for all-solid-state lithium batteries using simple mechanical method. Int. J. Electrochem. Sci. (2017). https://doi.org/10.20964/2017.08.29
175. Zhang, N., Ding, F., Yu, S.H., et al.: Novel research approach combined with dielectric spectrum testing for dual-doped $Li_7P_3S_{11}$ glass–ceramic electrolytes. ACS Appl. Mater. Interfaces **11**, 27897–27905 (2019). https://doi.org/10.1021/acsami.9b08218
176. Minami, K., Hayashi, A., Tatsumisago, M.: Electrical and electrochemical properties of the $70Li_2S{\cdot}(30-x)P_2S_5{\cdot}xP_2O_5$ glass–ceramic electrolytes. Solid State Ionics **179**, 1282–1285 (2008). https://doi.org/10.1016/j.ssi.2008.02.014
177. Kondo, S., Takada, K., Yamamura, Y.: New lithium ion conductors based on Li_2S–SiS_2 system. Solid State Ionics **53/54/55/56**, 1183–1186 (1992). https://doi.org/10.1016/0167-2738(92)90310-l

178. Kanno, R.: Synthesis of a new lithium ionic conductor, thio-LISICON–lithium germanium sulfide system. Solid State Ionics **130**, 97–104 (2000). https://doi.org/10.1016/s0167-2738(00)00277-0
179. Kaib, T., Haddadpour, S., Kapitein, M., et al.: New lithium chalcogenidotetrelates, LiChT: synthesis and characterization of the Li^+-conducting tetralithium ortho-sulfidostannate Li_4SnS_4. Chem. Mater. **24**, 2211–2219 (2012). https://doi.org/10.1021/cm3011315
180. Trevey, J.E., Jung, Y.S., Lee, S.: High lithium ion conducting Li_2S–GeS_2–P_2S_5 glass–ceramic solid electrolyte with sulfur additive for all solid-state lithium secondary batteries. Electrochim. Acta **56**, 4243–4247 (2011). https://doi.org/10.1016/j.electacta.2011.01.086
181. Tsukasaki, H., Mori, S., Shiotani, S., et al.: Direct observation of a non-isothermal crystallization process in precursor $Li_{10}GeP_2S_{12}$ glass electrolyte. J. Power Sources **369**, 57–64 (2017). https://doi.org/10.1016/j.jpowsour.2017.09.070
182. Kwon, O., Hirayama, M., Suzuki, K., et al.: Synthesis, structure, and conduction mechanism of the lithium superionic conductor $Li_{10+\delta}Ge_{1+\delta}P_{2-\delta}S_{12}$. J. Mater. Chem. A **3**, 438–446 (2015). https://doi.org/10.1039/c4ta05231e
183. Zhang, Q., Wan, H., Liu, G., et al.: Rational design of multichannel continuous electronic/ionic conductive networks for room temperature vanadium tetrasulfide-based all-solid-state lithium-sulfur batteries. Nano Energy **57**, 771–782 (2019). https://doi.org/10.1016/j.nanoen.2019.01.004
184. Bron, P., Dehnen, S., Roling, B.: $Li_{10}Si_{0.3}Sn_{0.7}P_2S_{12}$—a low-cost and low-grain-boundary-resistance lithium superionic conductor. J. Power Sources **329**, 530–535 (2016). https://doi.org/10.1016/j.jpowsour.2016.08.115
185. Ooura, Y., Machida, N., Naito, M., et al.: Electrochemical properties of the amorphous solid electrolytes in the system Li_2S–Al_2S_3–P_2S_5. Solid State Ionics **225**, 350–353 (2012). https://doi.org/10.1016/j.ssi.2012.03.003
186. Kato, Y., Saito, R., Sakano, M., et al.: Synthesis, structure and lithium ionic conductivity of solid solutions of $Li_{10}(Ge_{1-x}M_x)P_2S_{12}$ (M = Si, Sn). J. Power Sources **271**, 60–64 (2014). https://doi.org/10.1016/j.jpowsour.2014.07.159
187. Zhou, L.D., Assoud, A., Zhang, Q., et al.: New family of argyrodite thioantimonate lithium superionic conductors. J. Am. Chem. Soc. **141**, 19002–19013 (2019). https://doi.org/10.1021/jacs.9b08357
188. Minafra, N., Culver, S.P., Krauskopf, T., et al.: Effect of Si substitution on the structural and transport properties of superionic Li-argyrodites. J. Mater. Chem. A **6**, 645–651 (2018). https://doi.org/10.1039/c7ta08581h
189. Yubuchi, S., Uematsu, M., Deguchi, M., et al.: Lithium-ion-conducting argyrodite-type Li_6PS_5X (X = Cl, Br, I) solid electrolytes prepared by a liquid-phase technique using ethanol as a solvent. ACS Appl. Energy Mater. **1**, 3622–3629 (2018). https://doi.org/10.1021/acsaem.8b00280
190. Machida, N., Kashiwagi, J., Naito, M., et al.: Electrochemical properties of all-solid-state batteries with ZrO_2-coated $LiNi_{1/3}Mn_{1/3}Co_{1/3}O_2$ as cathode materials. Solid State Ionics **225**, 354–358 (2012). https://doi.org/10.1016/j.ssi.2011.11.026
191. Okada, K., Machida, N., Naito, M., et al.: Preparation and electrochemical properties of $LiAlO_2$-coated $Li(Ni_{1/3}Mn_{1/3}Co_{1/3})O_2$ for all-solid-state batteries. Solid State Ionics **255**, 120–127 (2014). https://doi.org/10.1016/j.ssi.2013.12.019
192. Takada, K., Ohta, N., Zhang, L.Q., et al.: Interfacial modification for high-power solid-state lithium batteries. Solid State Ionics **179**, 1333–1337 (2008). https://doi.org/10.1016/j.ssi.2008.02.017
193. Kim, J., Kim, M., Noh, S., et al.: Enhanced electrochemical performance of surface modified $LiCoO_2$ for all-solid-state lithium batteries. Ceram. Int. **42**, 2140–2146 (2016). https://doi.org/10.1016/j.ceramint.2015.09.126
194. Ito, S., Fujiki, S., Yamada, T., et al.: A rocking chair type all-solid-state lithium ion battery adopting Li_2O–ZrO_2 coated $LiNi_{0.8}Co_{0.15}Al_{0.05}O_2$ and a sulfide based electrolyte. J. Power Sources **248**, 943–950 (2014). https://doi.org/10.1016/j.jpowsour.2013.10.005

Jinghua Wu is an associate professor at Ningbo Institute of Materials Technology and Engineering, Chinese Academy of Science (NIMTE, CAS). He received his Bachelor of Science (BS) degree from Shandong University, China, in 2006 and his Ph.D. degree from NIMTE in 2012. After postdoctoral research at the National Institute for Materials Science (NIMS, Japan) and Soochow University, he joined NIMTE as an associate professor in 2018. His research interest focuses on sulfide electrolyte-based solid-state batteries and solid-state lithium-sulfide batteries.

Lin Shen is currently pursuing his Ph.D. under the supervision of Professor Xiayin Yao at Ningbo Institute of Materials Technology and Engineering, Chinese Academy of Sciences (NIMTE, CAS). He received his bachelor's degree from the College of Materials Science and Engineering, Beijing University of Chemical Technology in 2017. His research work focuses on developing solid-state electrolytes with high ionic conductivity and excellent interface performances as well as their applications in solid-state batteries.

Zhihua Zhang received his Ph.D. degree from Ningbo Institute of Materials Technology and Engineering, Chinese Academy of Sciences (NIMTE, CAS) in 2019. Afterwards, he worked as a senior research engineer at the battery R&D department at Ganfeng Lithium Co., Ltd. for one year. Currently, he is a post-doctor at NIMTE. His research focuses on electrolyte materials and electrodes for all-solid-state batteries, including interface behavior researches and battery devices.

Gaozhan Liu is currently pursuing her Ph.D. under the supervision of Professor Xiayin Yao at Ningbo Institute of Materials Technology and Engineering, Chinese Academy of Sciences (NIMTE, CAS). She received her bachelor's degree in the College of Materials Science and Engineering at Wuhan University of Technology in 2016. Her research work focuses on developing sulfide solid-state electrolytes with good electrochemical performance and excellent stability as well as their applications in all-solid-state batteries.

Zhiyan Wang is currently pursuing her Ph.D. degree under the supervision of Professor Xiayin Yao at Ningbo Institute of Materials Technology and Engineering, Chinese Academy of Sciences (NIMTE, CAS). She received her bachelor's degree and master's degree in the College of Chemical and Environmental Engineering, Yangtze University in 2016 and 2019, respectively. Her research work focuses on the development of composite polymer electrolytes with excellent electrochemical and physicochemical stability as well as their application in solid-state batteries.

Dong Zhou received his Ph.D. degree from the Technical University of Berlin in 2017. Afterward, he worked as a postdoctoral fellow at the MEET Battery research center, the University of Muenster for two years. Currently, he is a research assistant at Ningbo Institute of Materials Technology and Engineering, Chinese Academy of Sciences. His research interest is focused on investigating working mechanisms and/or failure modes of various types of rechargeable batteries by nondestructive synchrotron X-ray absorption and imaging techniques.

Hongli Wan received her Ph.D. degree from Ningbo Institute of Materials Technology and Engineering, Chinese Academy of Sciences (NIMTE, CAS) in 2020. Currently, she is a post-doctor at Department of Chemical and Biomolecular Engineering, University of Maryland-College Park. Her research focuses on materials synthesis and interfacial modification for all-solid-state batteries.

Xiaoxiong Xu is the chief scientist of Ganfeng Lithium Co., Ltd., and the general manager of Zhejiang Fengli New Energy Technology Co., Ltd. He got his Ph.D. degree from Shanghai Institute of Ceramics, Chinese Academy of Sciences (SICCAS) in 2007. Then, he joined the National Institute for Materials Science (NIMS), Japan, as a postdoctoral fellow from 2007 to 2011. Dr. Xu's research work focuses on solid-state lithium batteries with high performances. To date, he has published more than 60 peer-review journal papers and applied for over 100 patents. He is the recipient of the outstanding research award from the Chinese Ceramic Society.

Xiayin Yao is a professor at Ningbo Institute of Materials Technology and Engineering, Chinese Academy of Sciences (NIMTE, CAS). He received Ph.D. from Institute of Solid-State Physics and NIMTE, CAS in 2009. After that, he joined NIMTE and worked there until now. He worked as a research fellow or a visiting scholar in Hanyang University, Republic of Korea (2012–2013), Nanyang Technological University, Singapore (2013–2014) and the University of Maryland, College Park, USA (2018–2019). So far, he has co-authored over 110 peer-reviewed journal papers and applied more than 50 Chinese patents. His major interests include developing solid-state electrolytes with high ionic conductivities, solid-state lithium–sulfur batteries as well as solid-state sodium batteries.